AD NUMBER

AD877808

NEW LIMITATION CHANGE

TO

Approved for public release, distribution unlimited

FROM

Distribution authorized to DoD only; Specific Authority; Nov 70. Other requests shall be referred to ONR, Code 468, Washington, DC 20368.

AUTHORITY

ONR ltr dtd 29 Aug 73

PANAMETRICS
A Subsidiary of Esterline Corporation • 221 Crescent Street • Waltham, Massachusetts 02154 • (617) 899-2719
ESTERLINE

Measurement of Elastic Moduli of Materials at Elevated Temperature

Progress Report for the 32nd Quarterly Period Ending November 15, 1970

Performed for

Office of Naval Research
under
Contract N0014-71-C-0050

Prepared by

E. P. Papadakis
K. A. Fowler
L. C. Lynnworth

I. BACKGROUND

This work was supported by the Office of Naval Research under Contract N0014-71-C-0050.

II. DISCUSSION

The work reported here is in two categories, (1) a continuation of the research conducted to date, and (2) the initiation of work on two new but related subjects as enumerated in the terms of the contract which commenced August 16, 1970. Both theoretical and experimental work has been undertaken. New equipment has been built, and still more is under construction. A list of the projects undertaken follows.

A. Modulus in Refractory Metals at Elevated Temperatures

Young's modulus has been measured in wires of rhenium, tungsten-25% rhenium alloy, and rhodium-50% iridium alloy at temperatures up to 2250C (2000C for the Rh-50 Ir).

B. Attenuation in Refractory Metals at Elevated Temperatures

The attenuation of extensional waves at about 160 kHz has been measured in the above wires during several heating and cooling cycles. Rhenium is being studied extensively.

C. Ferrite Stub Fixture

A fixture has been designed and built to permit magnetostrictive wire transducers to operate at frequencies approaching 500 kHz. The fixture limits the ringing field from the coil to a short region within the wire, defining a half-wavelength region at the end of a long wire.

D. Momentary Contact High-Temperature Attenuation Measurement Equipment

Buffer rods and transducers are being prepared for both longitudinal and shear wave measurements on steel and other materials in a muffle tube vacuum furnace by the momentary contact method. Preliminary measurements indicate that the method will yield useful new data.

E. Broadband Transducer Studies

The pressure and phase profiles in the field of broadband transducers have been calculated from the theory of piston radiators. Several applications utilizing the bandwidth of such transducers have been demonstrated.

F. Focused Transducer Studies

The study of focused transducers has commenced on the experimental level to verify theories and develop applications.

G. Flexural Modulus and Decrement Device for Measuring Plastics

A resonant device for low-frequency flexural testing analogous to the torsion pendulum for torsional testing has been investigated theoretically. A preliminary model is being constructed to test specimens of the same geometry as the standard ASTM tensile specimens.

H. Pulse-Echo-Overlap System for Ultrasonic Travel Time

An apparatus for measuring the travel time (delay) of ultrasonic waves in specimens by the pulse-echo-overlap method has been constructed from equipment currently available. The ultimate accuracy of the system can approach 5 ppm, and improvements will be made to try to achieve this goal.

I. Computer Programming

A program written at the NASA-Lewis Research Center for the computer-plotting of graphs from computer-generated tables of results has been adapted for use in plotting quantities such as modulus versus temperature derived from input data such as length, density, thermal expansion, and ultrasonic delay time versus temperature. The program will be extended to cover attenuation versus temperature in the future.

III. DETAILS OF NEW WORK

A. Modulus in Refractory Metals

Young's modulus has been computed from ultrasonic extensional wave travel time measurements in several refractory metal wires by the formulas

$$v_e = 2L/t_e \tag{1}$$

and

$$Y = \rho v_e^2 \tag{2}$$

where L is specimen length, t_e is round trip travel time of extensional waves, v_e is extensional wave velocity, ρ is density, and Y is Young's modulus. The travel times t_e were measured as a function of temperature at the thermocouple calibration facility of Englehard Industries in Newark, New Jersey, by means of a Panatherm® 5010 instrument. Specimens were fabricated and pretested at Panametrics from wire supplied by Englehard. The wire configuration was as follows: A remendur magnetostrictive stub 1/2 inch long, a tungsten lead-in wire 16 inches long, and a specimen 2 inches long. The temperature in the furnace was determined by an L & N optical pyrometer.

Corrections for thermal expansion were applied in the calculations to arrive at values of length L and density ρ as functions of temperature. The corrections were known accurately[1] for rhenium and W-25% Re, and were approximated by interpolation from tabulated data[2] for Ir-50% Rh. A computer program was written to calculate Y and plot Y versus temperature automatically. (See Section I.)

Results of Y versus temperature are given in Figs. 1 through 4 for Re, W-25% Re (2 samples), and Ir-50% Rh. The points represent several cycles from room temperature to the maximum temperature in Figs. 1 through 3. In all cases the specimens were annealed at 2000C for 1/2 hour and brought to room temperature before the measurements were initiated. No significant hysteresis in modulus was observed. These curves follow the general trend of modulus versus temperature in metals.

B. Attenuation in Refractory Metals at Elevated Temperatures

During the measurements of delay time reported in Section A, photographs were taken of the echo amplitudes from the specimens. The amplitudes of the first three echoes were used to compute the attenuation in the specimens and the reflection coefficient between the lead-in wires and the specimens.[3] The attenuation versus temperature is shown in Figs. 5 through 8. It will be noted that attenuation is not a monotonic function of temperature in the Re and W-25% Re run in these tests, but that it depends on the heating cycle and the direction of temperature change. In rhenium (Fig. 5) a peak of variable magnitude appears near 1900C (2175K). The level of 0.03 N/cm is reached between 1500C and 1900C on different runs. Attenuation coefficient of 0.03 N/cm is equivalent to 6 dB of loss in one round trip through a specimen 2 inches (5 cm) long. (Sample lengths in our tests are typically 2 inches long.) The peak at 1900C does not appear to be the same peak observed earlier.[4] The earlier data extrapolated to 160 kHz would predict a peak near 2700K (2430C), above our temperature range. The present peak near 1900C is probably related to the peak (or plateau) near 2000-2100C reported earlier[3] for measurements near 100 kHz. Further work is called for.

In W-25% Re alloy the data below 2000C is inconclusive, but above 2000C the attenuation definitely rises with a steep slope of up to 1×10^{-4} N/cm-^{o}C, reaching 0.03 N/cm by 2300C.

The Ir-50 Rh alloy was run only once, not cycled, so Fig. 8 is not as definitive as the previous curves. The level of 0.03 N/cm is reached on a steep slope at 1600C, and a peak may be present at 1800C. A plateau, if not a peak, is in evidence.

C. Ferrite Stub Fixture

To facilitate the measurement of ultrasonic attenuation versus frequency in wires it would be advantageous to have a transducer of variable length. The transducer length is defined by the length of the magnetostrictive wire influenced by the applied magnetic field. This effective length defines a half-wavelength at the center-frequency of the pulse generated by the transducer. To increase the length of the transducer, the magnetostrictive wire is moved further into the solenoidal coil, and vice versa. The effective length cannot be made arbitrarily short, however, because fringing fields follow the ferromagnetic wire for some distance.

To eliminate this problem and create shorter, variable-length transducers, a ferromagnetic reluctance loop was designed and constructed of ferrite. See Fig. 9. In this loop the magnetostrictive wire fits through a hole in a disc of ferrite. The fringing field passes out into the ferrite instead of continuing down the wire. The flux is brought around through other ferrite pieces to the end of the wire. Thus, the half-wavelength region in the wire is the portion between the end of the wire and the ferrite disc. This length is varied by positioning the ferrite plug abutting the end of the wire.

Two experiments were performed to establish the operating limits and characteristics of the device. First, electrical pulses of adjustable length were applied to the coil with the magnetostrictive wire inserted a given distance. The pulse length for maximum echo amplitude was determined, and the upper and lower limiting pulse lengths for echo distortion were also determined. The widths of the central half-cycle of the echoes were taken as representative of half a cycle of the center frequency of the echoes. Thus the frequency limits of the system for a given wire insertion distance were determined. See Fig. 10. Operation was obtained from 60 to 400 kHz. The upper limit is more than twice the frequency obtained previously with fringing coils.

Second, the effective bandwidth of the device was found by an inverse method. Usually the transducer length is held constant and the loss is plotted as a function of frequency. In the inverse method used here, the frequency of an rf burst was held constant and the loss was plotted as a function of insertion length. See Fig. 11. Bandwidths of over 45% for two transductions were observed. Operation up to 500 kHz was possible with rf bursts. This device will be used to make measurements of materials properties at various frequencies versus a second variable such as temperature.

D. Momentary Contact High-Temperature Attenuation Measurement Equipment

Both shear and longitudinal wave attenuation can be obtained from momentary contact measurements in hot bulk specimens using pressure coupling.[5, 6] This method of measuring attenuation depends upon the presence of a buffer rod between the transducer and the specimen. The ultrasonic wave travel time in the buffer rod must be more than three times that in the specimen to permit the observation of two reverberations in the specimen as well as the first echo from the buffer/specimen interface. Then the attenuation and the reflection coefficient can be calculated.[3]

Buffer rods to fit the translation mechanism in a muffle tube vacuum furnace have been built, and 2 MHz transducers installed. See Fig. 12. These will permit operation at 2, 6, and 10 MHz in overtone operation. The buffer rod with a slightly convex face (actually lapped out-of-flat from a ground surface) contacts one face of the specimen while a ring support contacts the opposite face. Thus the ultrasonic wave encounters a steel/vacuum interface at the far end of the specimen.

Preliminary results with longitudinal waves in 52100 steel are shown in Fig. 13. A single specimen was run from room temperature to 925C in steps. At each increment in temperature it was measured at 2, 6, and 10 MHz. The data show the pressure-dependent magnetic ordering at the Curie temperature, about 725C. Just below the Curie temperature there is an absorption peak due to the wave's perturbing the ordering. Just above, this absorption disappears because no ordering is possible. At still higher temperatures, grain growth probably occurs, increasing the loss due to grain scattering.

E. Broadband Transducer Studies

The pressure and phase profiles in the field of a plane-wave broadband transducer have been calculated. Several experiments utilizing the spectral content of the pulses from these transducers have also been performed. These calculations and experiments have been written up as Technical Memorandum No. 6, and oral presentations have been made at two national meetings in October. A copy of the memorandum is attached as Appendix A. It constitutes the contents of this section of this quarterly report.

F. Focused Transducer Studies

Focused transducers are useful in two areas: (1) detecting small flaws in materials, and (2) applying high intensity waves over small volumes. Applications range from inspecting steel billets to performing brain surgery.

Interesting physical problems in diffraction theory and nonlinear acoustics arise during focusing. Smith and Beyer[7] have recently investigated the monofrequency case, observing harmonic generation and field distributions. We intend to pursue the broadband focusing problem.

The transducer assembly sketched in Fig. 14 was built with an aluminum buffer rod containing a spherical depression of spherical

radius 1 inch. A Panametrics VIP-10 transducer was clamped to the opposite end, and the assembly tested in a water tank. The target was the squared-off end of a wire 1 mm (0.040 inch) in diameter The focal point of the assembly was found by manipulating the buffer ro o the point yielding maximum echo amplitude from the wire. Then a plitude was recorded as a function of buffer rod position in x-y-z coord ates. Amplitude plots are shown in Fig. 15. The sharpness of the focus is evident.

G. Flexural Modulus and Decrement Device for Measuring Plastics

At present, the standard measurement of Young's modulus of rigid and viscoelastic plastics is usually performed on tensile testing machines.[8] The modulus is the slope of the stress-strain curve, at a particular strain. Various problems arise including the fact that the modulus is a function of strain and strain rate in this test.

Ultrasonic measurements, on the other hand, may be above some relaxation frequencies, and hence yield moduli which are higher than the static or low-frequency values. Structural designers usually want zero-frequency moduli, for cases involving static (not dynamic) loads.

We have considered several ways to measure Young's modulus at very low frequencies. Analogs to the torsion pendulum have been explored. A balanced resonator concept seems promising. The resonator is a structure similar in appearance to a slice through an I-beam. See Fig. 16. The "web" is the spring element, and consists of the sample to be tested. The "flanges" are two elongated masses into which the ends of the sample are clamped. These masses are pivoted at their centers of gravity and provide the inertial element in the resonator. The resonator is set into motion such that the web element flexes as a leaf spring, and the masses rotate about their pivots. According to the theory of the bending of beams, the stiffness is directly proportional to Young's modulus of the web material. With large masses and thin webs, the frequency of operation can be depressed below 1 Hz. Thus the balanced resonator is an attractive acoustic approach to the low-frequency measurement problem in plastics.

We have derived the equations of motion of the structure in Fig. 16:

$$-YI_1 \frac{d^2y}{dx^2}\Big|_\ell - \frac{a}{2} YI_1 \frac{d^3y}{dx^3}\Big|_\ell = I_2 \frac{d^2\theta}{dt^2} + \eta \frac{d\theta}{dt} \tag{3}$$

$$YI_1 \frac{d^3y}{dx^3}\Big|_\ell = m \frac{d^2y_m}{dt^2} \tag{4}$$

$$YI_1 \frac{d^4y}{dx^4} - \mu \omega^2 y = 0 \tag{5}$$

$$m y_m + \int^{\ell} \mu y \, dx = 0 \tag{6}$$

Equation (3) is the torque equation for the masses about their pivots. Equation (4) is the force on the center of mass of one mass. Equation (5) is the equation for flexural motion of the web member. Equation (6) is a statement that the center of mass of the total device stays fixed in space; the web moves one way a great deal while the masses translate slightly in the opposite direction. Equation (6) is actually the integral of Eq. (4). In these equations, the quantities are defined as follows:

Y = Young's modulus of spring member (web),

I_1 = Geometrical moment of inertia of web cross section

y = displacement

x = coordinate along web, origin at center

ℓ = length of web from center to end mass

a = width of end mass

I_2 = Mechanical moment of inertia of end mass

ϑ = rotation angle of end mass

η = friction coefficient

m = mass of an end mass

y_m = displacement of center of end mass

μ = mass per unit length of web

ω = angular frequency.

The solution[9] to Eq. (5) is

$$y(x) = B_1 \sinh rx + B_2 \cosh rx + \\ + B_3 \sin rx + B_4 \cos rx \qquad (7)$$

where r is given by

$$r = (\mu \omega^2/EI_1)^{1/4} \ . \qquad (8)$$

Only symmetrical solutions for y(x) are desired, so the odd terms are dropped, and Eq. (7) becomes

$$y(x) = B_2 \cosh rx + B_4 \cos rx \ . \qquad (9)$$

In general the solution to Eqs. (3) through (6) is separable, so

$$y = X(x)\, T(t)$$

$$= X(x) \exp (j\omega t) \qquad (10)$$

with sinusoidal time dependence and spatial dependence

$$X(x) = B_2 \cosh rx + B_4 \cos rx \ . \qquad (11)$$

The angle θ is

$$\theta = \frac{dX}{dx}\Big|_{\ell} \qquad (12)$$

by continuity of slope at the ends of the web. This implies that the

position y_m of the center of each end mass is

$$X_m = X_\ell + \frac{a}{2} \left.\frac{dX}{dx}\right|_\ell . \tag{13}$$

Use of Eqs. (12) and (13) in Eqs. (3) and (6) yields

$$-YI_1 \left.\frac{d^2X}{dx^2}\right|_\ell - \frac{YI_1 a}{2} \left.\frac{d^3X}{dx^3}\right|_\ell + \omega^2 I_2 \left.\frac{dX}{dx}\right|_\ell - j\omega\eta \left.\frac{dX}{dx}\right|_\ell = 0 \tag{14}$$

and

$$m \left(X_\ell + \frac{a}{2} \left.\frac{dX}{dx}\right|_\ell \right) + \int_0^\ell \mu X \, dx = 0 . \tag{15}$$

Application of these boundary conditions to the web solution in Eq. (11) yields two equations,

$$-YI_1 (B_2 r^2 \cosh r\ell - B_4 r^2 \cos r\ell)$$

$$-(YI_1 a/2) (B_2 r^3 \sinh r\ell + B_4 r^3 \sin r\ell)$$

$$+ \omega^2 I_2 (B_2 r \sinh r\ell - B_4 r \sin r\ell)$$

$$-j\omega\eta (B_2 r \sinh r\ell - B_4 r \sin r\ell) = 0 \tag{16}$$

and

$$m (B_2 \cosh r\ell + B_4 \cos r\ell)$$

$$+(ma/2) (B_2 r \sinh r\ell - B_4 r \sin r\ell)$$

$$+\mu \left[(B_2/r) \sinh r\ell + (B_4/r) \sin r\ell \right] = 0 . \tag{17}$$

At resonance, the hyperbolic and circular components of the displacement will be in definite proportions, so B_2 and B_4 are related by

$$B_2 = g B_4 \tag{18}$$

where g is a constant which can be evaluated from Eq. (17) as

$$g = \frac{(mar/2 - \mu/r) \sin r\ell - m \cos r\ell}{(mar/2 + \mu/r) \sinh r\ell + m \cosh r\ell} \quad . \tag{19}$$

Insertion of this into Eq. (16) yields

$$-YI_1 r (g \cosh r\ell - \cos r\ell)$$

$$-(YI_1 a r^2/2) (g \sinh r\ell + \sin r\ell)$$

$$+\omega^2 I_2 (g \sinh r\ell - \sin r\ell)$$

$$-j\omega\eta (g \sinh r\ell - \sin r\ell) = 0 \quad . \tag{20}$$

Equation (20) is the basic equation for the resonance of the balanced resonator. It is a complex transcendental equation involving both circular and hyperbolic functions. Iteration on an electronic data processing machine seems the best way to solve for the resonance frequency.

A computer program was written in Fortran IV G to do the iteration and compute the resonance frequency. The end masses were assumed rectangular of density ρ_m, width a, length b, and thickness c. The web was generalized to the case of a symmetrical laminated sandwich of half-thickness U_2, filler half-thickness U_1, outer layer width W_2, filler width W_1, and corresponding moduli Y_2 and Y_1 and densities ρ_2 and ρ_1. The parameters I_1, I_2, Y, and μ are

$$I_1 = \left[(W_1 - W_2) U_1^3 + W_2 U_2^3\right]/3 \tag{21}$$

$$I_2 = \rho_m a b c (a^2 + b^2)/12 \tag{22}$$

$$Y = \frac{(W_1 Y_1 - W_2 Y_2) U_1^2 + W_2 Y_2 U_2^2}{(W_1 - W_2) U_1^2 + W_2 U_2^2} \tag{23}$$

$$\mu = 2 U_1 W_1 \rho_1 + 2 (U_2 - U_1) W_2 \rho_2 \quad . \tag{24}$$

The program input is data on densities, moduli, dimensions, and damping. The output is resonant frequency as a function of any one of these with the others held constant. Curves have been produced of resonance frequency versus some of the more important variables such as web thickness (TWEB), web modulus (YWEB), and mass length (LMASS). See Figs. 17 through 19. Basic input data corresponded to Invar end masses 33 cm long, 5.7 cm wide, and 3.1 cm thick, and a Lucite web 5.0 cm long, 1.3 cm wide, and 0.5 cm thick. A structure of these dimensions was chosen deliberately to accommodate the ASTM standard plastic tensile specimens[8] of Types I, II, and III for sheet and plate material. With such a structure, the tensile specimens could be tested nondestructively at low frequency first, then pulled to destruction in the standard manner.

Examination of Figs. 17 through 19 will indicate that the resonant frequency varies with the reciprocal of the length of the end mass, with the square root of the modulus, and with the 3/2-power of the web thickness. These powers are approximate, but they show the functional dependence expected from the balanced resonator configuration.

A working model is being constructed to verify the theory and to be used as a test instrument for Young's modulus and internal friction in plastics at low frequencies.

H. Pulse-Echo-Overlap System for Ultrasonic Travel Time

An apparatus for measuring the travel time (delay) of ultrasonic waves in specimens by the pulse-echo-overlap method[10] has been constructed from standard electronic components. See Fig. 20 for a block diagram of the system. The principle of operation is as follows: Delay time between two echoes is measured by setting the period of an oscillator equal to the travel time between the echoes (by adjusting the oscillator frequency). The oscillator drives the x-axis of the oscilloscope on which the echoes are viewed. The echoes are overlapped because the first occurs on one sweep and the second occurs on the next sweep. The rest of the equipment synchronizes the input pulses with the sweep and intensifies the echoes of interest. If rf operation is desired, a pulsed rf generator is interposed between pulser #1 and the pulse limiter. The function of the latter is to limit the feedthrough of the input pulse to the oscilloscope while permitting the echoes to pass thence.

Figure 21 contains oscilloscope photographs of echoes in a 1-inch rhenium sensor on the end of a tungsten wire transmission line. On the

linear sweep three echoes are intensified. These three echoes are overlapped simultaneously on cycles 1, 2, and 3 of the driven sweep. The delay is computed from the accurately counted oscillator frequency as $t = 1/f$, and the attenuation and reflection coefficients may be found from the amplitudes of the three echoes. For any individual reading, the precision of the system is limited to roughly 1/100 of the period of the center frequency of the echoes (or to 1/100 of the period of the frequency of an rf burst when used). Accuracy can approach 5 ppm in velocity. Transit time accuracy is correspondingly about 1 ns at 10 MHz. By averaging many readings, even greater accuracy has been achieved.

I. Computer Programming

A program for computer-plotting of graphs from computer-generated tables of results[11] has been adapted for use in our modulus work. This computer program is versatile, being able to plot several curves on one graph with different symbols using coordinate scale factors either fed in or self-generated from the tabulated results.

A program has been written to compute moduli from ultrasonic delay times measured versus temperature. This program incorporates corrections for thermal expansion and utilizes the computer-plotting routine mentioned above. Figures 1 through 4 are examples of modulus data plotted automatically on the computer.

Another computer program has been written to compute the resonance frequency of the balanced resonator from its intrinsic and extrinsic variables. This program includes the solution of a complex transcendental equation.

A computer program, written earlier, was used in the broadband transducer field analysis.

IV. PUBLICATIONS, TALKS, COURSES

Our course, #2911, Ultrasonics, has been postponed until the spring term at the Northeastern University Extension School. Cooperative teaching will be carried on by C. A. Carey, K. A. Fowler, L. C. Lynnworth, and E. P. Papadakis.

The following papers, submitted recently, have been scheduled for publication:

"Traveling Wave Reflection Methods for Measuring Ultrasonic Attenuation in Thin Rods and Wires," E. P. Papadakis, J. Appl. Phys. (Nov. 1970).

"Effects of Input Amplitude Profile Upon Diffraction Loss and Phase Change in a Pulse-Echo System," E. P. Papadakis, J. Acoust. Soc. Am. (Nov. 1970).

"Elastic Wave Velocities in Various Alloy Strips," E. P. Papadakis, Metallurgical Transactions (early 1971).

"Ultrasonic Waveguide Effects in Inhomogeneous Rods of Radial Symmetry," E. P. Papadakis, J. Acoust. Soc. Am. (Feb. 1971).

The following papers, submitted recently, are under review by technical journals:

"The Role of Reaction Rates and Cross-Linking in the Growth of the Elastic Moduli in Solidifying Epoxy Resins," E. P. Papadakis (to J. Appl. Phys.)

"Nonuniform Pressure Device for Bonding Thin Slabs to Substrates," E. P. Papadakis (to Rev. Sci. Instr.)

The following talks were delivered recently:

L. C. Lynnworth and E. P. Papadakis, "Ultrasonic Thermometry," 1970 Ultrasonics Symposium (IEEE Group on Sonics and Ultrasonics, sponsor) October 21, 1970 (Invited).

E. P. Papadakis and K. A. Fowler, "The Radiation Field of Broadband Transducers and Their Temporal and Frequency Response," 1970 Ultrasonics Symposium (IEEE Group on Sonics and Ultrasonics, sponsor) October 21, 1970.

K. A. Fowler and E. P. Papadakis, "Video Pulse Ceramic Transducers for Ultrasonic Inspection and Measurements," 1970 Fall Conference (ASNT, sponsor) October 21, 1970.

K. A. Fowler, "Acoustic Emission Transducers and an Experimental Method of Verifying Their Performance," Joint Meeting of the Boston Chapters of ASNT, IEEE, ANS, ASM, ASTM, ASME, September 23, 1970 (Invited). A preprint is in Appendix B.

K. A. Fowler, "An Acoustic Emission Simulation Test Set," The Acoustic Emission Working Group, Chicago, November 12-13, 1970.

V. SUMMARY

A. New Apparatus

Three new pieces of apparatus have been built and tested:

(1) Ferrite stub fixture for increasing the frequency range of digital pulses and allowing multifrequency operation of one transducer; (2) Pulse-Echo-Overlap system for measuring ultrasonic wave travel time to an accuracy of 5 ppm; (3) Focused transducer for studying ultrasonic lens "optics" and testing solid objects with focused energy.

Two other new pieces of apparatus are being built and perfected:

(4) Buffer rod set for making attenuation measurements in hot materials by the momentary contact method using pressure coupling of both longitudinal and shear waves; (5) Balanced resonator for making low-frequency flexural modulus and damping measurements on plastics.

B. New Measurements

Young's modulus has been measured in Re, W-25% Re, and Ir-50% Rh wires. The attenuation of extensional waves near 160 kHz was also measured in these alloys. Several measurements utilizing the spectral content of the pulses from broadband transducers have also been performed.

C. Theory

The pressure and phase profiles in the radiation field of a plane-wave broadband transducer have been computed. We derived the equations of motion of the balanced resonator. We determined the resonance frequency as a function of size, densities, and moduli. Such a resonator is being tested for low-frequency flexural modulus measurements in plastics.

D. Computer-Aided Calculations

Computer programs have been written and/or utilized for

(1) Broadband transducer field analysis,

(2) Balanced resonator frequency calculations,

(3) Modulus calculations,

(4) Computer-plotting of graphs.

E. Communications

The new course on ultrasonics owes much of its subject matter to the results of research sponsored by the ONR. Several papers and talks have been published or given, or are scheduled.

ACKNOWLEDGMENTS

The authors are indebted to E. Zysk and A. Robertson of Englehard Industries, for supplying specimen material and performing the measurements on ultrasonic delay and echo amplitudes from which the moduli and attenuation values were calculated. J. E. Bradshaw, R. A. Fisher, and D. R. Patch of this laboratory, made many contributions in design, fabrication and testing.

REFERENCES

1. J. B. Conway and A. C. Losekamp, "Thermal Expansion Characteristics of Several Refractory Metals to 2500°C," Trans. Met. Soc. AIME 236, 702-709 (1966).

2. Handbook of Chemistry and Physics, 40th Edition, pp 2101-2103 and 2239-2249, Chemical Rubber Publishing Company, Cleveland, Ohio, 1958.

3. Progress Report for the 28th Quarterly Period, Nonr-3918(00), Nov. 15, 1969.

4. Progress Report for the 24th Quarterly Period, Nonr-3918(00), Nov. 15, 1968.

5. Progress Report for the 30th Quarterly Period, Nonr-3918(00), May 15, 1970.

6. Annual Summary Report, Nonr-3918(00), August 15, 1970.

7. C. W. Smith and R. T. Beyer, "Ultrasonic Radiation Field of a Focusing Spherical Source at Finite Amplitudes," J. Acoust. Soc. Am. 46, 806-813 (1969).

8. Standard D-638-68, "Standard Method of Test for Tensile Properties of Plastics," 1970 Annual Book of ASTM Standards, Part 27, pp 169-182, ASTM, Philadelphia, Pa., 1970.

9. F. B. Hildebrand, Advanced Calculus for Engineers, p 210, Prentice-Hall, Inc., New York, 1949.

10. E. P. Papadakis, "Ultrasonic Phase Velocity by the Pulse-Echo-Overlap Method Incorporating Diffraction Phase Corrections," J. Acoust. Soc. Am. 42, 1045-1051 (1967).

11. L. T. Dellner, "A Set of 360 Fortran (Level G or H) Subroutines for Generating Printed Plots," NASA TM X-1700, Lewis Research Center, Cleveland, Ohio, December 1968.

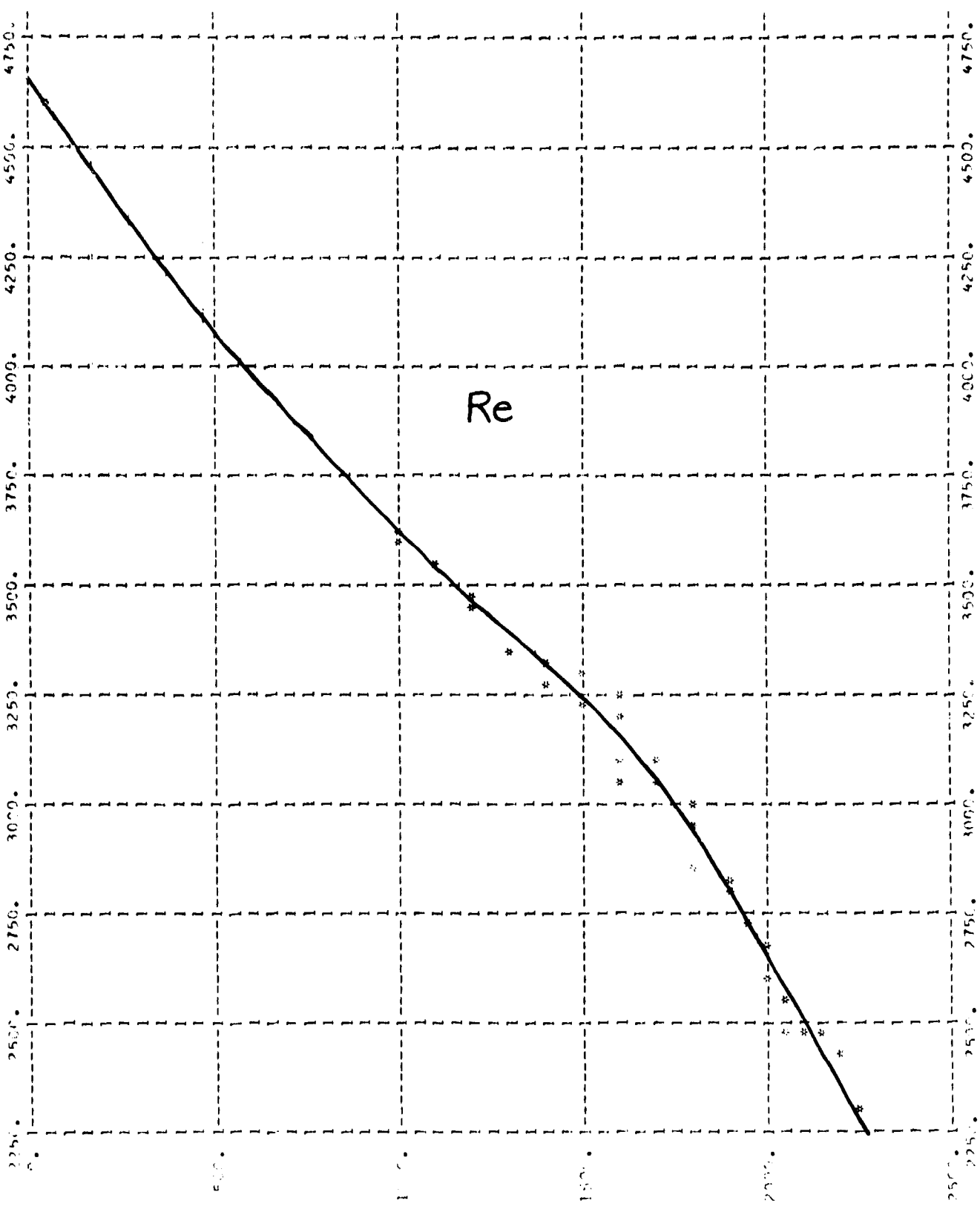

Fig. 1. Young's modulus in rhenium sample

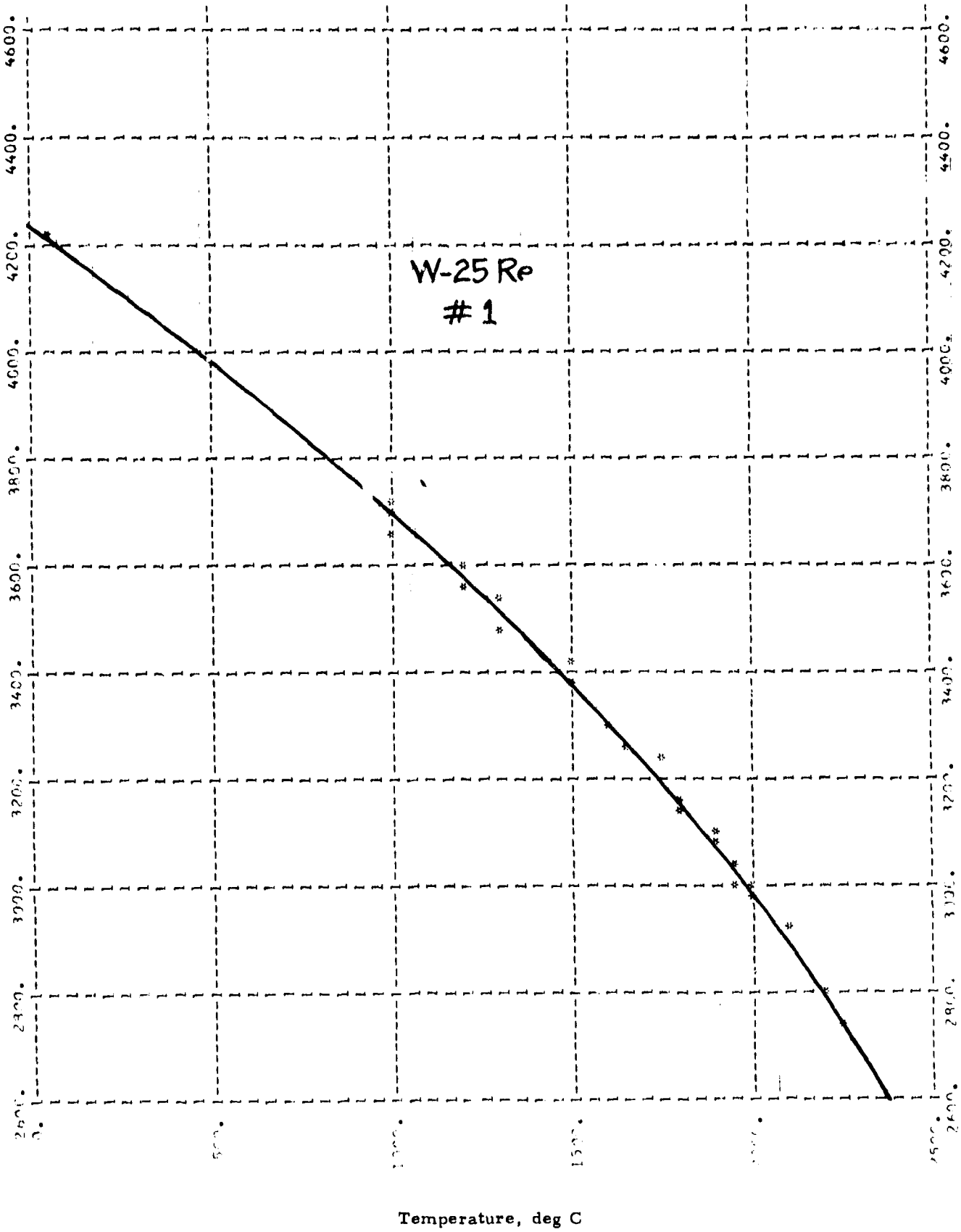

Fig. 2. Young's modulus in W-25 Re alloy sample #1

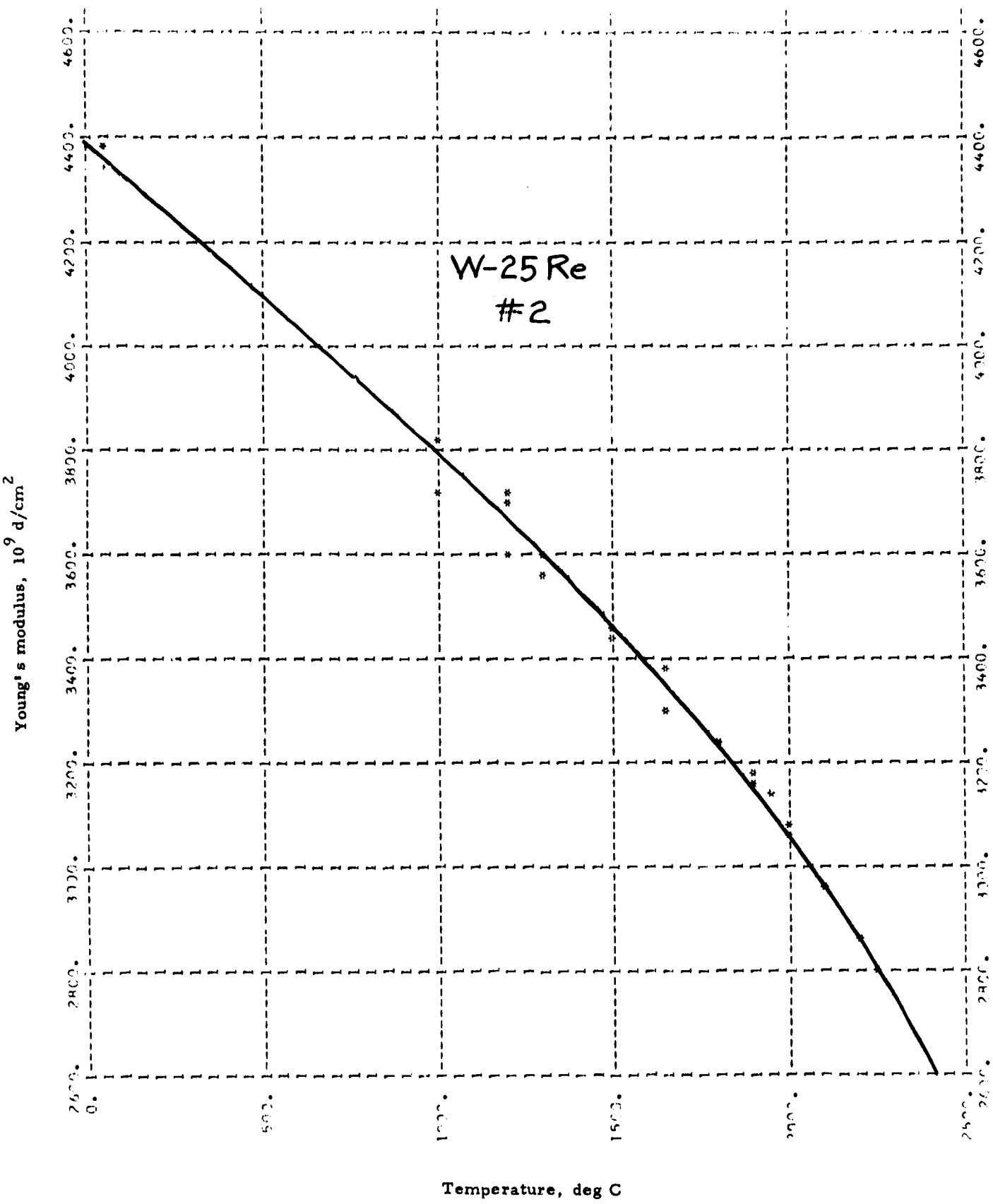

Fig. 3. Young's modulus in W-25 Re alloy sample #2

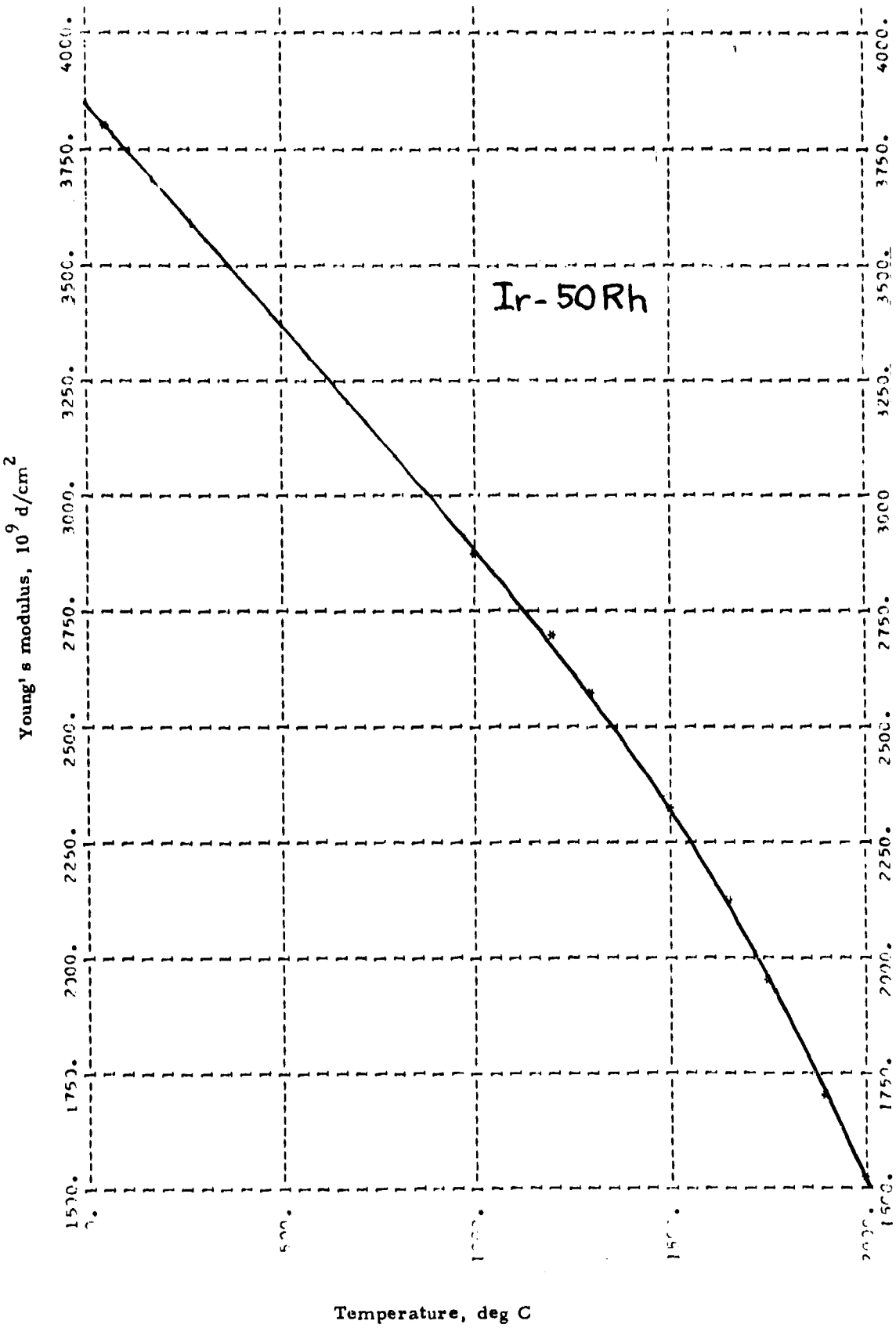

Fig. 4. Young's modulus in Ir-50 Rh sample

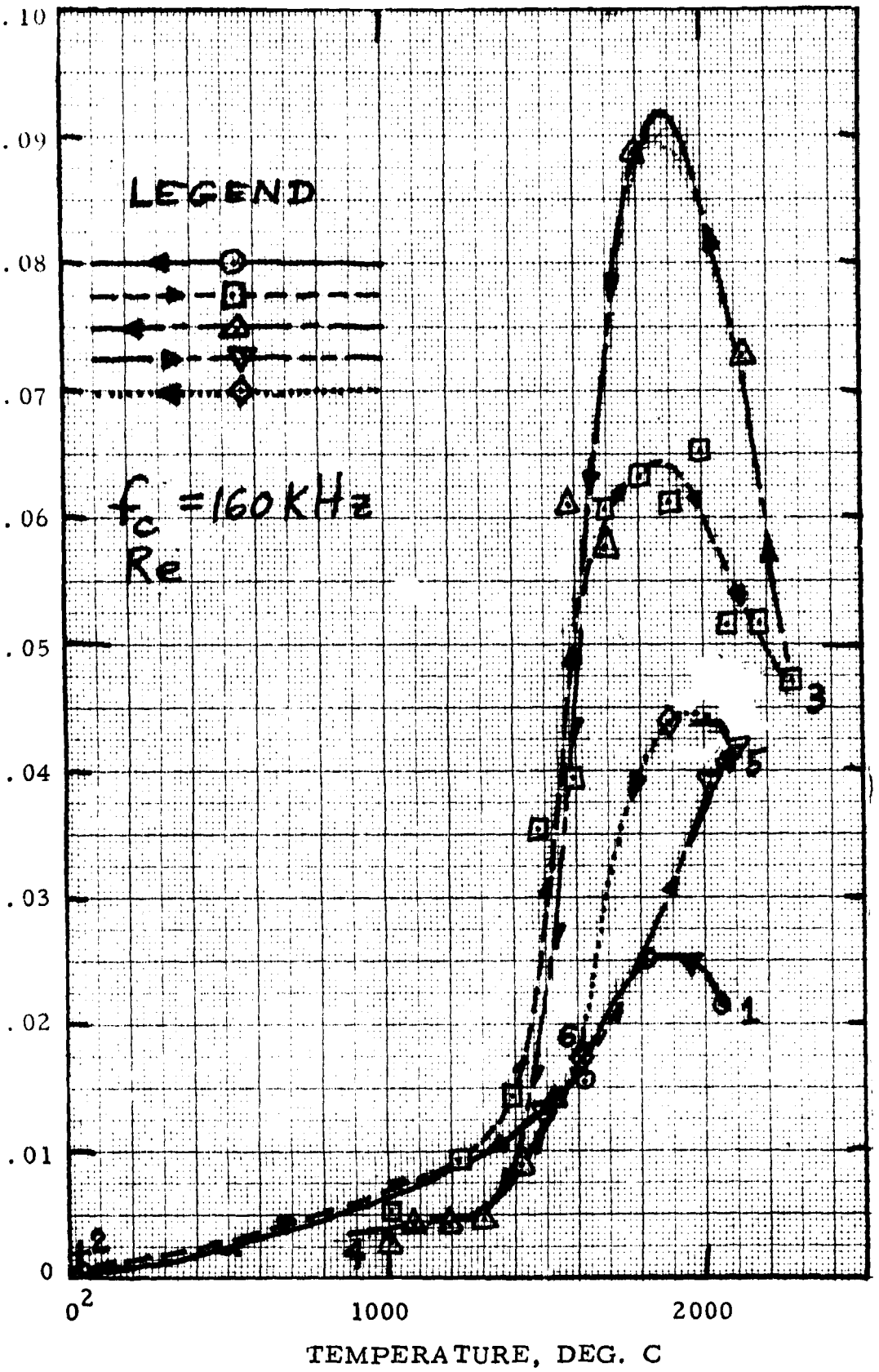

Fig. 5. Attenuation in rhenium wire cycled several times at the Englehard Industries thermocouple calibration facility.

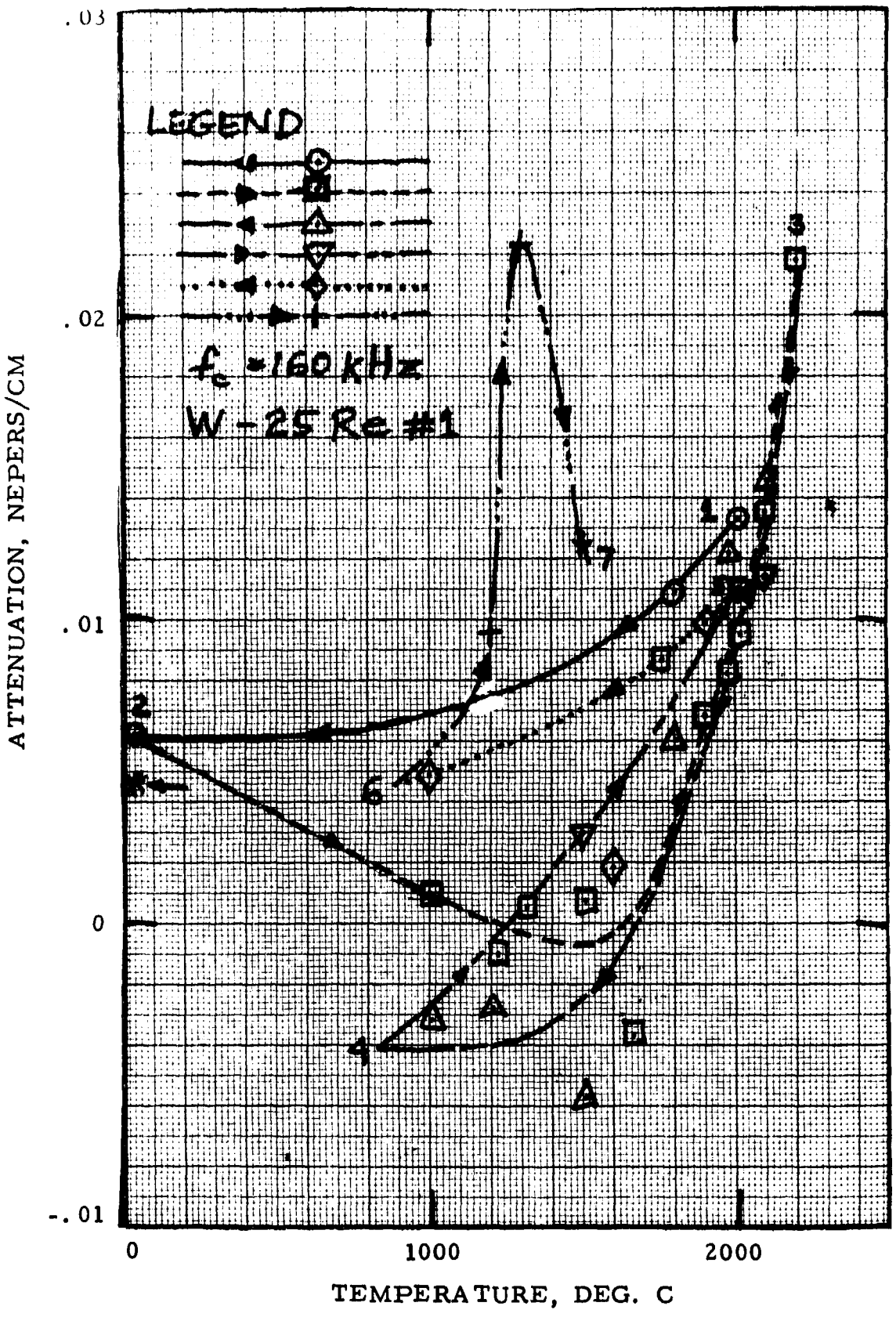

Fig. 6. Attenuation in one sample of W-25 Re wire cycled several times at the Englehard Industries thermocouple calibration facility.

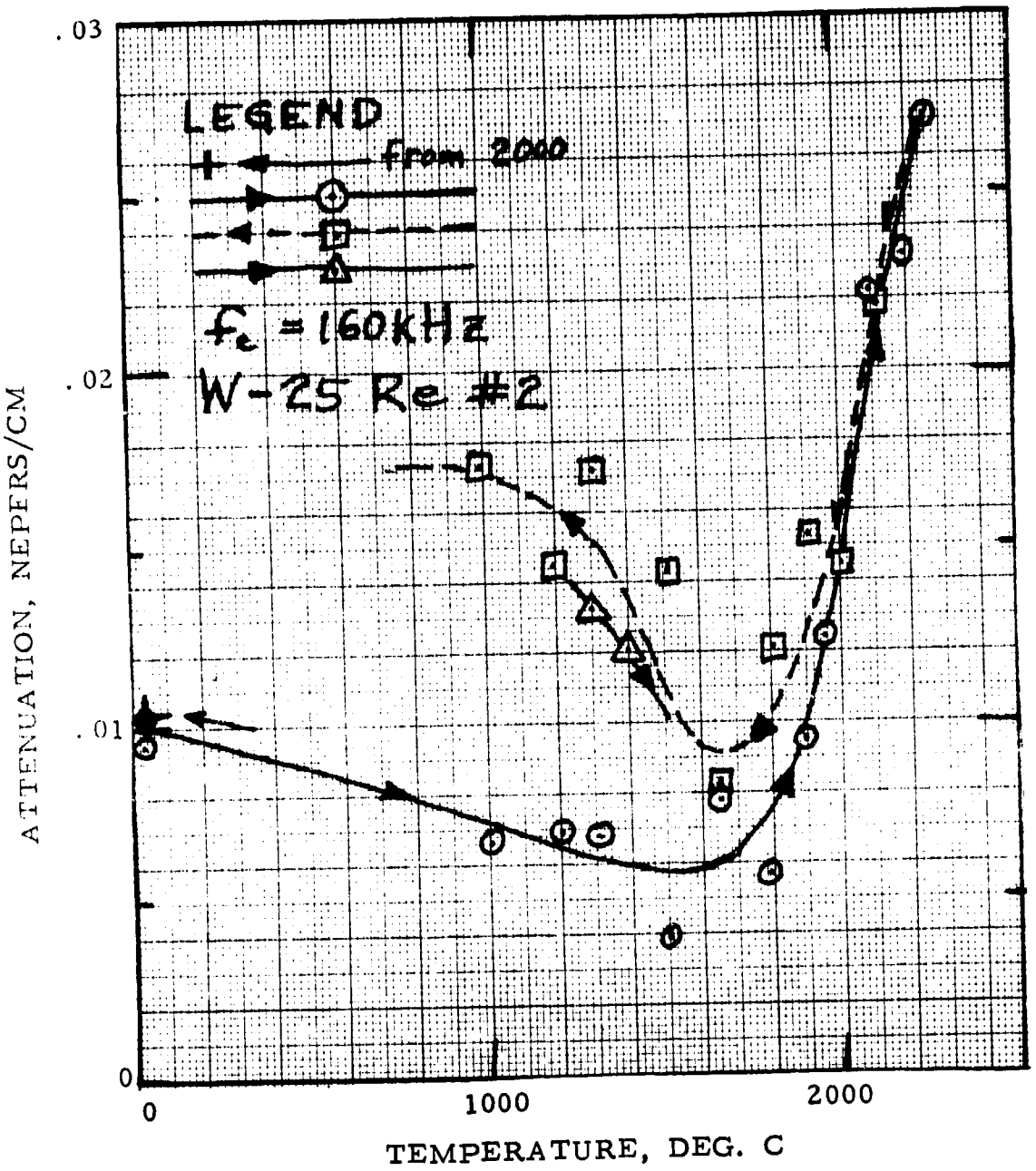

Fig. 7. Attenuation in a second W-25 Re wire sample cycled several times at the Englehard Industries thermocouple calibration facility.

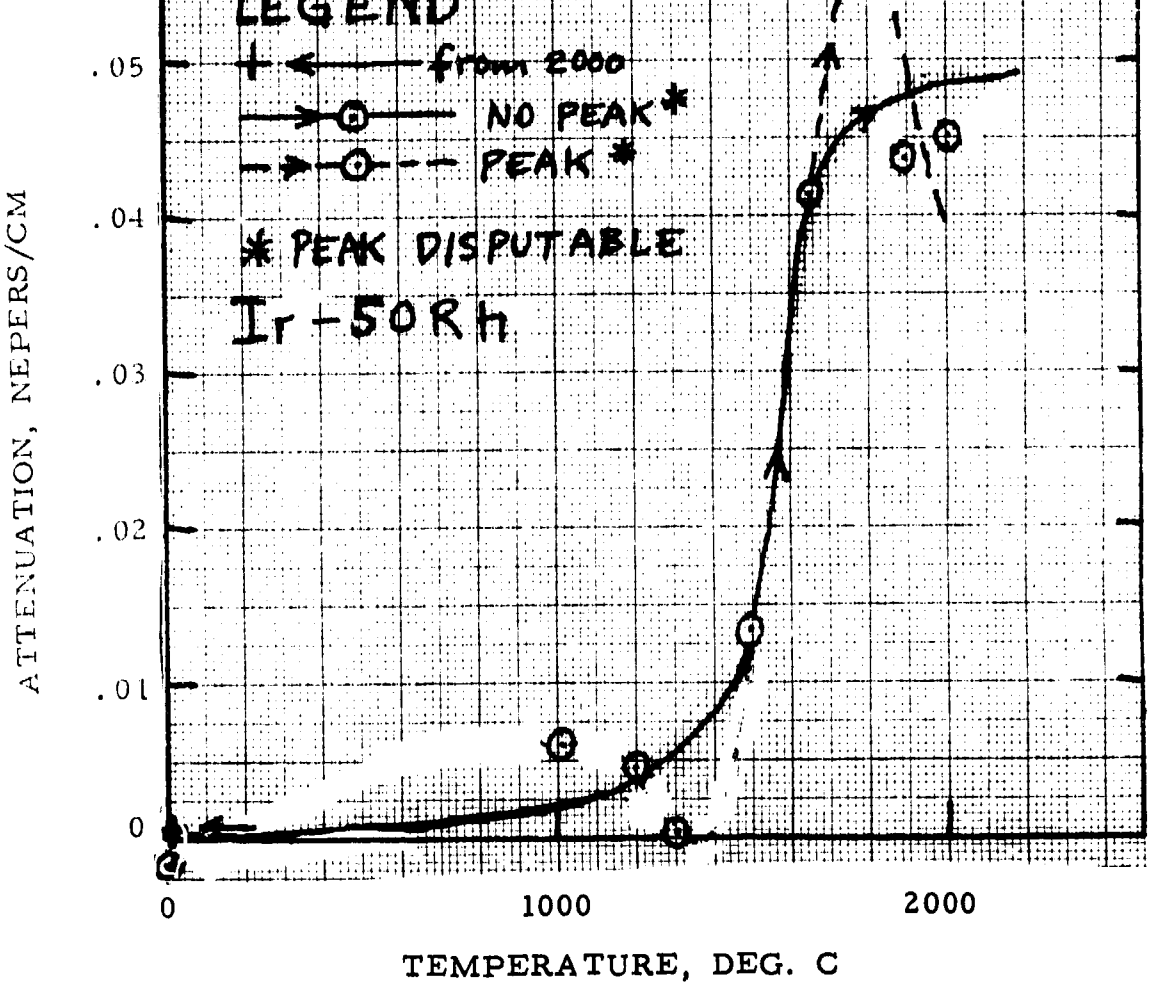

Fig. 8. Attenuation in Ir-50 Rh wire measured at the Englehard Industries thermocouple calibration facility.

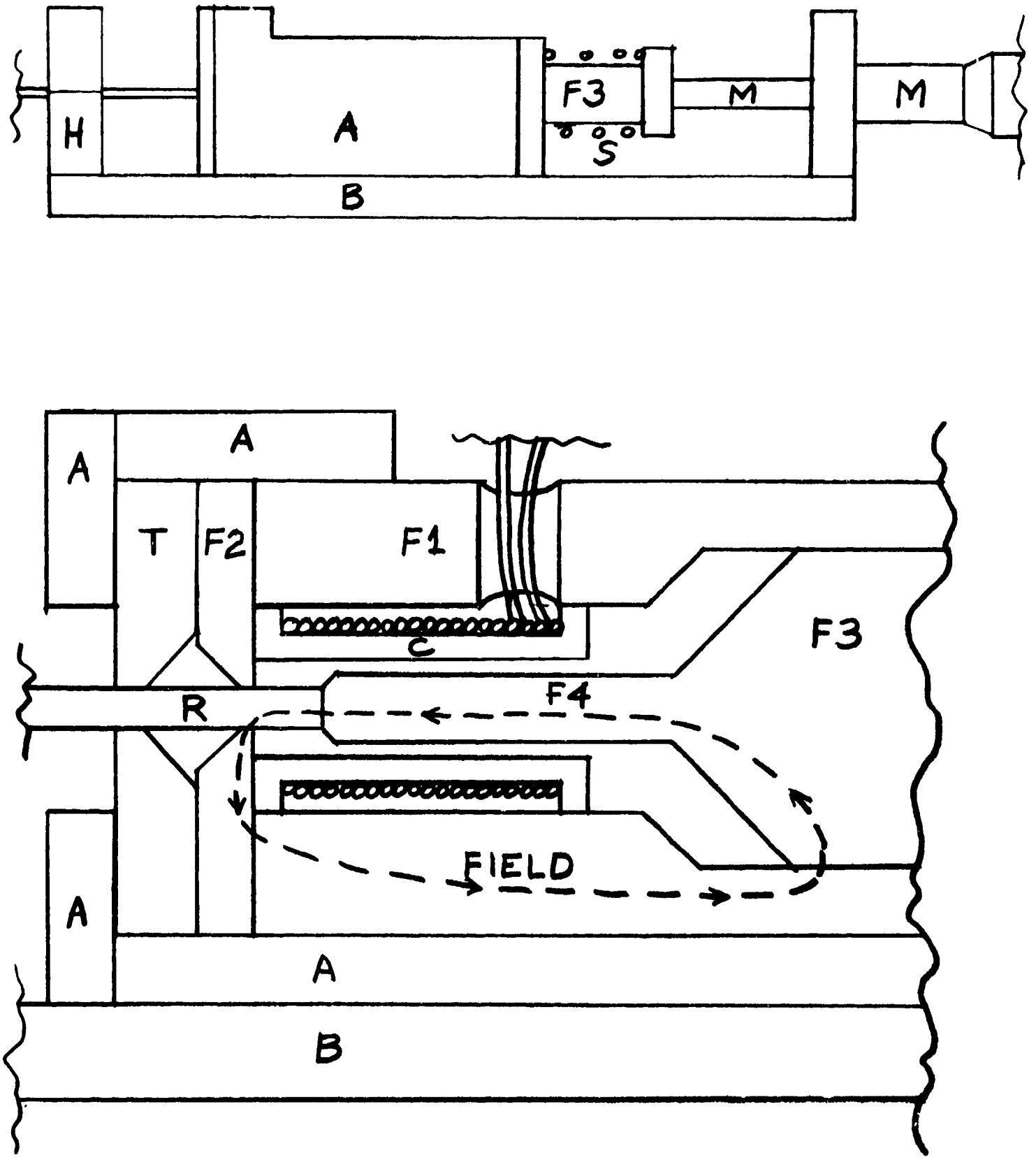

Fig. 9. Elevation and detail of ferrite core stub transducer. An aluminum holder A on a baseplate B contains a ferrite cylinder F1 with a faceplate F2 and a sliding plug F3 pushed by a micrometer M and retracted by a spring S. The end of the plug F3 is a ferrite rod F4 which touches the end of the Remendur transducer wire R passing through F2 and a Teflon bushing T. The path of the magnetic field is shown. Fringing fields penetrating far into the Remendur are minimized.

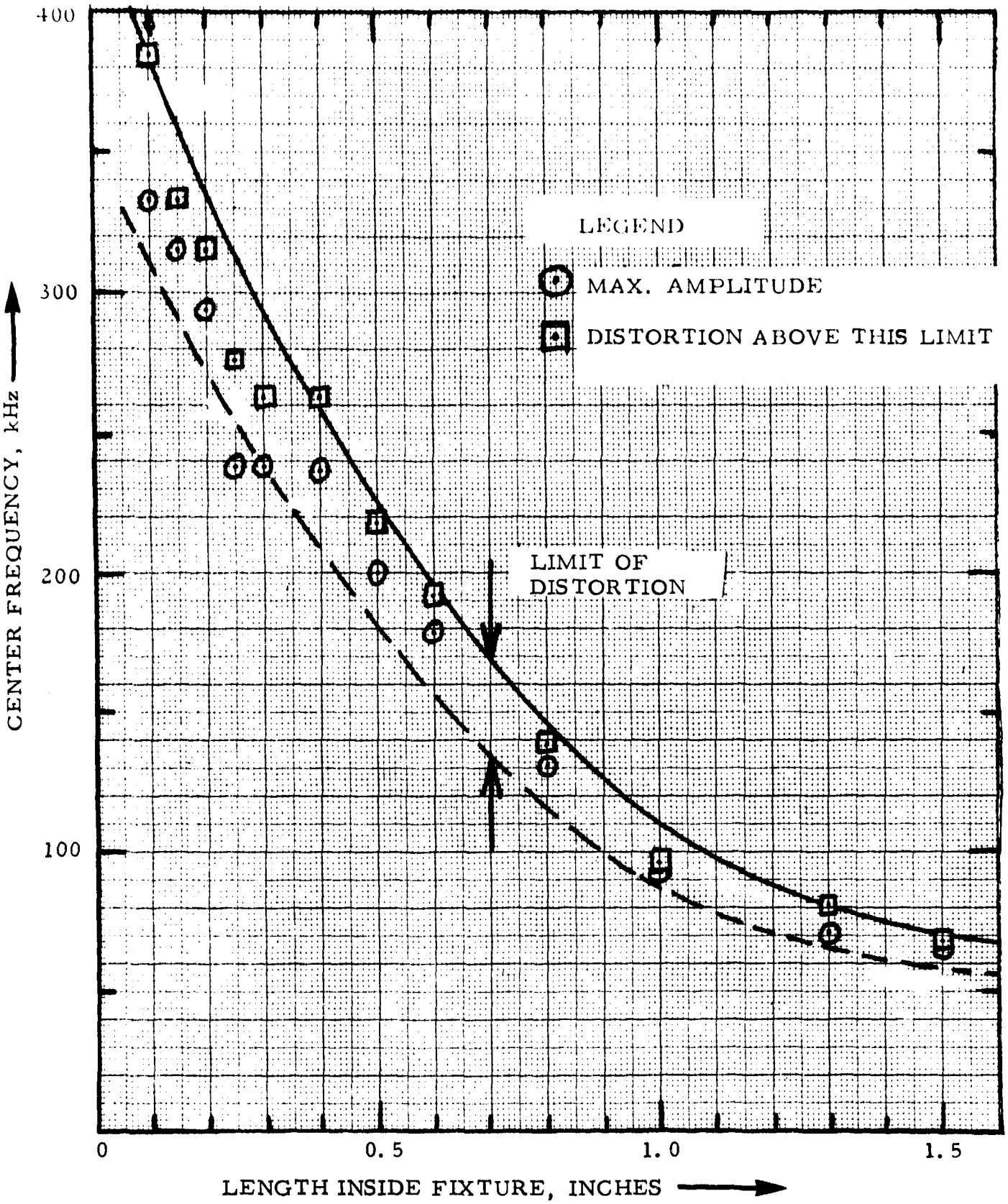

Fig. 10. Limits on center frequency of ferrite core stub transducer assembly with remendur wire extending inside fixture a given distance.

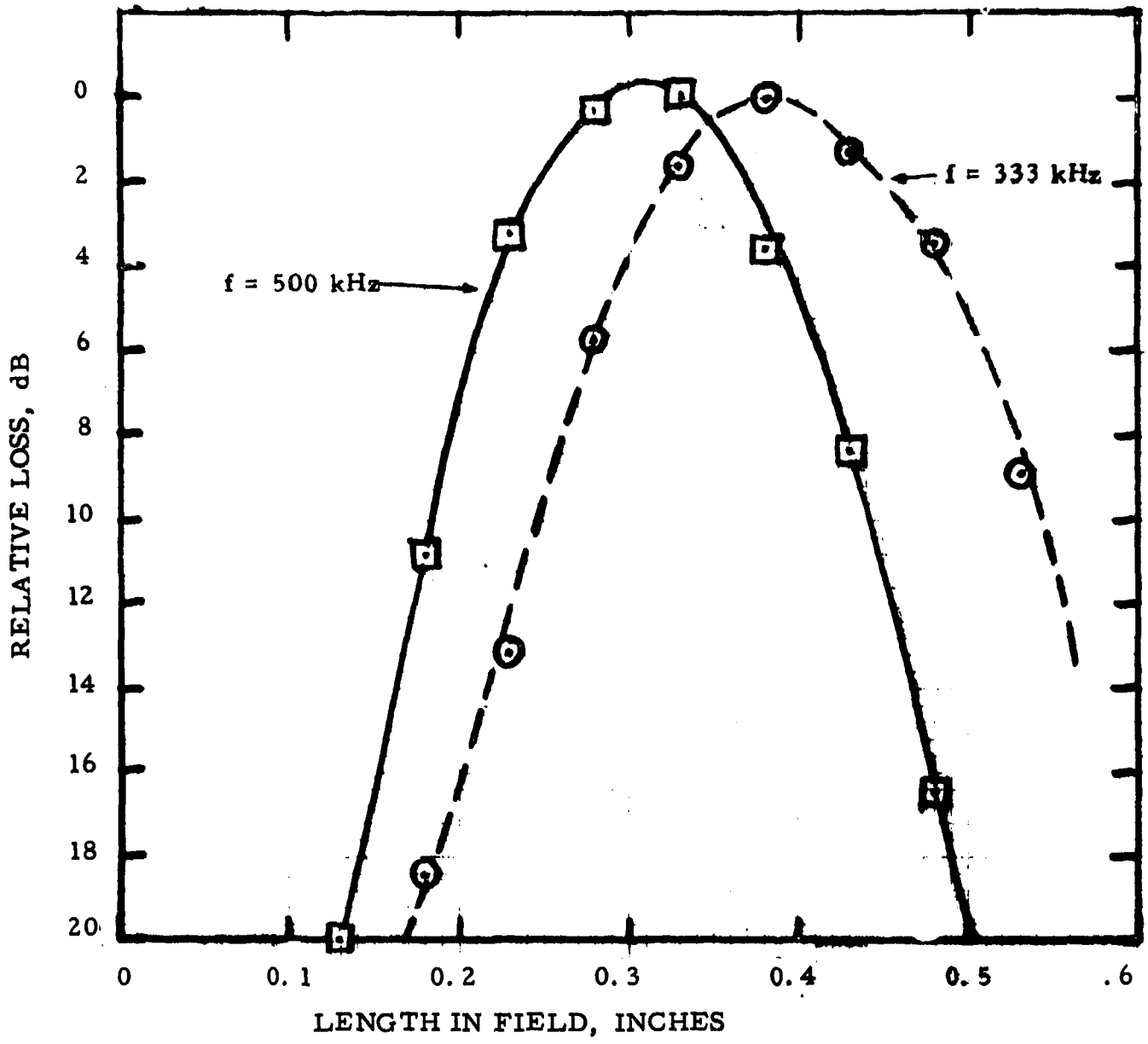

Fig. 11. Effective bandwidth of the ferrite core stub transducer assembly using remendur wire. The abscissa is plotted in the units of half-wavelength with frequency held constant instead of the usual abscissa of frequency with transducer length held constant.

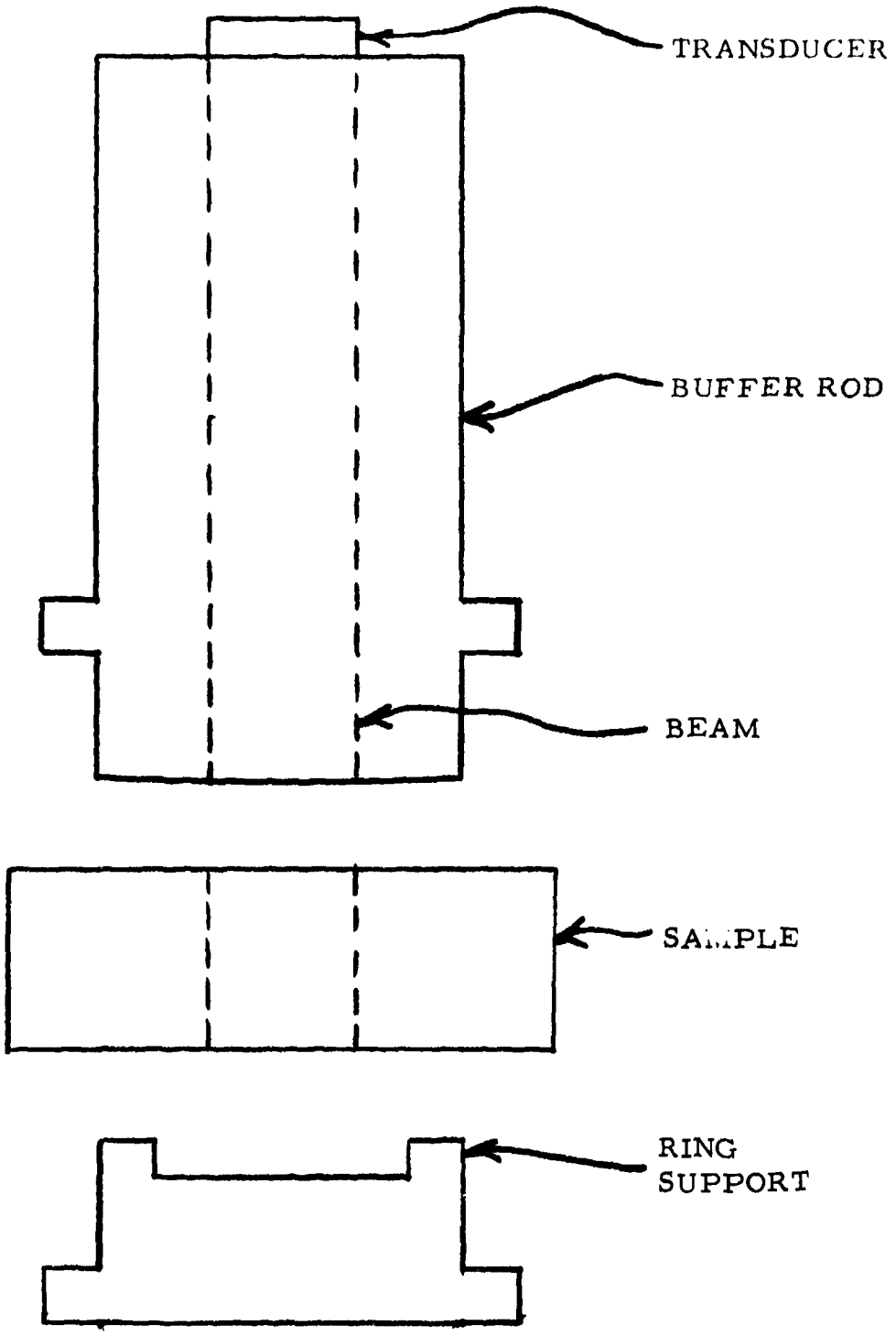

Fig. 12. Schematic representation of buffer rod system for attenuation measurements in the muffle tube vacuum furnace by the momentary contact pressure coupling method.

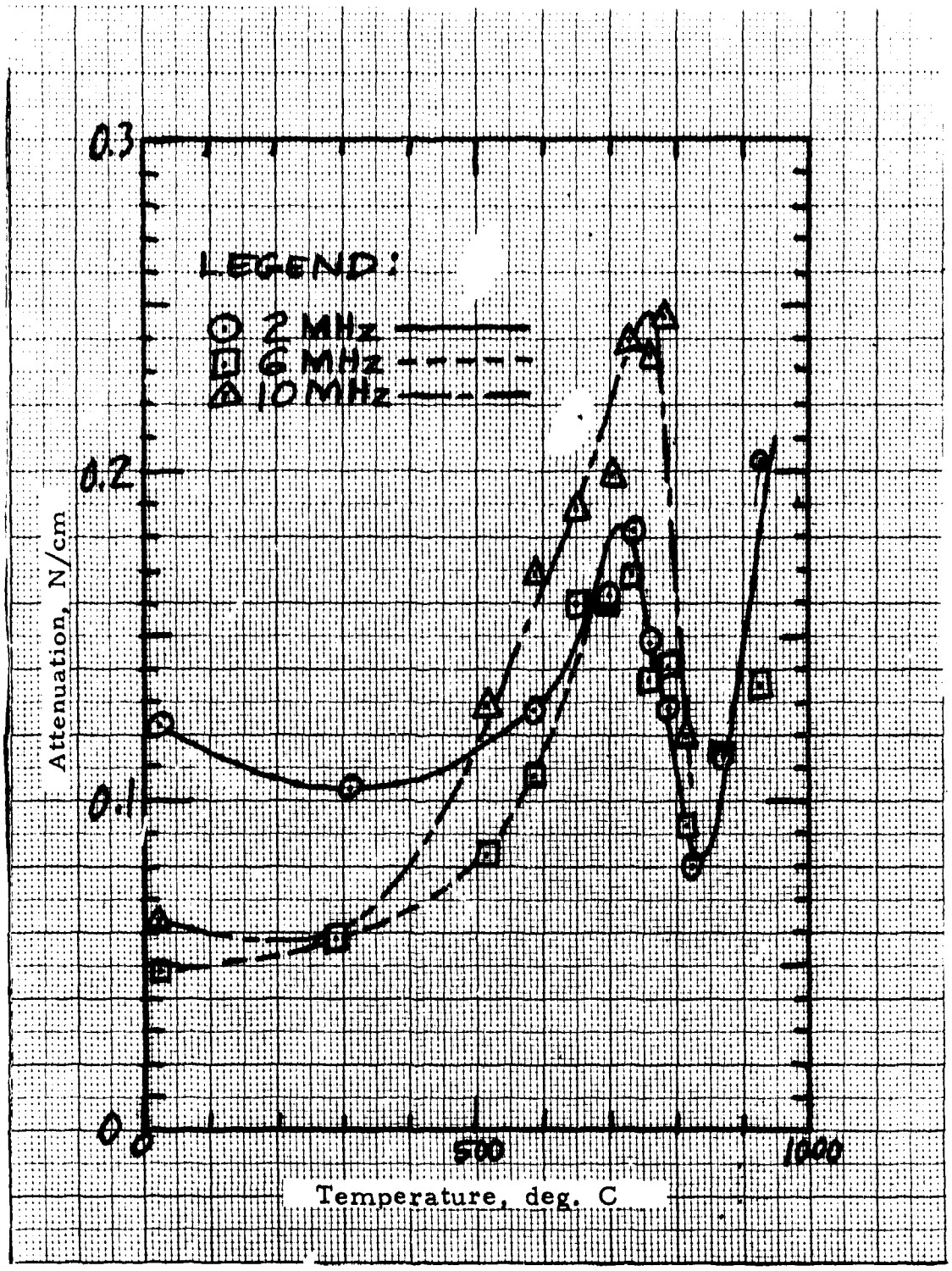

Fig. 13. The attenuation in SAE 52100 steel as measured by the momentary contact method with pressure coupling of longitudinal waves. The absorption peak due to magnetic ordering below the Curie temperature is evident.

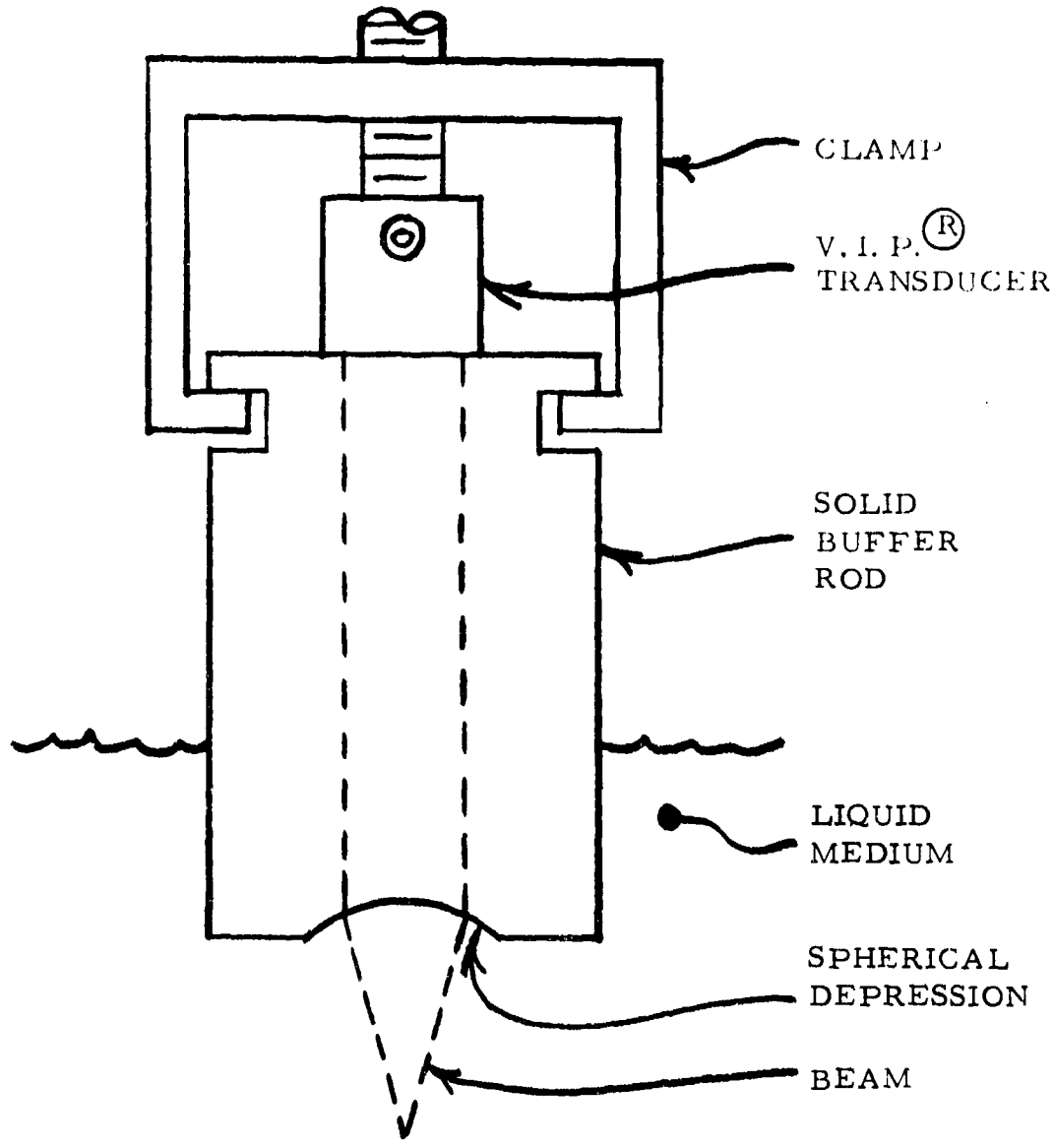

Fig. 14. Configuration of the focusing transducer built to investigate beam shapes and aberations.

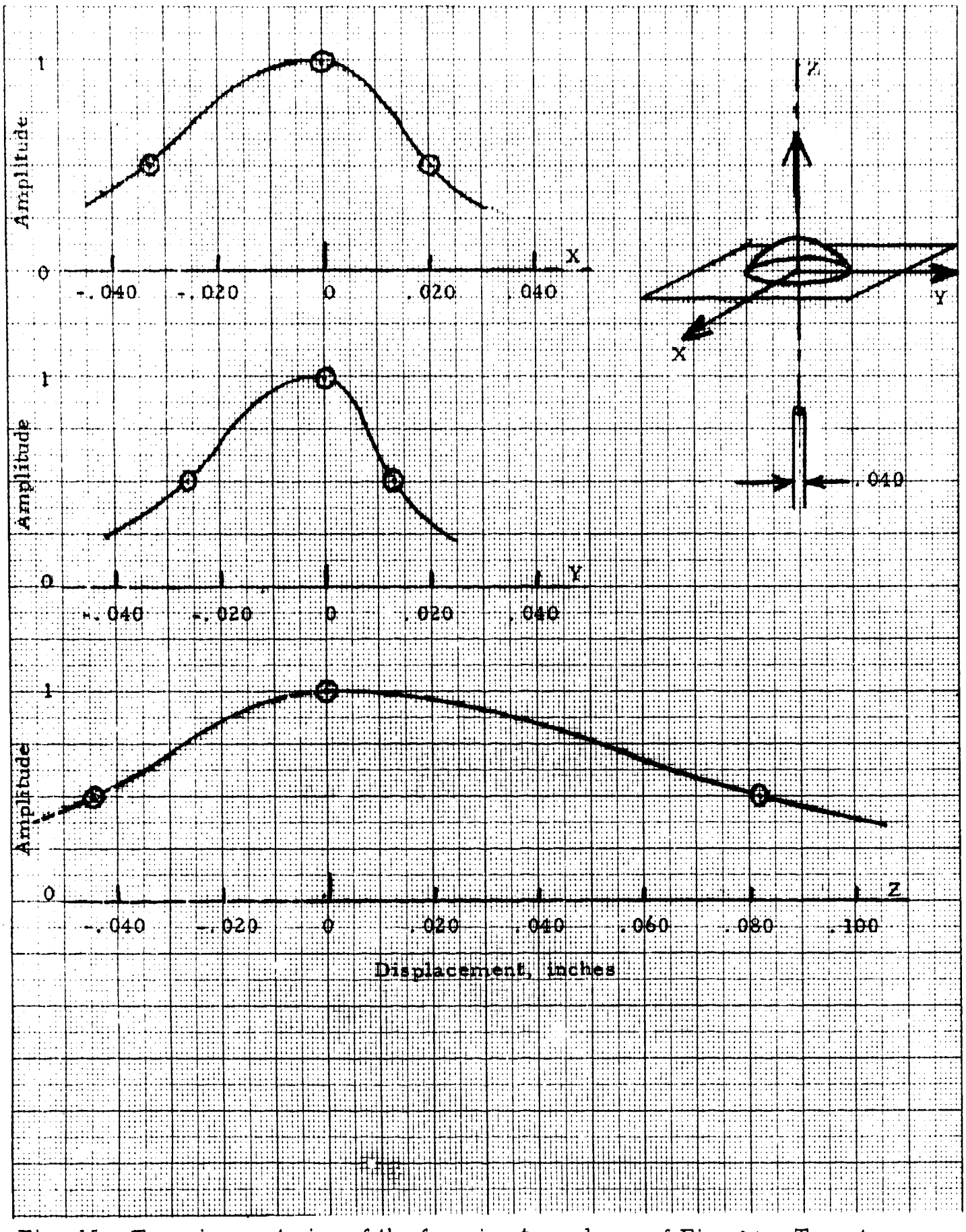

Fig. 15. Focusing spot size of the focusing transducer of Fig. 14. Target configuration also shown.

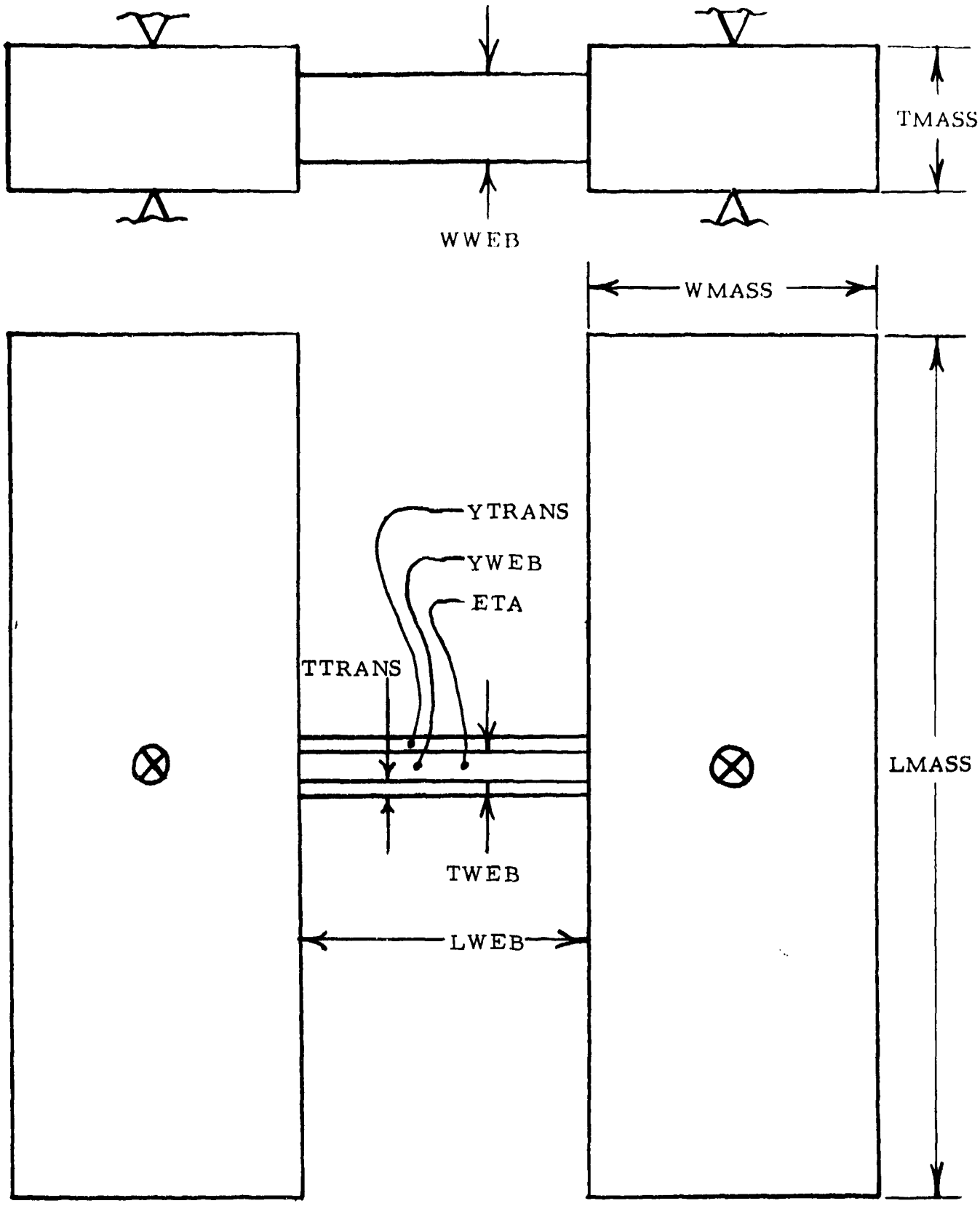

Fig. 16. Balanced resonator coniguration consisting of two pivoted end masses and a laminated elastic web. Dimensicns as well as moduli Y and damping η can be varied.

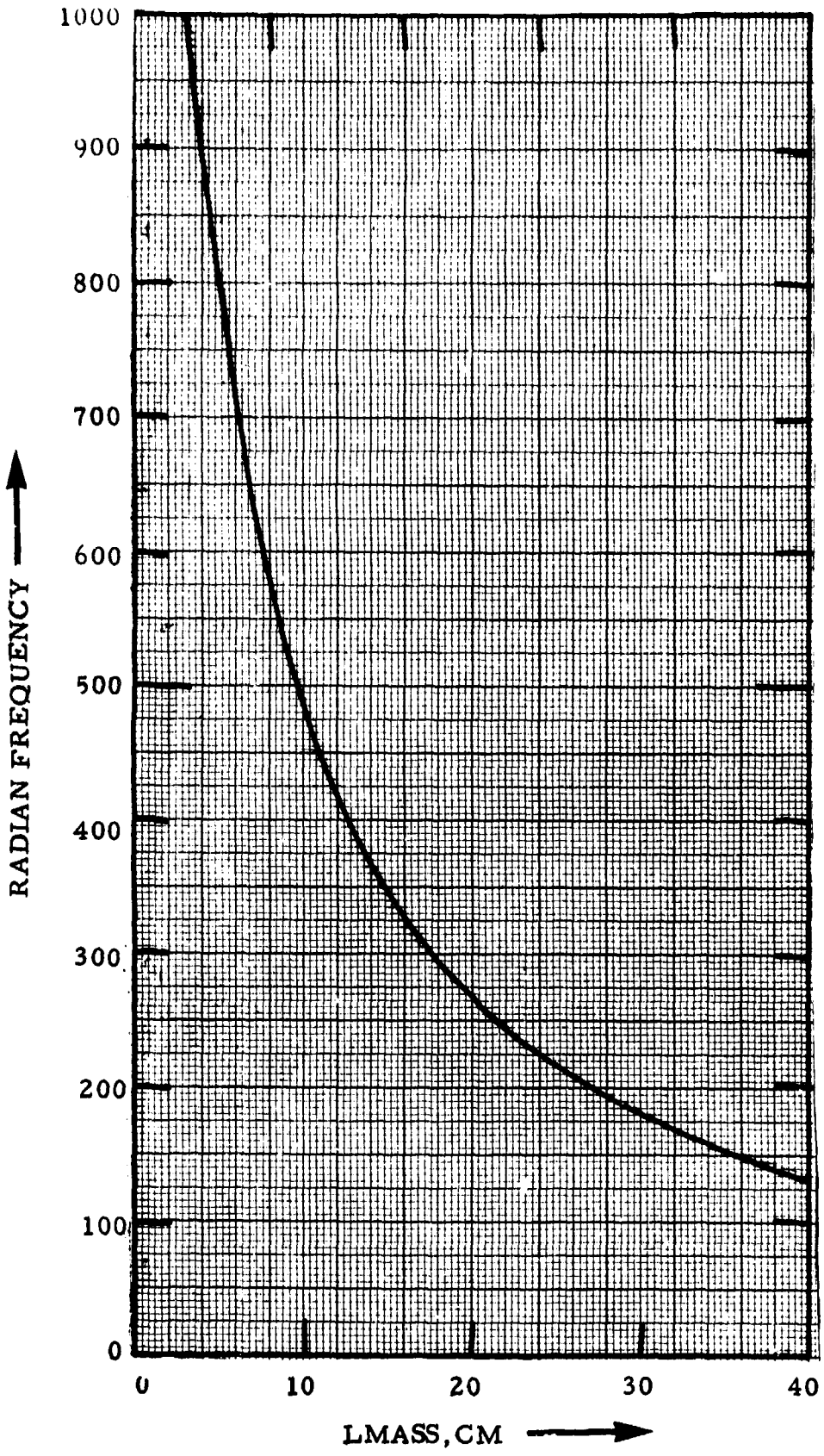

Fig. 17. Frequency of the balanced resonator versus length of the end masses with other parameters constant.

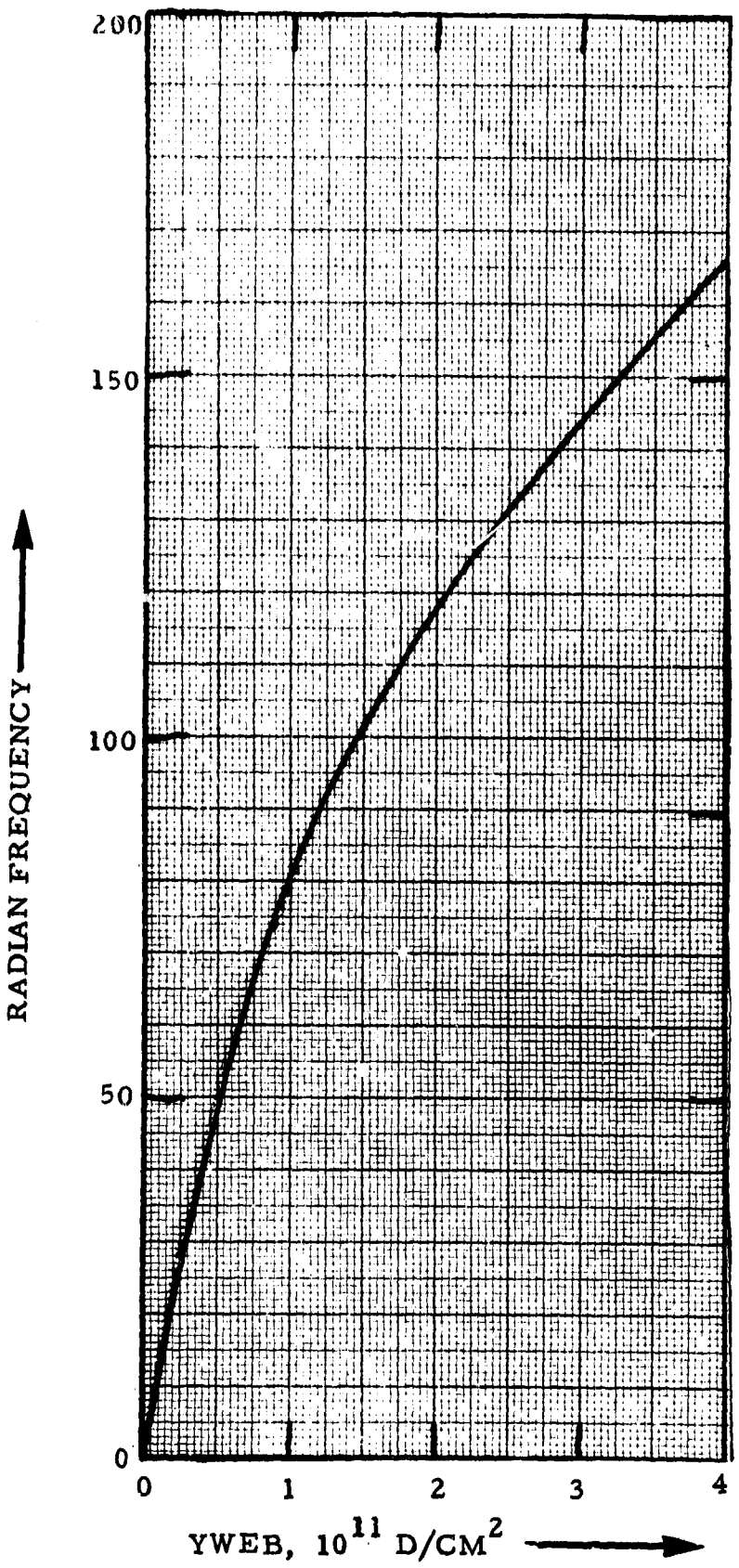

Fig. 18. Frequency of the balanced resonator versus modulus of the web with other parameters constant.

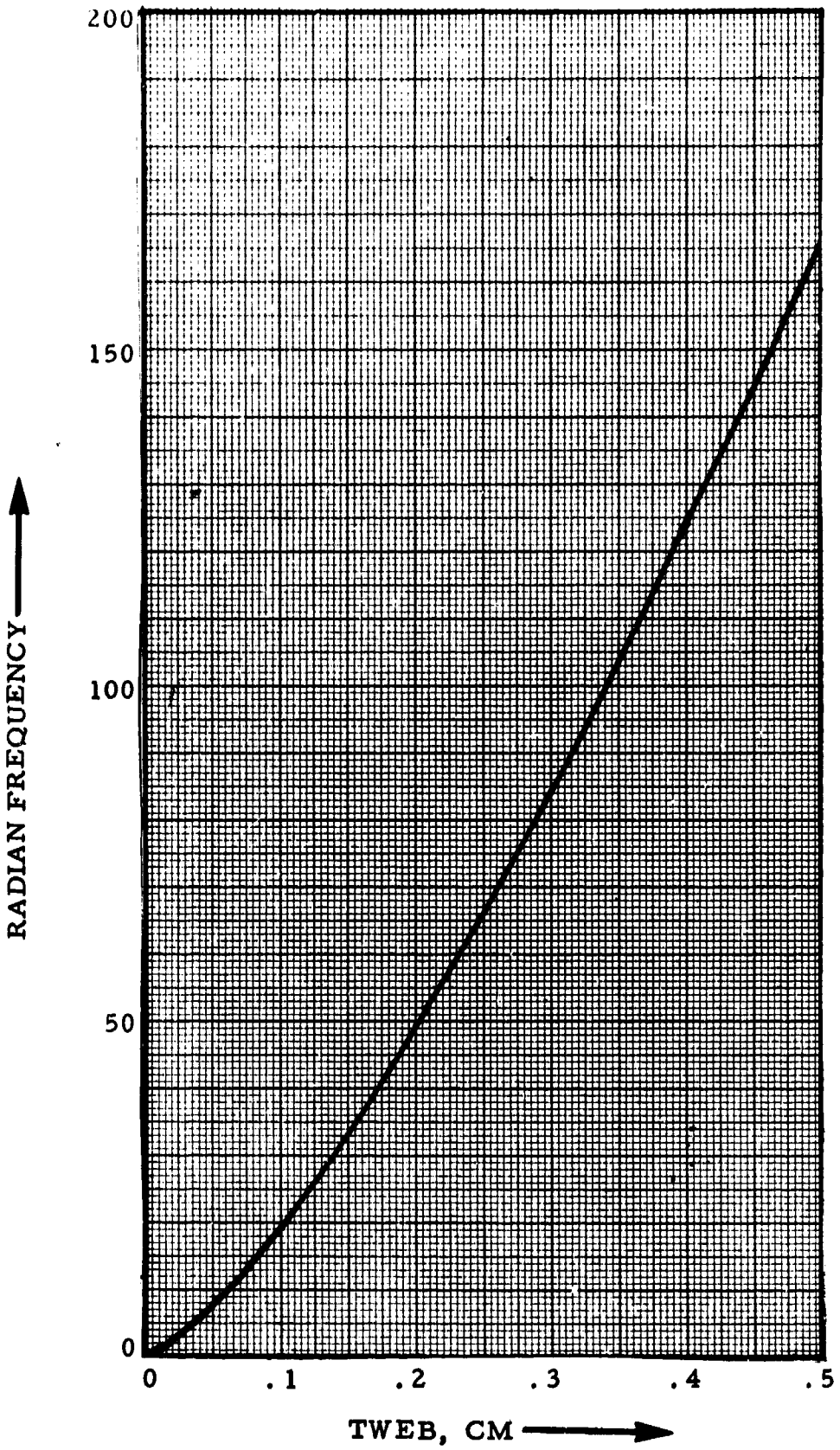

Fig. 19. Frequency of the balanced resonator versus thickness of the web with other parameters constant.

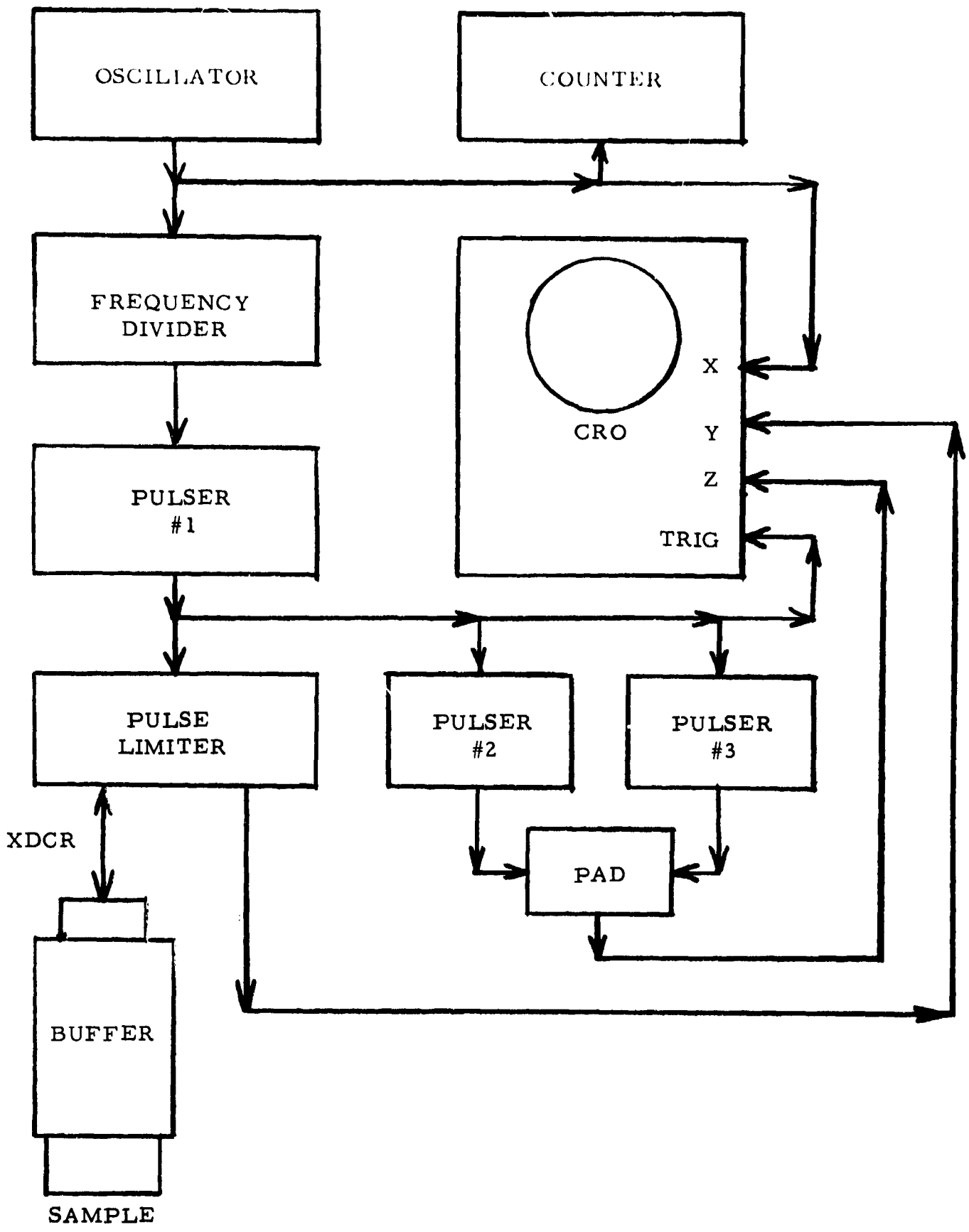

Fig. 20. Pulse-echo-overlap system built up from commercially available equipment for laboratory use.

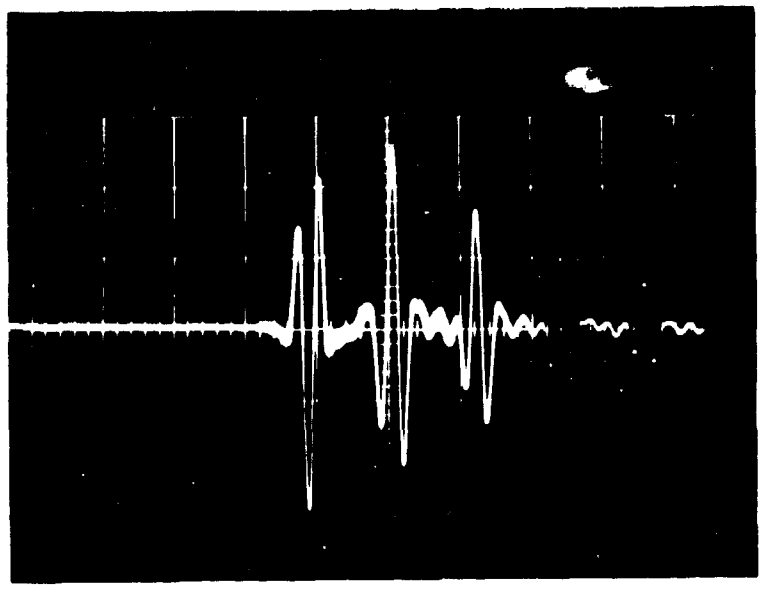

LINEAR SWEEP

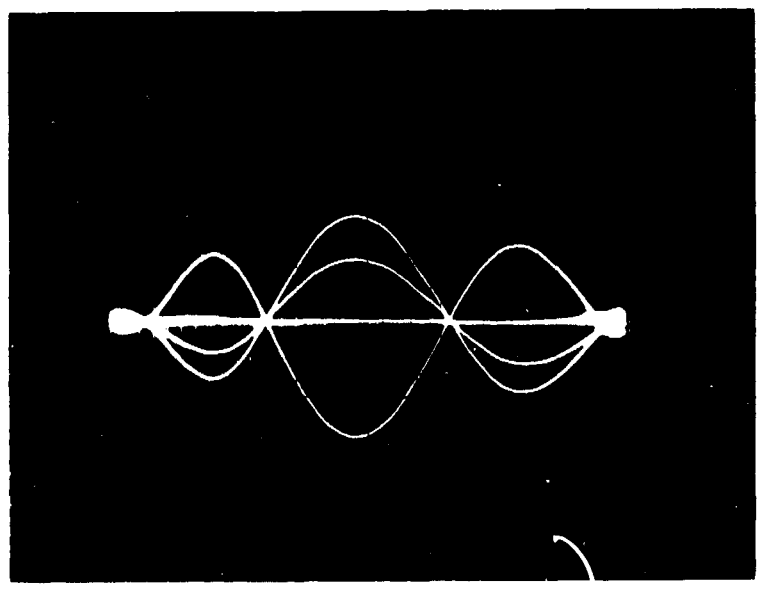

DRIVEN SWEEP

Fig. 21 Top: Three echoes intensified for the pulse-echo-overlap measurement. Bottom: These echoes overlapped by driving the x-axis of the oscilloscope with a frequency equal to the reciprocal of the travel time between echoes.

PANAMETRICS
A Subsidiary of Esterline Corporation · 221 Crescent Street · Waltham, Massachusetts 02154 · (617) 899-2719
ESTERLINE

Technical Memorandum No. 6

October 1970

Broadband Transducers: Radiation Field and Selected Applications

by

E. P. Papadakis
Head, Physical Acoustics Department

and

K. A. Fowler
Chief, Materials Evaluation Branch

Presented in part at

IEEE Ultrasonics Symposium
San Francisco, California, October 21-23, 1970

and

ASNT Fall Conference
Cleveland, Ohio, October 19-22, 1970

UR-90

ABSTRACT

In many applications broadband ultrasonic transducers capable of producing short video pulses are required. Previously, plane-wave analysis with equivalent circuits has proven successful in predicting pulse shape in the time and frequency domains. The present approach is to recognize that piston sources radiate nonplanar waves, and that the frequency spectrum of a broadband piston source can be measured experimentally. With the spectrum as a weighing function for the field profiles of a monofrequency piston source, a superposition is performed to find the pressure and phase profiles in the radiation field of a broadband transducer. Experimental measurements are presented that take advantage of the broadband pulse technique combined with spectrum analysis. These include thickness gaging of thin materials and interface layers, and relative viscosity measurements.

I. INTRODUCTION

The ultrasonic field of a piston source many wavelengths in diameter and driven with a single frequency is well-known.[1, 2] In a plane in front of the source there is a pressure profile and a phase profile. These profiles change with distance from the face of the source to infinity. In particular, along the centerline of the source there are maxima and zeroes in pressure in the Fresnel zone.[3, 4] Beyond the Fresnel zone the pressure drops to zero inversely with distance.

Although narrow band ultrasonic measurements have been widely used for many applications such as the determination of ultrasonic attenuation and velocity as functions of frequency and for ultrasonic flaw detection, there are also many applications which either require or are enhanced by broadband pulsed operation of ultrasonic transducers. These include digital storage delay lines,[5] high-resolution nondestructive flaw detection,[6] and pulse-echo spectrum analysis.[7]

In all cases, elastic pulses short in space and time must be generated, propagated, and received. Bandwidths upward of 40% are required to make the pulse duration less than two wavelengths of the center frequency of the pulse spectrum. Much work has already been published[8, 9] on the ultrasonic pulse problem. Plane wave analysis has been used in this previous work. The present paper deals with the theory of pulse propagation as a single-aperture diffraction problem, utilizing a weighted superposition of the fields of single-frequency piston sources[1, 2] at various frequencies within the band. New pressure and phase profiles are calculated for broadband operation. From these profiles, scattering factors for objects of various sizes and shapes could be calculated. Experiments utilizing broadband transducers for physical measurements and nondestructive testing by spectrum analysis are reported.

II. THEORY

If the piston source is driven by a spectrum of frequencies, the on-axis zeroes of pressure disappear and become minima. With increased bandwidth, the maxima and minima become more nearly equal, the pressure profiles smooth out, and the phase profiles vary less. Figure 1 shows the contrast between the profiles computed for a monochromatic

transducer and a broadband transducer. The latter computation will be described below. The amplitude and phase are plotted in a plane at the $Y_1^{(-)}$ point. This is defined[3] to be at the last zero along the axis in the Fresnel zone of a transducer. There, the S-parameter[1] is $S = z\lambda/a^2 = 0.5$. The pressure of the monochromatic wave has a central zero while the phase fluctuates rapidly. On the other hand, the pressure in the broadband pulse shows no zero. Such a pressure distribution would permit the detection of small flaws along the axis, while the narrow-band pulse might not detect them.

The method of obtaining the pressure and phase in the broadband pulse follows. Let the pressure of a monochromatic transducer be expressed as

$$p = C\, e^{j(\omega t - kz - \delta)} \tag{1}$$

where the phase $\omega t - kz$ for a plane wave cancels, leaving the phase δ relative to the plane wave. Then p, C, and δ are functions of S, the normalized distance along the axis of the transducer, and of x, the radial distance from the axis. They are implicitly functions of frequency f, since $S = z\lambda/a^2 = zv/a^2 f$ is a function of f. The equation for p reduces to

$$p(f) = C(f)\left[(\cos\delta(f) - j\sin\delta(f))\right] \tag{2}$$

Introducing a spectral density function B(f) for the broadband pulse,

$$dp(f) = B(f)\, C(f)\left[\cos\delta(f) - j\sin\delta(f)\right] \tag{3}$$

Integrating, one finds

$$p = \int_0^\infty BC\,(\cos\delta - j\sin\delta)\,df$$

$$= \int_0^\infty BC\cos\delta\,df - j\int_0^\infty BC\sin\delta\,df \tag{4}$$

This may be equated to

$$p = A (\cos \epsilon - j \sin \epsilon) \tag{5}$$

with

$$A \cos \epsilon = \int_0^\infty BC \cos \delta \, df = A_1$$

and (6)

$$A \sin \epsilon = \int_0^\infty BC \sin \delta \, df = A_2 .$$

This introduces a new amplitude A and an effective phase ϵ for the broadband pulse, where

$$A = (A_1^2 + A_2^2)^{1/2}$$

and (7)

$$\epsilon = \tan^{-1} (A_2/A_1) .$$

For computational purposes, the integrals were turned into summations,

$$A_1 = \sum_{n=1}^{9} B_n C_n \cos \delta_n$$

and (8)

$$A_2 = \sum_{n=1}^{9} B_n C_n \sin \delta_n .$$

For the calculation of the profiles the quantity S_c was defined to be the value of S at the center frequency f_c of the spectral distribution,

$$S_c = zv/a^2 f_c . \tag{9}$$

For any other frequency f, the equivalent value of S was

$$S = S_c f_c / f . \tag{10}$$

Since C and δ were known as functions of S and x from previous computations,[2] it was only necessary to tabulate C and δ in the approximate order for the summations. The tabulation is given in Appendix A.

The spectral density was taken from the spectrum analysis of a real echo generated and received by a broadband transducer. The spectrum is shown in Fig. 2. Since this spectrum represents two transductions, the spectral density function B(f) was taken to be the square root of this envelope. Then it was scaled for various bandwidths. See Appendix B.

A program was written to do the summations and calculate A and ϵ, the pressure and phase. This program is listed in Appendix C. In Fig. 3(a) through (h) the results for the pressure profiles are presented at various values of S_c for various pulse bandwidths. The cw monochromatic case shows zeroes on the centerline at $S_c = 0.25$ and 0.50 as predicted by theory. See Fig. 3(b) and (d). $S_c = 0.50$ is the $Y_1^{(-)}$ point. The finite bandwidths do not have zeroes. Indeed, above 80% bandwidth the field is fairly flat out to 3/4 the radius of the transducer. Complete results are in Appendix D.

Figure 4 contains a plot of the pressure profiles at various distances from a transducer of 120% bandwidth for double transduction. The pressure in the near field is relatively smooth, and no strong minima appear along the axis.

In Fig. 5, the relative pressure along the centerline is plotted with bandwidth as a parameter. These pressure amplitudes plotted here represent the relative amplitudes as a function of path and do not represent the degree of sensitivity of the transducers versus bandwidth. The ratio of the heights of the last minimum to the last maximum is seen to increase with bandwidth. This ratio, plotted in Fig. 6, is suggested as one figure of merit for broadband nondestructive testing transducers. It represents the difference in amplitude of the echoes from equal flaws at different depths, not counting attenuation effects. Note that not much more field uniformity is gained by a bandwidth above 80%.

Frequently, transducers are used for immersed testing. Then part of the path is in water and part in solid material. Figure 7 contains

plots of the amplitude along the centerline in the solid for two water paths. One might want to work in the region of increasing amplitude with distance to cancel attenuation effects in the solid.

Broadband pulses are advantageous for flaw detection because the acoustic pressure does not show any serious minima, because they are narrow in space and time (permitting high depth resolution), and because the spectrum contains information about the material interrogated or the flaw observed. Increased bandwidth is achieved at the expense of sensitivity. Provided the signal-to-noise ratio is great enough, the loss in sensitivity can be compensated for by electronic amplification.

Concerning resolution, the graph in Fig. 8 shows the predicted pulse shape of an echo from a broadband transducer with a 10 MHz piezoelectric plate. Sittig's analysis[9] was used to account for the mechanical properties of the backing and faceplate materials and for the electrical terminations. The inset in this figure is an oscillogram of an echo from a transducer built to the same specifications. The details of pulse width and relative amplitude agree exactly. The width of the first half-cycle, about 60 ns, represents a round trip through about 0.1 mm of a metal.

III. EXPERIMENTAL

A. Thickness Measurements Utilizing Broadband Transducers and Spectrum Analysis

A broadband interrogation pulse combined with spectrum analysis permits a number of interesting thickness measurements in thin materials. These measurements take advantage of "impulse-induced resonance"* effects which result when a thin material interacts with a broadband ultrasonic pulse that contains frequency components corresponding to its resonant frequency. By the selective time-domain gating of pulses reflected or transmitted by the thin material and analysis of their frequency content the thickness is readily determined.

For the case of a half-wave resonator, i.e., material bound on both sides by a material of either substantially higher or lower acoustic impedance, the thickness (t) is related to the fundamental resonant frequency (f_r) and the longitudinal wave velocity (V_L) by:

$$t = \frac{V_L}{2 f_r}$$

*K. A. Fowler, patent applied for.

The frequency f_r is determined from the spectrum of the "impulse-induced resonance" signals in a way to be shown below.

The advantages of this method of thickness measurement are that front and back surface echoes from very thin material do not have to be resolved and the percentage error in the measurement holds constant as the thickness decreases, whereas in conventional thickness gaging, the absolute magnitude of the error holds constant and the percentage error increases.

Figure 9 shows oscillograms of a broadband ultrasonic pulse in water reflected from a thick steel sample, and the frequency spectrum of that echo. Figure 10(a) shows a block diagram of the instrumentation used for making impulse induced thickness measurements. Also shown in Figs. 10(b) and (c) are the sample holder, and a schematic of the pulse-echo signal and gate timing, respectively. Figures 11(a) through (d) show impulse induced resonance signals and spectra for steel samples of several thicknesses in the range of 0.025 to 0.008 in. (0.635 to 0.203 mm).

The 0.025 in. (0.635 mm) thick sample reflects a resonance signal containing both the fundamental and second harmonic resonances. This is because both frequency components are contained, in significant amounts, in the broadband pulse. This method of measurement could be extended to thicker samples; however, it is desirable to have the fundamental resonant frequency fall in the bandwidth of the transducer in order to avoid misinterpretation of the result.

At a sample thickness of 0.015 in. (0.381 mm) the second harmonic frequency peak has disappeared because it is almost higher than the useful bandwidth of the transducer. In the thickness range of 0.015 to 0.007 in. (0.381 to 0.178 mm) only the fundamental frequencies appear. As the resonant frequency increases above 8 MHz the impulse-induced resonance amplitude decreases, reflecting the lower output of these frequencies by the transducer. A thickness of 0.007 in. (0.178 mm) corresponding to a resonance of 16.1 MHz represents the useful limit of this transducer. It is apparent, then, that with a transducer having a 30 MHz usable bandwidth steel thickness as small as 0.003 to 0.004 in. (0.076 to 0.102 mm) could be measured with considerable accuracy.

The progressive shift in resonant frequency with decreasing thickness, together with the computed "ultrasonic" thickness, is summarized in the following table. The samples used were from a standard "feeler" gage.

TABLE I

Thickness Determined by Ultrasonic Spectroscopy

Actual Thickness		Resonant Frequency	Ultrasonic Thickness	
0.025 in.	0.635 mm	4.60 MHz	0.0250 in.	0.635 mm
.020	.508	5.65	.0204	.518
.018	.457	6.50	.0177	.449
.015	.381	7.65	.0150	.381
.012	.305	9.55	.0120	.305
.010	.254	11.40	.0101	.256
.009	.229	12.65	.0091	.231
.008	.203	13.95	.0082	.208
.007	.178	16.10	.0071	.180

The thickness of intermediate layers such as adhesive or liquid layers may be measured in several ways based on the principles already described and demonstrated. The experimental setup shown in Fig. 12 was used to illustrate intermediate layer thickness measurement. The spectrum of the pulse incident on the intermediate water layer was nearly identical to that shown in Fig. 9. Spectra of the gated pulse-echo signal for four gate positions are shown in Fig. 13.

Gate position A includes the interface echo and one or two reverberations in the intermediate water layer. The spectrum shows two minima not occurring in the spectrum of the incident pulse. These minima represent the loss of energy at these frequencies due to the increased transmission coefficient of the layer at its resonant frequency. With the gate in position B, the interface echo is eliminated and the impulse-induced resonance spectrum is displayed. As in the case of the 0.025 in. (0.635 mm) thick steel both the fundamental and second harmonic frequency are included in the frequency band of the transducer. Note that the minima in the spectrum with the gate in position A correspond exactly to the maxima with the gate in position B.

Gate position C includes pulse-echo signal 2 which is the second round trip in the fused quartz. This pulse which has now undergone two reflections from the intermediate layer is even more depleted of frequency components

corresponding to the resonant frequency of the layer. Finally, the gate was positioned to include echo 3. This pulse has been transmitted by the layer to the aluminum and reflected from the bottom of the aluminum through the layer a second time to the transducer. This pulse is now relatively narrow band, rich in the fundamental and second harmonic frequency of the layer.

It is clear from the preceding and Fig. 13 that the thickness of a layer may be determined from the spectrum of a broadband pulse reflected by it or transmitted through it.

B. Relative Viscosity Measurement in Liquids

It is well known that the attenuation of ultrasound in liquids is related to the viscosity. In the classical case, the attenuation is directly proportional to the viscosity and the square of the frequency. Using a broadband transducer one may then relate the spectral content of pulse transmitted through a fixed liquid path to the viscosity of the liquid.

A demonstration of this type of measurement was made using the same transducer used in making the thickness measurements for the sheet steel samples. The water path of the sample holder in that experiment (see Fig. 10b) was used as a liquid cell. The cell was filled with liquids of various viscosities and covered with a fine ground quartz block. The spectral content of the pulse reflected from the quartz block was then analyzed.

In Fig. 14(a) through (c) the influence of viscosity on the spectrum of the reflected pulse is illustrated. The spectral output of the transducer when the liquid attenuation is negligible is shown in Fig. 9. This spectrum should be compared with those in Fig. 14. The amplitude of the spectrum display has been normalized for each liquid to clearly show the frequency dependence. There is, in addition to the frequency dependent attenuation, a substantial drop in signal amplitude as the viscosity increases.

A number of practical applications are apparent that may utilize this principle. For example, one may wish to monitor the progress or rate of polymerization of material in a vessel. In other cases, it may be necessary to know when the interface between two liquids pumped through the same pipe reach a certain point in the line. By combining accurate velocity and attenuation measurements it is possible to monitor these changes without penetrating the system. This is demonstrated in Fig. 15 which shows the spectra of pulses transmitted across identical sections of pipe containing 10% and 40% polystyrene in ethyl benzene,

respectively. The 10% solution has a viscosity of 40 cps while the 40% solution has a viscosity of 10,000 cps. The spectra, which were again brought to the same display amplitude show the higher order harmonic overtones of the pulse reverberations in the pipe wall. It will be noted that in the pulse transmitted across the pipe containing the higher viscosity liquid, the higher frequency components are missing.

In practical application it is not necessary to display the entire frequency spectrum. A narrow band receiver adjusted for an appropriate frequency peak would accomplish the objective. Ideally, both the attenuation and velocity of sound through the liquid would be measured.

C. Measurements in Attenuating Materials

Broadband ultrasonic transducers may be used to advantage for making ultrasonic measurements in highly attenuating materials.[7a] Although this subject will be dealt with more completely in a subsequent paper, the salient features will be mentioned here.

As illustrated in Fig. 14, the material transmitting the ultrasonic pulse acts as a filter. The broadband pulse permits the material to "choose" the frequencies it can transmit efficiently as long as those frequencies are significant in the output of the transducer. When the pulse is received there is no ambiguity about which cycle to use in order to make accurate velocity measurements for in most cases only one cycle is received. Further, the spectrum of the received pulse may be used to determine certain factors that may be of interest from the standpoint of quality control of such materials.

IV. SUMMARY

In summary, we have computed the pressure and phase profiles in the field of a transducer generating a broadband pulse. The results show that the pressure is free from zeroes and even sharp minima if the bandwidth is wide enough. We have also computed the pulse shape to be expected from transducers of various damped configurations. These transducers are useful because of the uniformity of their pressure fields, the short duration of their pulses, and the information-carrying capability of their broad spectral content. Experiments have been presented that demonstrate the utility of broadband pulse techniques for physical measurements.

V. ACKNOWLEDGMENTS

The authors are indebted to R. E. Fisher for fabricating the broadband transducers used in this study, and to R. E. Fisher and J. E. Bradshaw for performing many necessary measurements. Conversations with E. K. Sittig of Bell Telephone Laboratories, O. R. Gericke of AMMRC, and S. Lees of the Forsyth Dental Center provided encouragement and useful information. This work was supported in part by the Office of Naval Research.

REFERENCES

1. H. Seki, A. Granato and R. Truell, J. Acoust. Soc. Am. 28, 230-238 (1956).

2. E. P. Papadakis, J. Acoust. Soc. Am. 40, 863-876 (1966).

3. R. C. McMasters, Nondestructive Testing Handbook, Vol. II, Ronald Press Co., N. Y., 1959, Sect. 44, pp. 12-19.

4. W. P. Mason, Physical Acoustics and the Properties of Solids, D. Van Nostrand Co., Inc., Princeton, N. J., 1958, p. 96.

5. J. H. Eveleth, Proc. IEEE 53 (10), 1406-1428 (1965).

6. (a) R. C. McMasters, op. cit., sect. 43, p. 5.

   (b) S. Lees and F. E. Barber, Science 161, 477-478 (1968).

7. (a) O. R. Gericke, Matl. Res. & Stds. 5, 23-30 (1965).

   (b) O. R. Gericke, J. Metals 18, 932-937 (1966).

8. (a) V. E. Ivanov, L. G. Merkulov and L. A. Yakovlev, Zavodskaya Laborotoriya 28, 1459-1464 (1962).

   (b) M. Redwood, Appl. Matl. Res. 2, 76-84 (1963).

   (c) G. Kossoff, Trans. IEEE SU-13, 20-30 (1966).

9. (a) E. K. Sittig, Trans. IEEE SU-14, 167-174 (1967).

   (b) E. K. Sittig, Trans. IEEE SU-16, 2-10 (1969).

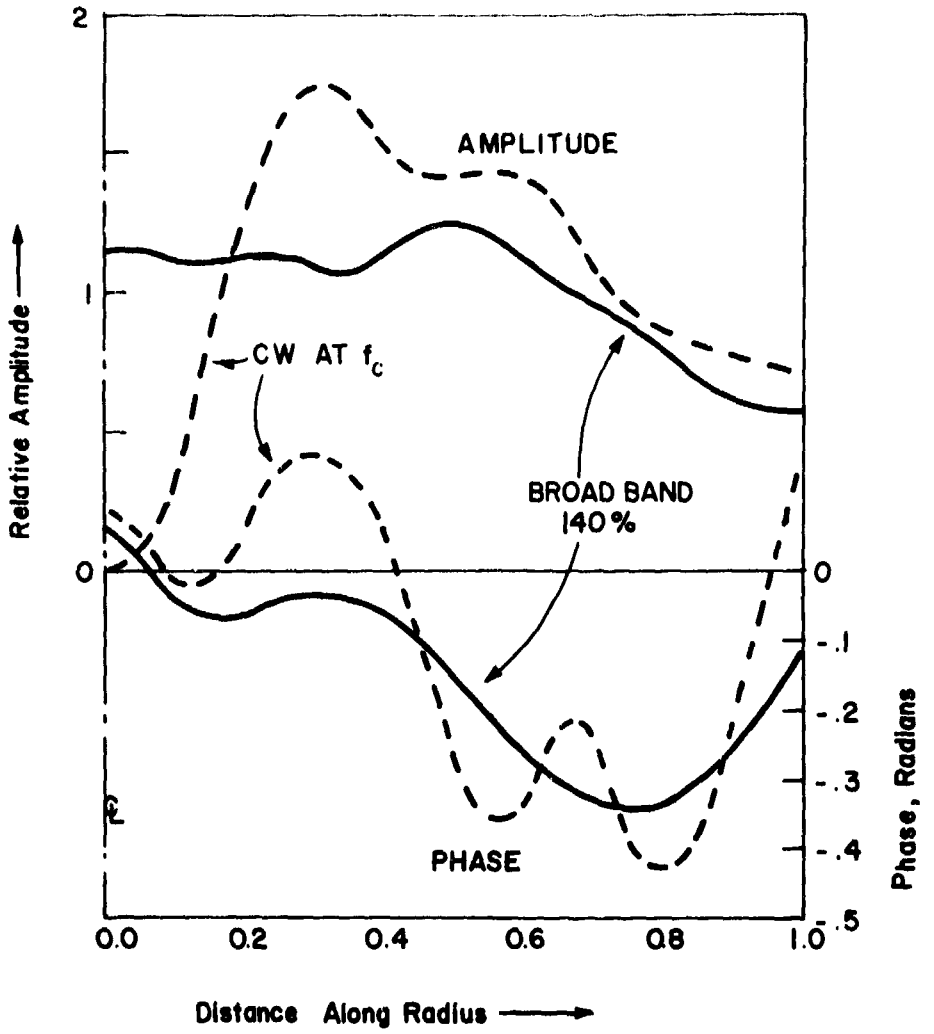

Fig. 1. Pressure and phase profiles at the $Y_1^{(-)}$ point ($S_c = 0.5$) for a broadband pulse and a monochromatic burst compared.

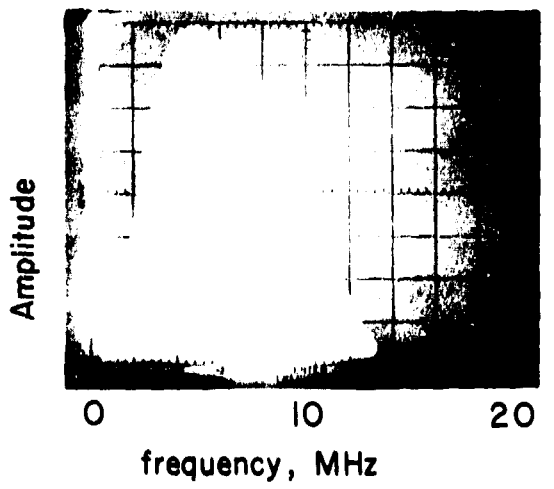

Fig. 2. Spectrum of a broadband echo used to determine the spectral density function for the computations.

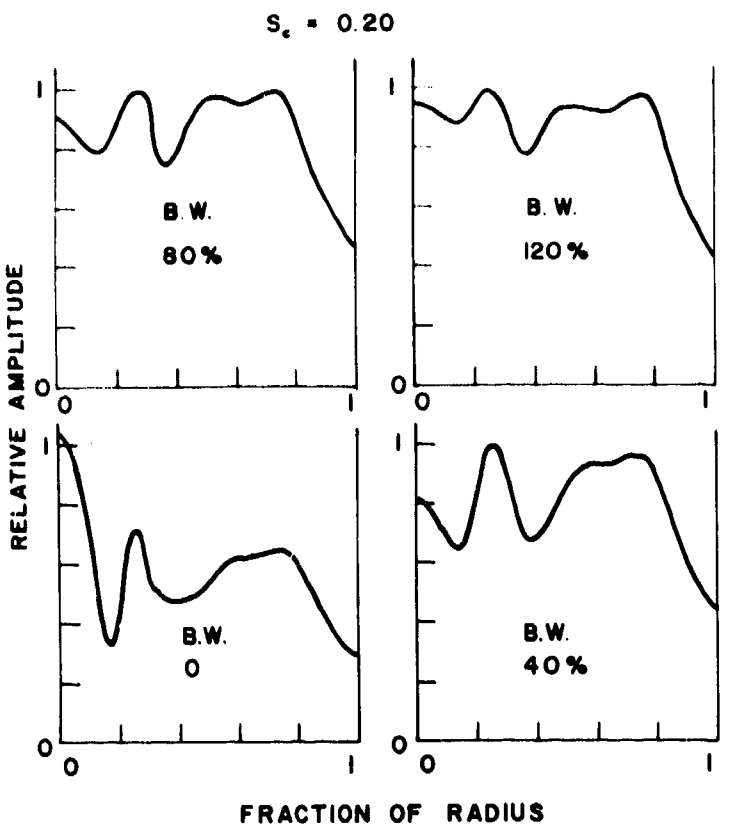

Fig. 3(a)

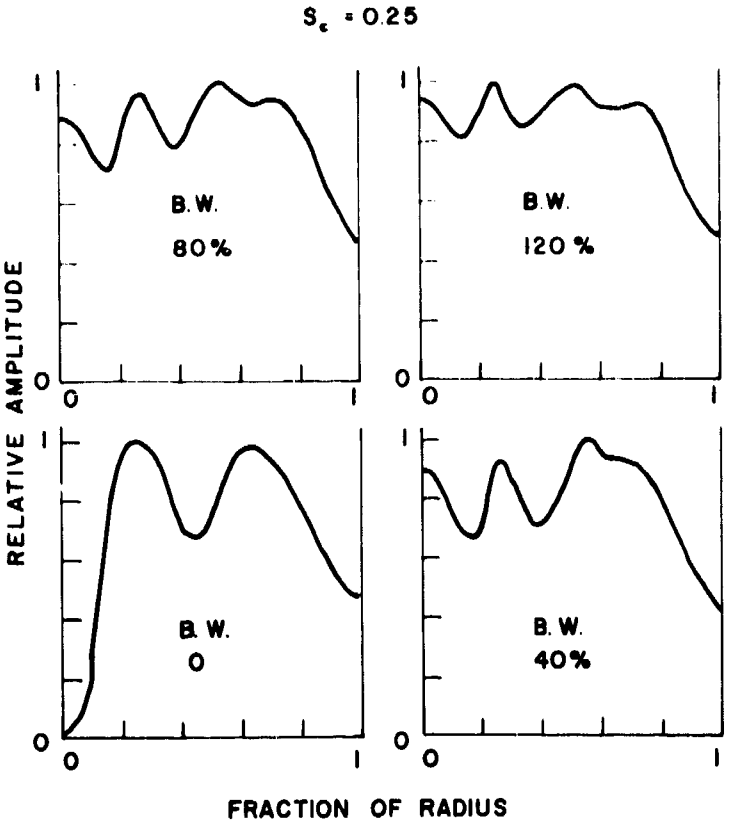

Fig. 3(b)

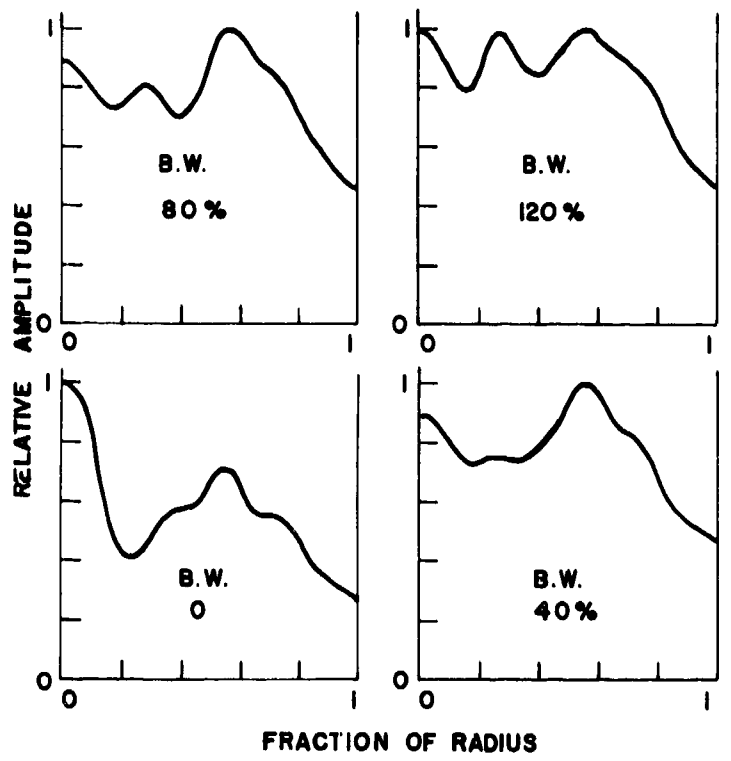

Fig. 3(c)

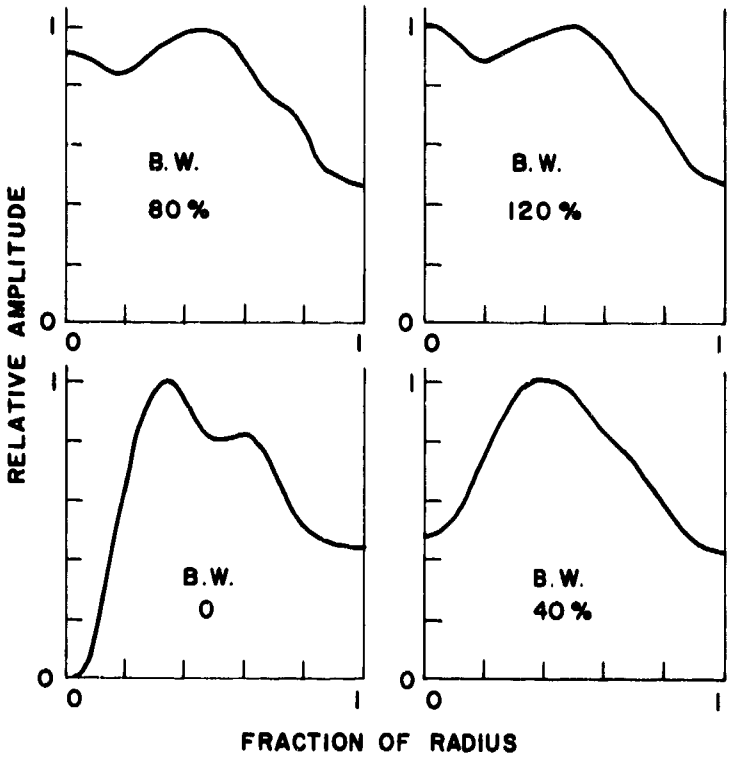

Fig. 3(d)

Fig. 3. Pressure profiles for various bandwidths at several values of S_c.

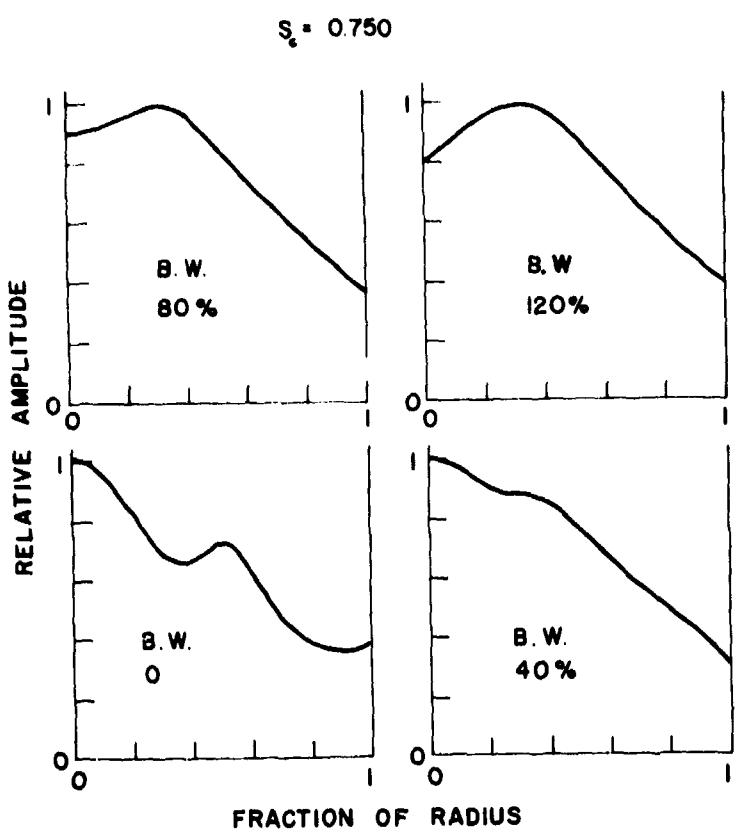

Fig. 3(e)

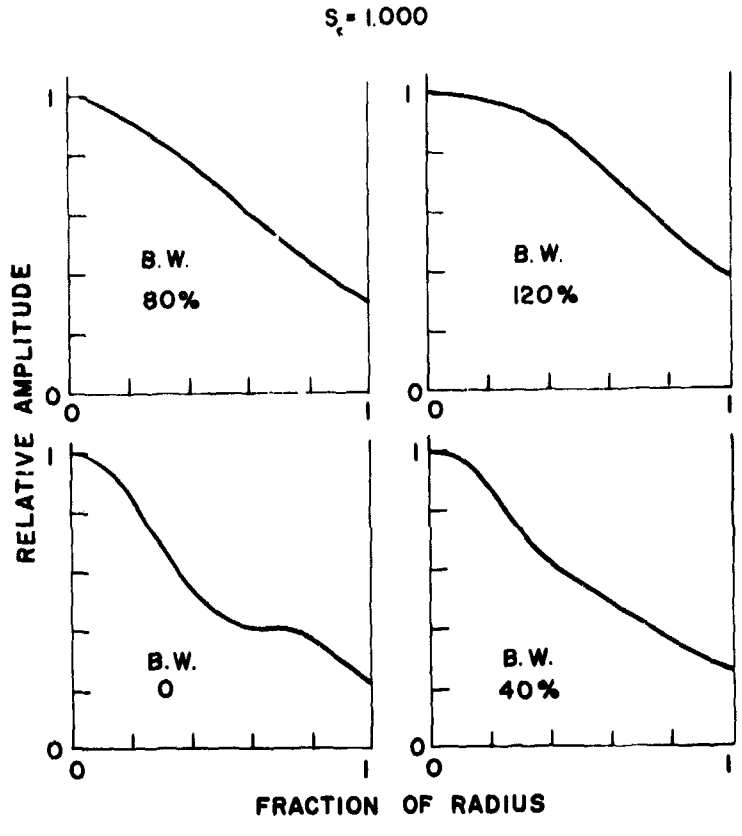

Fig. 3(f)

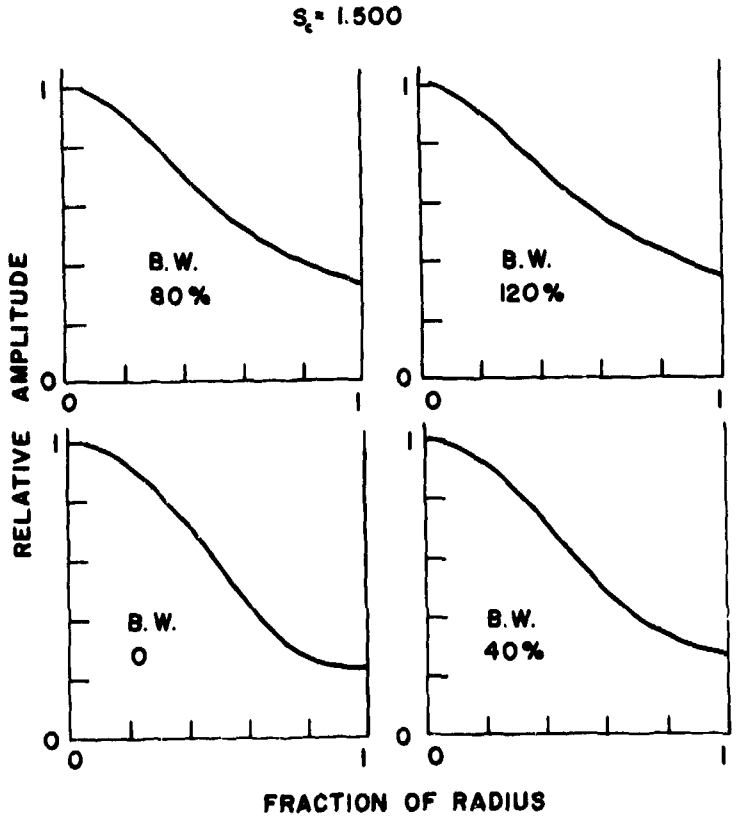

Fig. 3(g)

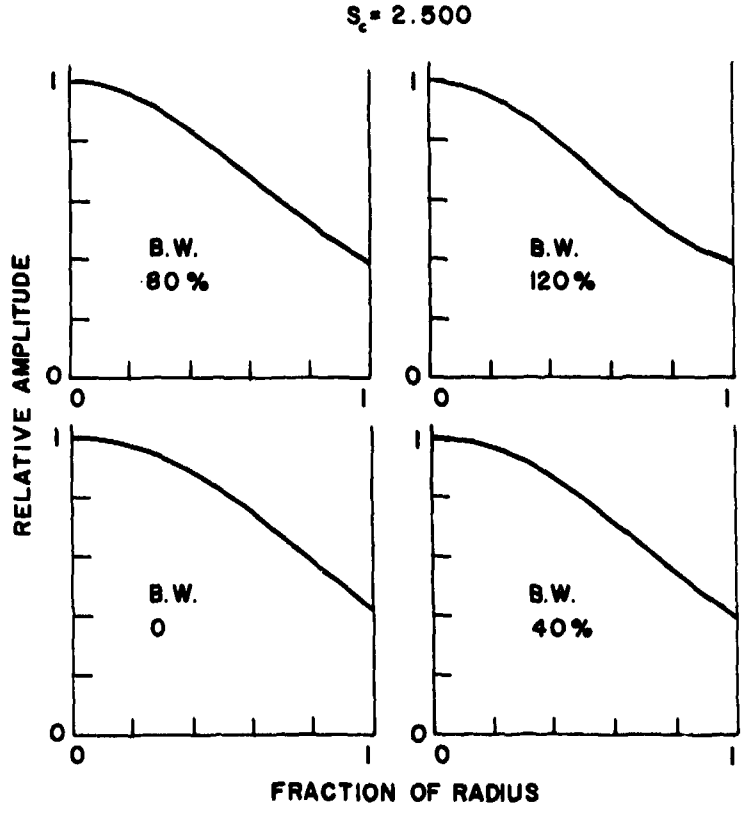

Fig. 3(h)

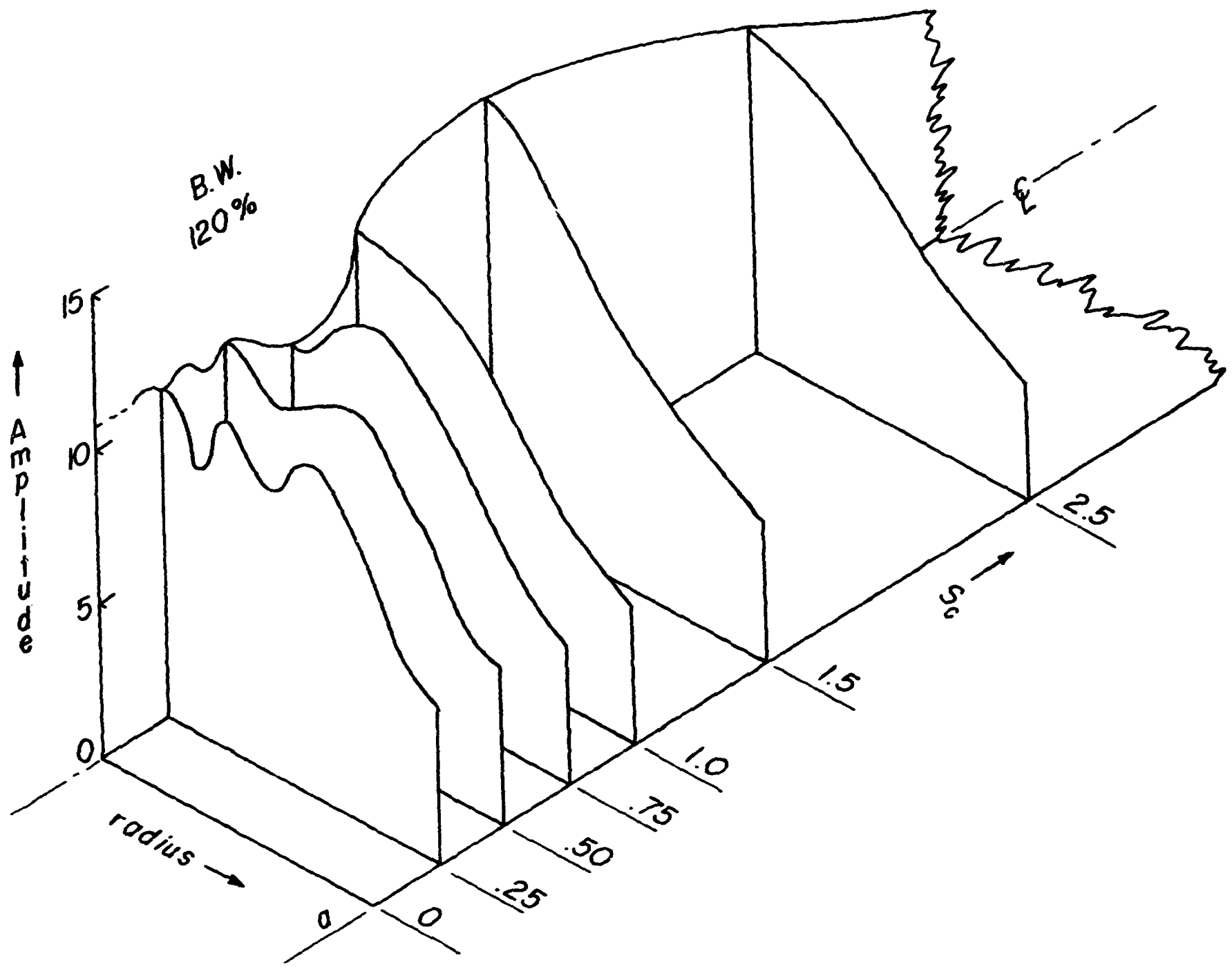

Fig. 4. Pressure profile contour map for the field of a transducer with 120% bandwidth.

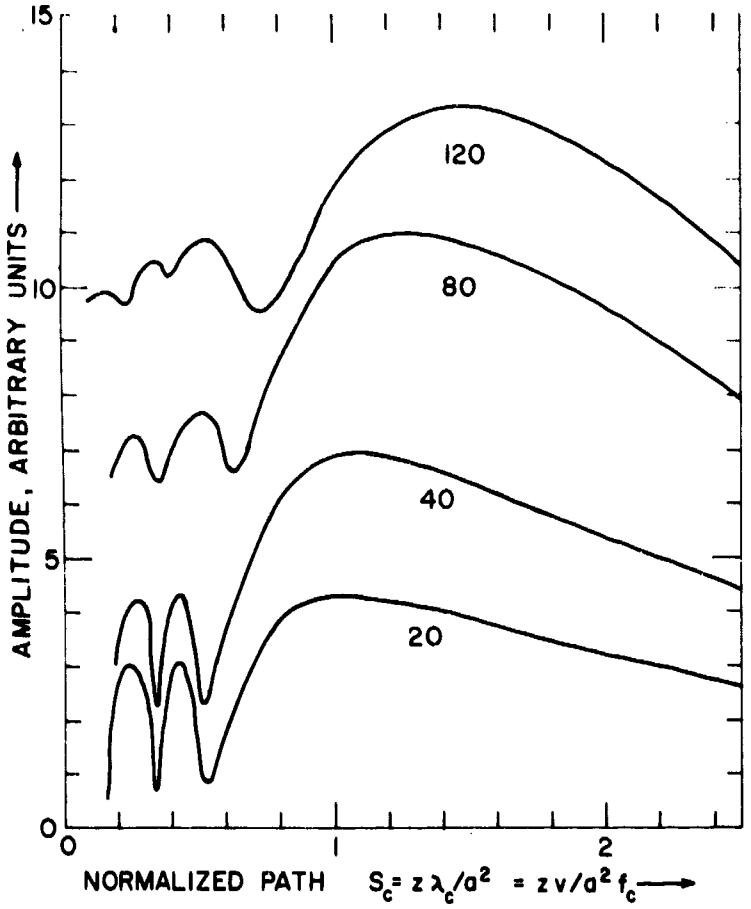

Fig. 5. Centerline pressure of the transducer field for various bandwidths.

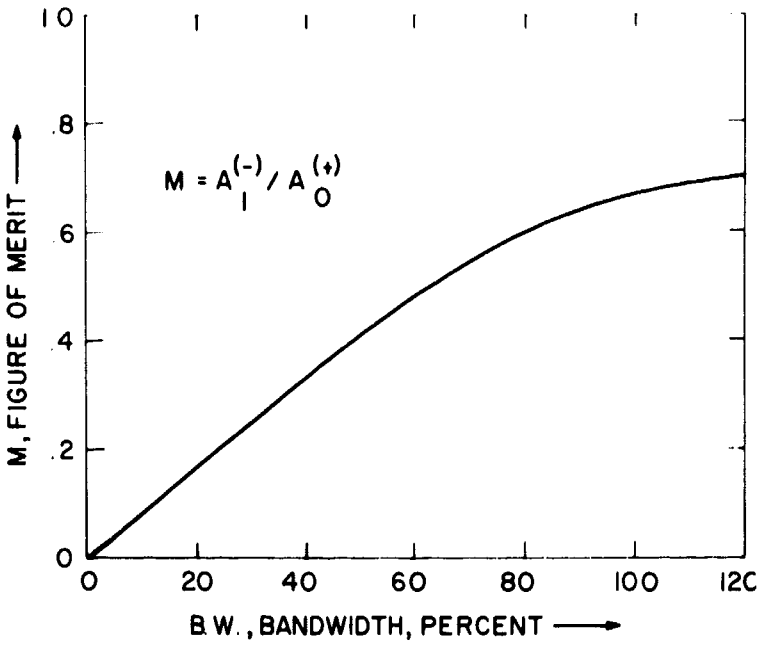

Fig. 6. Ratio of the depth of the $A_1^{(-)}$ minimum to the $A_0^{(+)}$ maximum centerline pressure as a function of bandwidth. This ratio is proposed as a figure of merit for NDT broadband transducers.

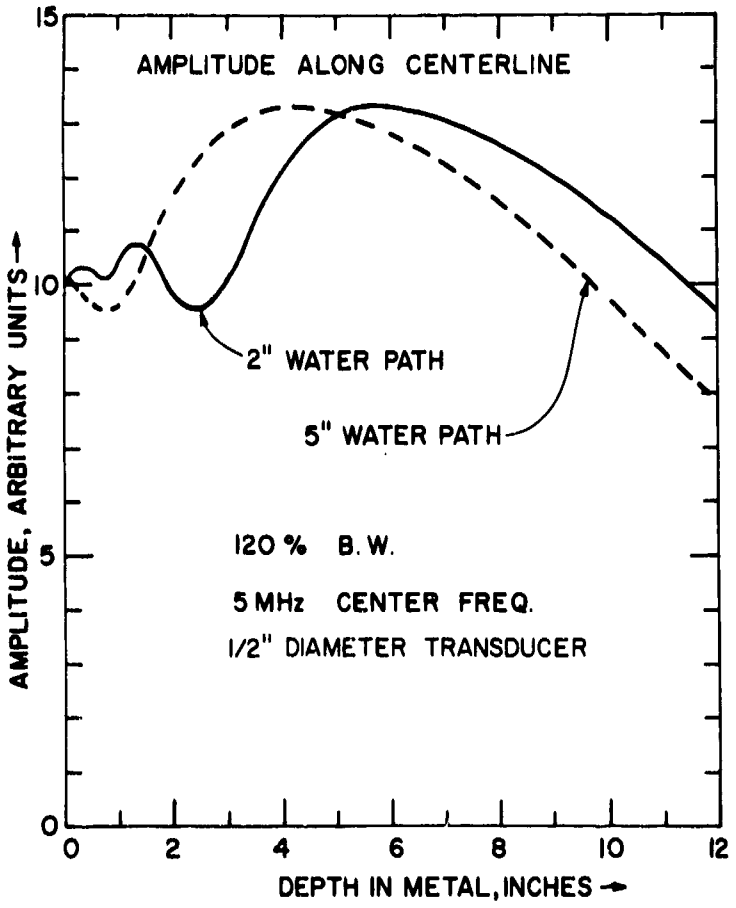

Fig. 7. Pressure along the transducer centerline in immersed testing. The pressure in the solid under test is plotted for two water paths.

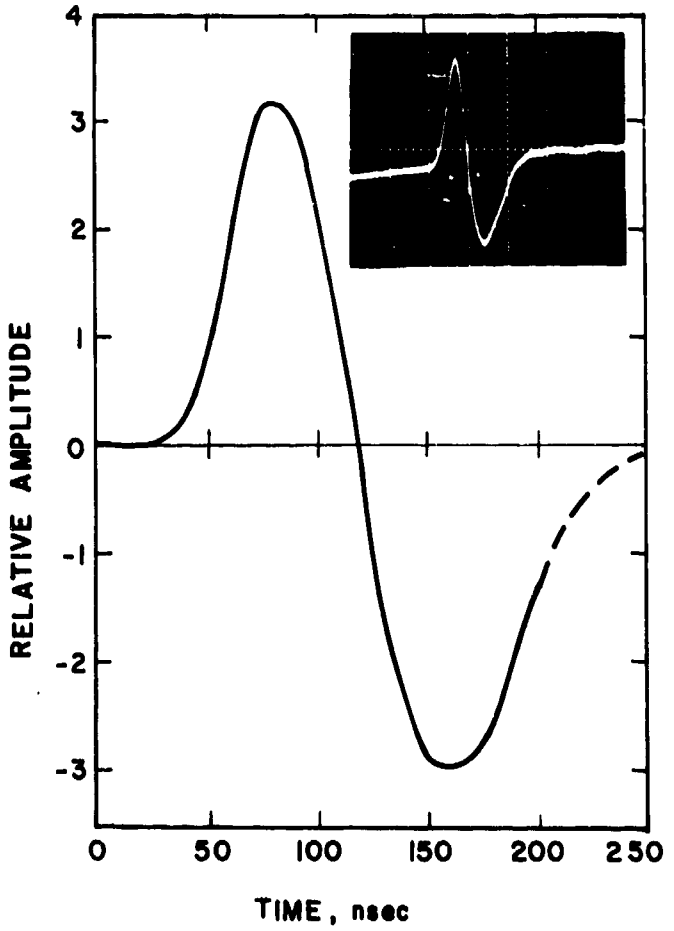

Fig. 8. Pulse shape and duration for the echo from a broadband transducer with a 10 MHz piezoelectric plate. Experiment and theory agree quantitatively.

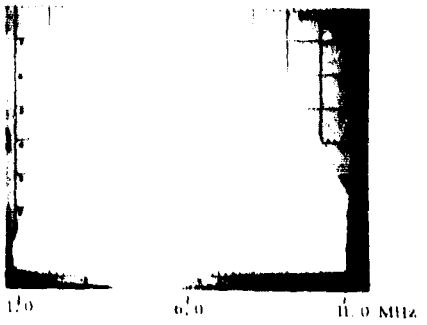

Spectrum
Linear Scale

6 MHz Center Frequency
300 KHz Bandwidth
1 MHz/div.
3 db Fractional
Bandwidth = 118%

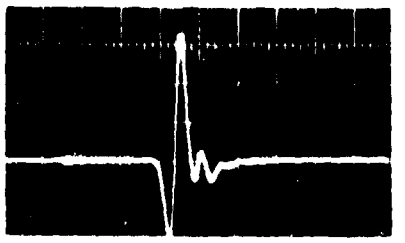

Pulse Signal

0.1V/div.
0.2 μs/div.

Fig. 9 Oscillograms of a Wideband Ultrasonic Pulse Reflected from a Water-Steel Interface and its Spectrum.

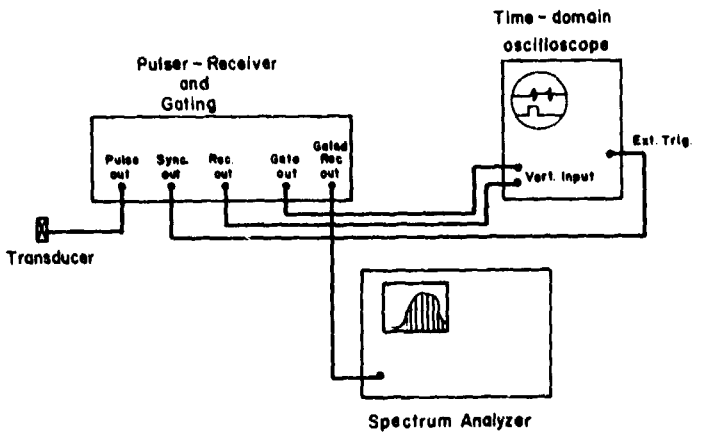

(a)

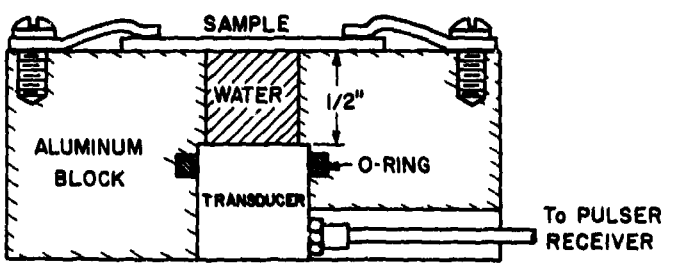

(b)

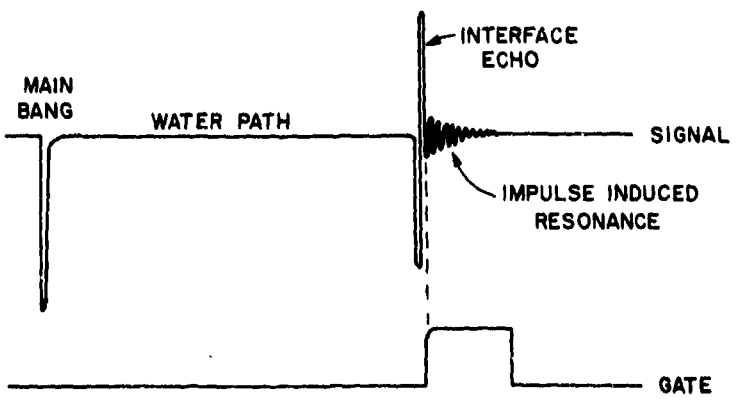

(c)

Fig. 10 Experimental Setup for Ultrasonic Spectroscopy of Impulse-Induced Resonance Signals for Thickness Measurement.

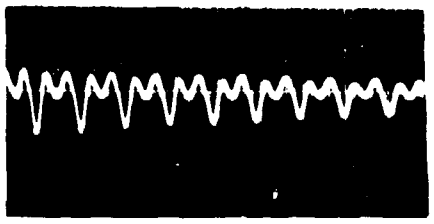

Gated Portion of Signal
0.1V/cm
0.2 μs/cm

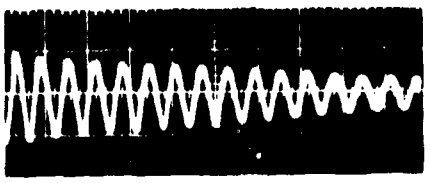

Gated Portion of Signal
0.1V/cm
0.2 μs/cm

Spectrum of Gated Signal
Linear Scale
8 MHz Center Frequency
300 KHz Bandwidth
1 MHz/div.

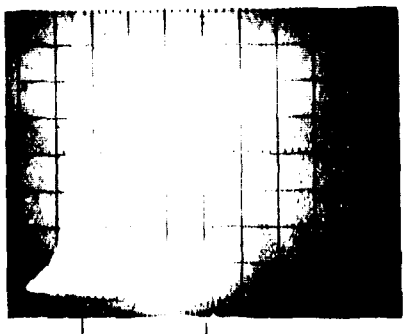

Spectrum of Gated Signal
Linear Scale
11 MHz Center Frequency
300 KHz Bandwidth
1 MHz/div

a. 0.025 in. (0.635 mm) Thick Steel Sheet

b. 0.015 in. (0.381 mm) Thick Steel Sheet

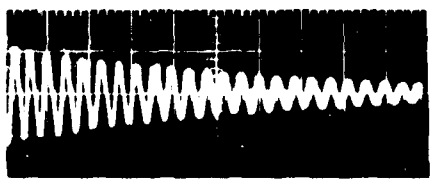

Gated Portion of Signal
0.05V/cm
0.2μs/cm

Gated Portion of Signal
0.02V/cm
0.2 μs/cm

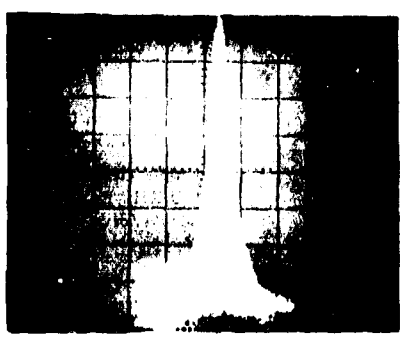

Spectrum of Gated Signal
Linear Scale
11 MHz Center Frequency
300 KHz Bandwidth
1 MHz/div

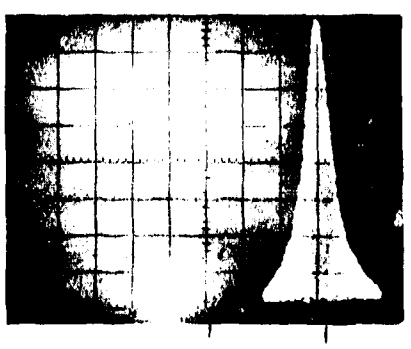

Spectrum of Gated Signal
Linear Scale
11 MHz Center Frequency
300 KHz Bandwidth
1 MHz/div

c. 0.010 in. (0.254 mm) Thick Steel Sheet

d. 0.008 in. (0.203 mm) Thick Steel Sheet

Fig. 11 Reflected Ultrasonic Signal and Corresponding Frequency Spectrum for Steel Sheet Samples of Several Thicknesses.

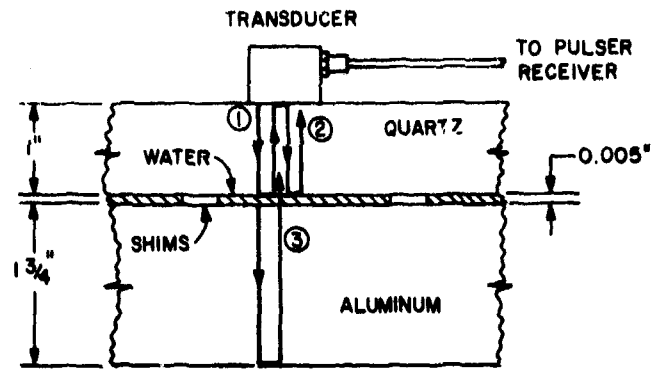

Fig. 12 Experimental Arrangement for Demonstrating Thickness Measurement of an Intermediate Layer of Low Acoustic Impedance.

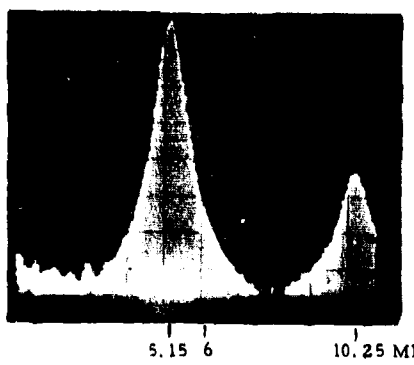

Spectrum in Gate B
Linear Scale

6 MHz Center Frequency
300 KHz Bandwidth
1 MHz/div

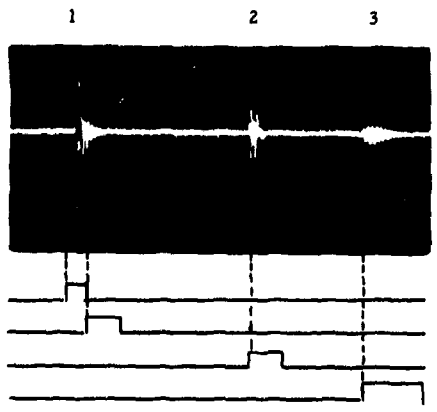

Pulse-Echo Signal

0.1V/cm
0.2μs/cm

Gate Timing

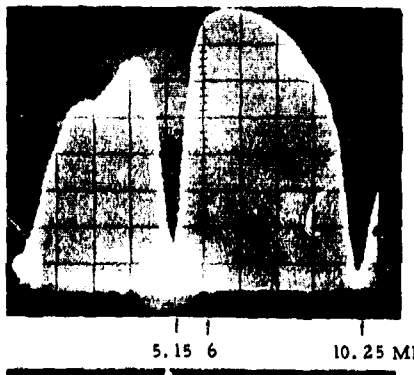

Spectrum in Gate C
Linear Scale

6 MHz Center Frequency
300 KHz Bandwidth
1 MHz/div

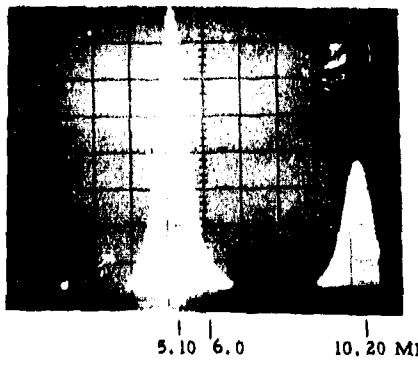

Spectrum in Gate D
Linear Scale

6 MHz Center Frequency
300 KHz Bandwidth
1 MHz/div

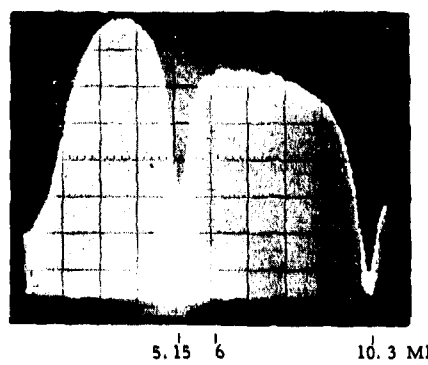

Spectrum in Gate A
Linear Scale

6 MHz Center Frequency
300 KHz Bandwidth
1 MHz/div

Fig. 13 Thickness Measurement of a Bond Layer Using a Broadband Ultrasonic Pulse and Spectrum Analysis.

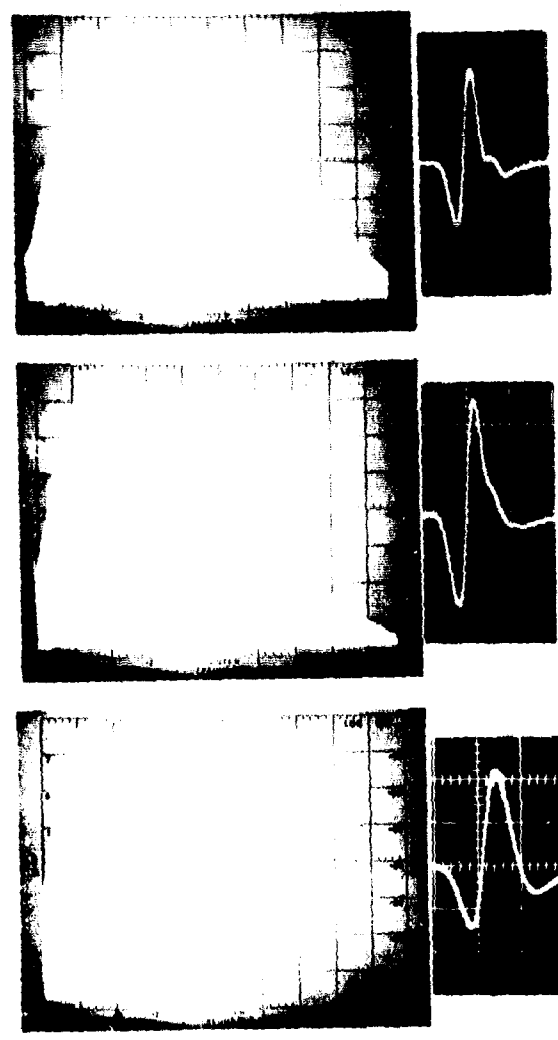

a. Low Viscosity Silicone Oil
Time Domain
0.2 μsec/cm
Frequency Domain
Linear Scale
6 MHz Center Frequency
100 KHz Bandwidth
1 MHz/div

b. Medium Viscosity Silicone Oil
Time Domain
0.2 μsec/cm
Frequency Domain
same as a.

c. Glycerine
Time Domain
0.2 μsec/cm
Frequency Domain
same as a.

Fig. 14 Effect of Liquid Viscosity on the Waveform and Spectrum of Pulses Reflected from a Submerged Interface.

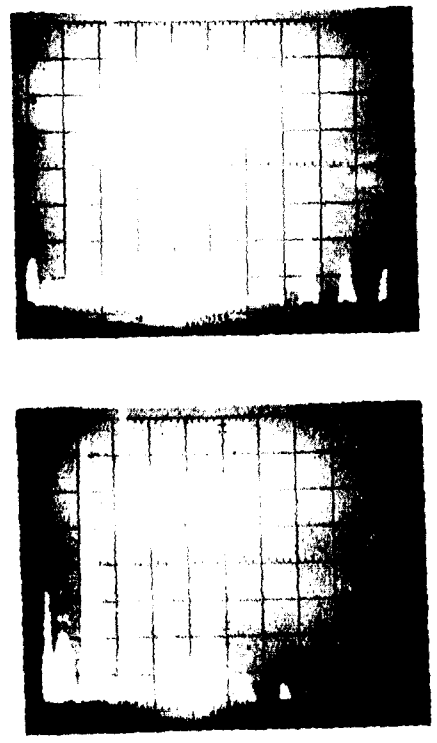

a. 10% Polystyrene in Ethyl Benzene
Viscosity - 40 cps
Linear Scale
3 MHz Center Frequency
30 KHz Bandwidth
0.5 MHz/div

b. 40% Polystyrene in Ethyl Benzene
Viscosity - 10,000 cps
Linear Scale
3 MHz Center Frequency
30 KHz Bandwidth
0.5 MHz/div

Fig. 15 The Spectral Content of Broadband Pulses Transmitted Across Identical Sections of 4" Diameter Pipe Containing Liquids of Differing Viscosity.

APPENDIX A

Tabulation of Pressure and Phase as Functions of S and x for Various Values of S_c

	x/a	0.025		0.125		0.225		0.325		0.425		0.525		0.625		0.725		0.825		0.925	
t	S	C	δ	C	δ	C	δ	C	δ	C	δ	C	δ	C	δ	C	δ	C	δ	C	δ
1	1.000	2.45	0.00	2.26	0.00	1.95	-0.02	1.45	-0.09	1.15	-0.28	0.97	-0.48	0.95	-0.55	1.10	-0.46	0.95	-0.25	0.57	-0.05
2	0.500	0.05	0.07	0.64	-0.02	1.48	0.12	1.75	0.16	1.47	-0.01	1.43	-0.32	1.38	-0.28	1.00	-0.30	0.83	-0.42	0.76	-0.14
3	0.333	2.40	0.00	1.30	-0.06	0.85	-0.22	0.85	0.22	1.48	0.18	1.67	-0.12	1.26	-0.18	1.20	-0.36	0.87	-0.30	0.75	-0.23
4	0.250	0.02	0.60	1.05	0.07	1.49	-0.12	1.28	-0.14	0.98	0.26	1.51	0.08	1.47	-0.17	1.35	-0.30	1.00	-0.34	0.72	-0.23
5	S_c= 0.200	2.26	-0.10	0.75	-0.16	1.60	0.18	1.10	-0.28	1.10	0.09	1.35	0.22	1.10	-0.06	1.42	-0.19	1.10	-0.38	0.74	-0.30
6	0.167	1.50	-1.40	0.97	0.06	1.50	0.11	0.87	0.01	1.25	-0.19	1.20	0.16	1.31	0.00	1.47	-0.22	1.15	-0.38	0.76	-0.29
7	0.143	1.15	0.00	1.45	0.11	1.37	-0.22	0.76	0.09	1.30	-0.23	1.14	0.04	1.24	0.05	1.47	-0.18	1.16	-0.28	0.76	-0.28
8	0.125	2.35	-1.30	1.62	-0.31	1.22	-0.06	0.91	-0.11	1.29	-0.13	1.13	-0.04	1.20	0.16	1.46	-0.16	1.18	-0.18	0.76	-0.12
9	0.111	2.35	0.00	1.60	-0.30	1.10	0.18	1.05	-0.12	1.25	0.02	1.14	-0.13	1.15	0.28	1.45	-0.10	1.20	-0.38	0.76	-0.16
1	1.250	2.37	-0.31	2.26	-0.30	1.97	-0.27	1.67	-0.24	1.31	-0.23	1.00	-0.28	0.79	-0.41	0.70	-0.52	0.69	-0.50	0.69	-0.34
2	0.625	1.47	0.93	1.26	0.64	1.31	0.10	1.88	-0.17	1.80	-0.20	1.36	-0.18	1.04	-0.39	1.11	-0.46	0.88	-0.26	0.60	-0.26
3	0.417	1.40	-0.92	1.13	-0.31	1.21	0.39	1.36	0.25	1.65	-0.11	1.50	-0.08	1.31	-0.33	1.16	-0.34	0.82	-0.29	0.77	-0.30
4	0.312	2.30	0.31	1.28	-0.11	1.00	-0.37	0.98	0.32	1.39	0.12	1.65	-0.01	1.33	-0.27	1.23	-0.24	0.90	-0.39	0.73	-0.17
5	S_c= 0.250	0.02	0.60	1.05	0.07	1.49	-0.12	1.28	-0.14	0.98	0.26	1.51	0.08	1.47	-0.17	1.35	-0.30	1.00	-0.34	0.72	-0.23
6	0.208	2.15	-0.38	0.80	0.42	1.60	-0.02	1.15	-0.23	1.05	0.12	1.38	0.16	1.42	-0.05	1.41	-0.21	1.08	-0.37	0.74	-0.31
7	0.179	2.05	0.86	0.65	-0.16	1.55	0.18	0.98	0.00	1.20	-0.05	1.25	0.12	1.35	-0.05	1.45	-0.17	1.12	-0.37	0.75	-0.30
8	0.156	0.85	-0.84	1.20	0.19	1.45	-0.03	0.81	-0.04	1.27	-0.26	1.15	0.11	1.28	0.04	1.47	-0.23	1.15	-0.37	0.76	-0.28
9	0.139	1.85	0.30	1.50	0.02	1.33	-0.30	0.77	0.10	1.30	-0.21	1.13	0.02	1.23	0.06	1.47	-0.16	1.17	-0.23	0.77	-0.27
1	1.560	2.11	-0.56	2.05	-0.55	1.90	-0.53	1.69	-0.47	1.44	-0.38	1.17	-0.31	0.90	-0.28	0.69	-0.25	0.55	-0.30	0.51	-0.39
2	0.780	2.25	0.43	2.00	0.37	1.60	0.18	1.37	-0.16	1.40	-0.40	1.45	-0.40	1.23	-0.30	0.90	-0.25	0.70	-0.36	0.68	-0.34
3	0.520	0.35	1.16	0.77	0.26	1.49	0.09	1.77	0.11	1.40	0.02	1.43	-0.32	1.33	-0.35	0.90	-0.26	0.84	-0.40	0.71	-0.24
4	0.390	1.90	-0.65	1.27	-0.23	1.10	0.42	1.19	0.16	1.63	0.02	1.58	-0.08	1.26	-0.34	1.19	-0.26	0.80	-0.42	0.76	-0.13
5	S_c= 0.312	2.30	0.31	1.28	-0.11	1.00	-0.37	0.98	0.32	1.39	0.12	1.65	-0.01	1.33	-0.27	1.23	-0.24	0.90	-0.39	0.73	-0.17
6	0.260	0.10	1.20	1.10	-0.04	1.45	-0.07	1.30	-0.14	1.06	0.30	1.54	0.01	1.47	-0.24	1.29	-0.24	1.00	-0.38	0.72	-0.24
7	0.223	1.68	-0.86	0.90	0.40	1.58	-0.17	1.23	-0.05	0.96	0.14	1.43	0.09	1.45	-0.06	1.40	-0.23	1.06	-0.32	0.72	-0.30
8	0.195	2.30	0.10	0.70	-0.36	1.60	0.24	1.07	-0.24	1.14	0.08	1.32	0.21	1.39	-0.06	1.44	-0.17	1.10	-0.38	0.75	-0.31
9	0.173	2.05	1.15	0.82	-0.04	1.52	0.15	0.92	0.04	1.23	-0.14	1.22	0.13	1.33	-0.03	1.45	-0.19	1.14	-0.38	0.75	-0.30
1	2.500	1.47	-0.94	1.45	-0.92	1.41	-0.89	1.35	-0.83	1.27	-0.75	1.17	-0.65	1.06	-0.53	0.94	-0.39	0.82	-0.24	0.69	-0.08
2	1.250	2.37	-0.31	2.26	-0.30	1.97	-0.27	1.67	-0.24	1.31	-0.23	1.00	-0.28	0.79	-0.41	0.70	-0.52	0.69	-0.50	0.69	-0.34
3	0.833	2.38	0.30	2.15	0.27	1.73	0.14	1.38	-0.12	1.31	-0.33	1.30	-0.47	1.26	-0.38	0.96	-0.25	0.65	-0.25	0.58	-0.34
4	0.625	1.47	0.93	1.26	0.64	1.31	0.10	1.88	-0.17	1.80	-0.20	1.36	-0.18	1.04	-0.39	1.11	-0.46	0.88	-0.26	0.60	-0.12
5	S_c= 0.500	0.05	0.07	0.64	-0.02	1.48	0.12	1.75	0.16	1.47	-0.01	1.43	-0.32	1.38	-0.28	1.00	-0.30	0.83	-0.42	0.76	-0.14
6	0.417	1.40	-0.92	1.13	-0.31	1.21	0.39	1.36	0.25	1.65	-0.11	1.50	-0.08	1.31	-0.33	1.16	-0.34	0.82	-0.25	0.77	-0.30
7	0.357	2.30	-0.32	1.27	-0.10	0.93	0.14	0.96	0.12	1.57	0.18	1.65	-0.16	1.23	-0.20	1.18	-0.38	0.84	-0.28	0.81	-0.28
8	0.312	2.30	0.31	1.28	-0.11	1.00	-0.37	0.98	0.32	1.39	0.12	1.65	-0.01	1.33	-0.27	1.23	-0.24	0.90	-0.39	0.73	-0.17
9	0.278	1.75	0.88	1.18	-0.14	1.31	-0.14	1.26	0.08	1.21	0.19	1.59	-0.01	1.44	-0.13	1.29	-0.37	0.95	-0.28	0.72	-0.22
1	3.750	1.02	-1.15	1.01	-1.13	1.00	-1.11	0.98	-1.06	0.95	-1.00	0.92	-0.93	0.89	-0.84	0.84	-0.73	0.79	-0.61	0.74	-0.48
2	1.870	1.85	-0.72	1.82	-0.71	1.73	-0.67	1.60	-0.60	1.43	-0.51	1.23	-0.41	1.03	-0.29	0.82	-0.19	0.64	-0.11	0.49	-0.08
3	1.250	2.37	-0.31	2.26	-0.30	1.97	-0.27	1.67	-0.24	1.31	-0.23	1.00	-0.28	0.79	-0.41	0.70	-0.52	0.69	-0.50	0.69	-0.34
4	0.940	2.50	0.10	2.28	0.09	1.90	0.04	1.45	-0.08	1.18	-0.31	1.12	-0.50	1.10	-0.51	1.07	-0.38	0.84	-0.28	0.55	-0.08
5	S_c= 0.750	2.15	0.52	1.90	0.43	1.55	0.19	1.40	-0.18	1.48	-0.38	1.46	-0.36	1.20	-0.27	0.85	-0.28	0.75	-0.41	0.74	-0.30
6	0.625	1.47	0.93	1.26	0.64	1.31	0.10	1.88	-0.17	1.80	-0.20	1.36	-0.18	1.04	-0.39	1.11	-0.46	0.88	-0.26	0.60	-0.12
7	0.536	0.60	1.16	0.75	0.42	1.48	0.07	1.79	0.06	1.40	0.02	1.42	-0.30	1.29	-0.39	0.88	-0.26	0.83	-0.34	0.63	-0.30
8	0.469	0.45	-1.32	0.85	-0.23	1.47	0.21	1.63	0.24	1.55	-0.12	1.42	-0.26	1.38	-0.33	1.03	-0.41	0.83	-0.34	0.77	-0.12
9	0.417	1.40	-0.92	1.13	-0.31	1.21	0.39	1.36	0.25	1.65	-0.11	1.50	-0.08	1.31	-0.33	1.16	-0.34	0.82	-0.25	0.77	-0.30
1	5.000	0.77	-1.24	0.77	-1.24	0.76	-1.21	0.76	-1.18	0.75	-1.13	0.73	-1.08	0.71	-1.01	0.70	-0.93	0.67	-0.83	0.65	-0.73
2	2.500	1.47	-0.94	1.45	-0.93	1.41	-0.88	1.35	-0.83	1.27	-0.75	1.17	-0.65	1.06	-0.53	0.94	-0.39	0.82	-0.24	0.69	-0.08
3	1.670	2.01	-0.63	1.95	-0.61	1.84	-0.56	1.67	-0.50	1.45	-0.42	1.21	-0.32	0.96	-0.24	0.74	-0.19	0.57	-0.21	0.47	-0.28
4	1.250	2.36	-0.32	2.25	-0.31	2.02	-0.27	1.69	-0.24	1.33	-0.22	1.01	-0.28	0.81	-0.42	0.74	-0.56	0.73	-0.52	0.71	-0.35
5	S_c= 1.000	2.50	0.00	2.32	0.00	1.96	-0.02	1.53	-0.10	1.19	-0.27	1.06	-0.48	1.05	-0.56	1.01	-0.46	0.86	-0.26	0.65	-0.06
6	0.833	2.35	0.30	2.12	0.26	1.70	0.14	1.39	-0.12	1.33	-0.40	1.33	-0.47	1.22	-0.38	0.94	-0.26	0.69	-0.35	0.60	-0.34
7	0.714	2.00	0.62	1.75	0.50	1.45	0.18	1.47	-0.20	1.58	-0.54	1.46	-0.30	1.13	-0.26	0.85	-0.35	0.80	-0.44	0.72	-0.23
8	0.625	1.50	0.93	1.30	0.64	1.30	0.10	1.66	-0.17	1.80	-0.20	1.36	-0.28	1.05	-0.38	1.10	-0.46	0.88	-0.26	0.60	-0.10
9	0.555	0.90	1.10	0.90	0.56	1.40	0.06	1.80	-0.02	1.45	-0.02	1.40	-0.25	1.23	-0.43	0.90	-0.31	0.85	-0.25	0.64	-0.34
1	7.500	0.57	-1.40	0.54	-1.35	0.50	-1.33	0.50	-1.31	0.50	-1.28	0.50	-1.24	0.50	-1.19	0.50	-1.14	0.50	-1.07	0.50	-1.00
2	3.750	1.02	-1.15	1.01	-1.13	1.00	-1.11	0.98	-1.06	0.95	-1.00	0.92	-0.93	0.89	-0.84	0.84	-0.73	0.79	-0.61	0.74	-0.48
3	2.500	1.47	-0.94	1.45	-0.92	1.41	-0.89	1.35	-0.83	1.27	-0.75	1.17	-0.65	1.06	-0.53	0.94	-0.39	0.82	-0.24	0.69	-0.08
4	1.870	1.85	-0.72	1.82	-0.71	1.73	-0.67	1.60	-0.60	1.43	-0.51	1.23	-0.41	1.03	-0.29	0.82	-0.19	0.64	-0.11	0.49	-0.08
5	S_c= 1.500	2.16	-0.52	2.09	-0.54	1.94	-0.46	1.71	-0.40	1.44	-0.34	1.15	-0.26	0.88	-0.24	0.67	-0.28	0.56	-0.39	0.54	-0.44
6	1.250	2.37	-0.31	2.26	-0.30	1.97	-0.27	1.67	-0.24	1.31	-0.23	1.00	-0.28	0.79	-0.41	0.70	-0.52	0.69	-0.50	0.69	-0.34
7	1.070	2.48	-0.10	2.15	-0.11	1.95	-0.10	1.43	-0.12	1.15	-0.24	0.90	-0.42	0.85	-0.56	1.05	-0.53	1.10	-0.35	1.10	-0.10
8	0.940	2.50	0.10	2.28	0.09	1.90	0.04	1.45	-0.08	1.18	-0.31	1.12	-0.50	1.10	-0.51	1.07	-0.38	0.84	-0.28	0.55	-0.08
9	0.833	2.38	0.30	2.15	0.27	1.73	0.14	1.38	0.12	1.31	0.33	1.30	0.47	1.26	0.38	0.96	0.25	0.65	0.25	0.58	0.34
1	12.500	0.33	-1.44	0.30	-1.44	0.29	-1.43	0.29	-1.41	0.29	-1.39	0.29	-1.37	0.29	-1.34	0.29	-1.31	0.29	-1.27	0.29	-1.23
2	6.250	0.64	-1.32	0.64	-1.31	0.63	-1.29	0.62	-1.26	0.61	-1.23	0.60	-1.18	0.60	-1.12	0.59	-1.06	0.59	-0.98	0.58	-0.90
3	4.170	0.92	-1.19	0.91	-1.18	0.91	-1.15	0.89	-1.11	0.87	-1.06	0.85	-0.99	0.82	-0.91	0.79	-0.81	0.75	-0.70	0.71	-0.58
4	3.120	1.20	-1.06	1.19	-1.05	1.17	-1.02	1.14	-0.97	1.09	-0.90	1.04	-0.81	0.98	-0.71	0.91	-0.59	0.83	-0.45	0.76	-0.30
5	S_c= 2.500	1.47	-0.94	1.45	-0.92	1.41	-0.89	1.35	-0.83	1.27	-0.75	1.17	-0.65	1.06	-0.53	0.94	-0.39	0.82	-0.24	0.69	-0.08
6	2.080	1.71	-0.81	1.69	-0.79	1.62	-0.75	1.52	-0.69	1.39	-0.60	1.23	-0.49	1.06	-0.37	0.89	-0.24	0.72	-0.11	0.56	-0.01
7	1.790	1.92	-0.69	1.88	-0.67	1.78	-0.63	1.63	-0.56	1.44	-0.47	1.23	-0.37	1.00	-0.27	0.79	-0.18	0.60	-0.13	0.47	-0.15
8	1.560	2.11	-0.56	2.05	-0.55	1.90	-0.53	1.69	-0.47	1.44	-0.38	1.17	-0.31	0.90	-0.28	0.69	-0.25	0.55	-0.30	0.51	-0.39
9	1.390	2.25	-0.44	2.17	-0.42	1.98	-0.38	1.71	-0.33	1.40	-0.28	1.09	-0.24	0.83	-0.28	0.67	-0.40	0.62	-0.49	0.62	-0.45

APPENDIX B

Tabulation of Spectral Density
B(t) for Various Bandwidths

B. W., %	10	20	40	80	120
t	B(t)				
1	0.001	0.002	0.010	0.100	0.562
2	0.002	0.010	0.030	0.450	0.840
3	0.015	0.100	0.180	0.840	0.943
4	0.100	0.320	0.840	0.970	0.983
t_c 5	1.000	1.000	1.000	1.000	1.000
6	0.010	0.320	0.840	0.970	0.983
7	0.015	0.100	0.180	0.840	0.943
8	0.002	0.010	0.030	0.450	0.840
9	0.001	0.002	0.010	0.100	0.562

APPENDIX C
PROGRAM

```
101 FORMAT (10F9.4)
102 FORMAT (11H BANDWIDTH ,F9.4)
103 FORMAT (4H S ,F9.4)
104 FORMAT (11H AMPLITUDE )
105 FORMAT (7H PHASE )
    DIMENSION BAND(5),B(5,10),S(8),C(10,9),D(10,10),A(10),E(10)
    DIMENSION G(10)
    DO 100 I=1,5
    READ (5,101) BAND(I),B(I,1),B(I,2),B(I,3),B(I,4),B(I,5),B(I,6),
   1 B(I,7),B(I,8),B(I,9)
100 CONTINUE
    READ (5,101) S(1),S(2),S(3),S(4),S(5),S(6),S(7),S(8)
    DO 99 K=1,8
    SS=S(K)
    WRITE (6,103) SS
    DO 98 I=1,9
    READ (5,101) C(1,I),C(2,I),C(3,I),C(4,I),C(5,I),C(6,I),C(7,I),
   1 C(8,I),C(9,I),C(10,I)
    READ (5,101) D(1,I),D(2,I),D(3,I),D(4,I),D(5,I),D(6,I),D(7,I),
   1 D(8,I),D(9,I),D(10,I)
 98 CONTINUE
    DO 97 L=1,5
    BBB=BAND(L)
    WRITE (6,102) BBB
    DO 96 J=1,10
    SUMC=0.
    SUMS=0.
    DO 95 I=1,9
    BB=B(L,I)
    CC=C(J,I)
    DD=D(J,I)
    CD=COS(DD)
    SD=SIN(DD)
    COEF=BB*CC
    SUMC=COEF*CD+SUMC
 95 SUMS=COEF*SD+SUMS
    SCSQ=SUMC*SUMC
    SSSQ=SUMS*SUMS
    SUMA=SCSQ+SSSQ
    A(J)=SQRT(SUMA)
    QUO=SUMS/SUMC
 96 E(J)=ATAN(QUO)
    AMAX=A(1)
    DO 94 J=2,10
    ATEST=A(J)
    IF(ATEST-AMAX) 94,93,93
 93 AMAX=ATEST
 94 CONTINUE
    DO 92 J=1,10
 92 G(J)=A(J)/AMAX
    WRITE (6,104)
    WRITE (6,101) A(1),A(2),A(3),A(4),A(5),A(6),A(7),A(8),A(9),A(10)
    WRITE (6,106)
106 FORMAT (22H NORMALIZED AMPLITUDE )
    WRITE (6,101) G(1),G(2),G(3),G(4),G(5),G(6),G(7),G(8),G(9),G(10)
    WRITE (6,105)
    WRITE (6,101) E(1),E(2),E(3),E(4),E(5),E(6),E(7),E(8),E(9),E(10)
    WRITE (6,107)
107 FORMAT (/)
 97 CONTINUE
    WRITE (6,108)
108 FORMAT (1H1)
 99 CONTINUE
    WRITE (6,109)
109 FORMAT (23H COMPUTATION COMPLETED )
    WRITE (6,109)
    STOP
    END
```

APPENDIX D
RESULTS

```
S    0.2000
BANDWIDTH    1.2000
AMPLITUDE
 0.0980  0.0928  0.1050  0.0827  0.0964  0.0981  0.0966  0.1017  0.0820  0.0563
NORMALIZED AMPLITUDE
 0.9338  0.8841  1.0000  0.7874  0.8988  0.9346  0.9202  0.9614  0.7624  0.5360
PHASE
-0.3724 -0.0652 -0.0007 -0.0273 -0.0246 -0.0301 -0.0770 -0.2436 -0.3235 -0.2154

BANDWIDTH    0.8000
AMPLITUDE
 0.0692  0.0636  0.0779  0.0590  0.0696  0.0760  0.0750  0.0774  0.0600  0.0425
NORMALIZED AMPLITUDE
 0.8760  0.8166  1.0000  0.7575  0.8942  0.9754  0.9628  0.9938  0.7702  0.5461
PHASE
-0.4015 -0.0313 -0.0091 -0.0340 -0.0033  0.0244 -0.0756 -0.2405 -0.3394 -0.2404

BANDWIDTH    0.4000
AMPLITUDE
 0.0353  0.0303  0.0457  0.0327  0.0352  0.0421  0.0427  0.0436  0.0335  0.0231
NORMALIZED AMPLITUDE
 0.7719  0.6624  1.0000  0.7141  0.7694  0.9195  0.9331  0.9536  0.7326  0.5055
PHASE
-0.4468 -0.0047  0.0421 -0.1222  0.0279  0.1211 -0.0773 -0.2356 -0.3578 -0.2693

BANDWIDTH    0.2000
AMPLITUDE
 0.0280  0.0169  0.0278  0.0196  0.0210  0.0251  0.0256  0.0262  0.0201  0.0138
NORMALIZED AMPLITUDE
 1.0000  0.6036  0.9942  0.6997  0.7492  0.8979  0.9154  0.9340  0.7193  0.4934
PHASE
-0.2591 -0.0445  0.0845 -0.1701  0.0469  0.1488 -0.0711 -0.2211 -0.3613 -0.2795

BANDWIDTH    0.1000
AMPLITUDE
 0.0237  0.0100  0.0193  0.0134  0.0137  0.0167  0.0172  0.0175  0.0135  0.0091
NORMALIZED AMPLITUDE
 1.0000  0.4215  0.8168  0.5667  0.5772  0.7046  0.7276  0.7392  0.5713  0.3867
PHASE
-0.1690 -0.1071  0.1445 -0.2388  0.0728  0.1943 -0.0650 -0.2028 -0.3746 -0.2917
```

```
S    0.2500
BANDWIDTH    1.2000
AMPLITUDE
 0.1236  0.0861  0.1060  0.0955  0.0967  0.1088  0.1002  0.0900  0.0692  0.0543
NORMALIZED AMPLITUDE
 0.9528  0.7919  0.9750  0.8779  0.8890  1.0000  0.9211  0.8276  0.6362  0.4990
PHASE
 0.0959 -0.0199  0.0002 -0.0382 -0.0123 -0.0721 -0.2174 -0.2304 -0.3742 -0.2542

BANDWIDTH    0.8000
AMPLITUDE
 0.0727  0.0625  0.0759  0.0715  0.0727  0.0844  0.0767  0.0683  0.0522  0.0413
NORMALIZED AMPLITUDE
 0.8609  0.7406  0.8989  0.8470  0.8618  1.0000  0.9086  0.8095  0.6183  0.4889
PHASE
 0.0470  0.0161  0.0118  0.0199  0.0499 -0.0645 -0.2353 -0.2369 -0.3781 -0.2329

BANDWIDTH    0.4000
AMPLITUDE
 0.0416  0.0363  0.0366  0.0365  0.0415  0.0487  0.0421  0.0382  0.0282  0.0228
NORMALIZED AMPLITUDE
 0.8543  0.7456  0.7521  0.7483  0.8512  1.0000  0.8648  0.7837  0.5796  0.4685
PHASE
 0.0938 -0.0878 -0.0222  0.0872  0.1125 -0.0366 -0.2679 -0.2445 -0.3894 -0.1924

BANDWIDTH    0.2000
AMPLITUDE
 0.0301  0.0222  0.0207  0.0207  0.0251  0.0296  0.0251  0.0228  0.0169  0.0136
NORMALIZED AMPLITUDE
 1.0000  0.7353  0.6885  0.6876  0.8319  0.9814  0.8321  0.7571  0.5599  0.4520
PHASE
 0.1835 -0.0858 -0.1250  0.1542  0.1149 -0.0296 -0.2665 -0.2431 -0.3885 -0.1871

BANDWIDTH    0.1000
AMPLITUDE
 0.0290  0.0155  0.0128  0.0127  0.0170  0.0201  0.0165  0.0152  0.0111  0.0090
NORMALIZED AMPLITUDE
 1.0000  0.6187  0.5104  0.5070  0.6799  0.8048  0.6608  0.6080  0.4457  0.3614
PHASE
 0.2709 -0.1074 -0.2603  0.2467  0.1191 -0.0165 -0.2704 -0.2414 -0.3903 -0.1753
```

```
S   0.3120
BANDWIDTH   1.2000
AMPLITUDE
 0.0967  0.0834  0.1056  0.0901  0.0997  0.1031  0.0969  0.0974  0.0751  0.0555
NORMALIZED AMPLITUDE
 0.9101  0.8084  1.0000  0.8534  0.9438  0.9760  0.9177  0.9224  0.7111  0.5260
PHASE
 0.0713  0.0348 -0.0290 -0.0321 -0.0585  0.0106 -0.1619 -0.2694 -0.3397 -0.2700

BANDWIDTH   0.8000
AMPLITUDE
 0.0699  0.0579  0.0771  0.0662  0.0728  0.0805  0.0795  0.0746  0.0564  0.0418
NORMALIZED AMPLITUDE
 0.8673  0.7187  0.9574  0.8222  0.9040  1.0000  0.9872  0.9257  0.7004  0.5183
PHASE
 0.0739  0.0439  0.0009 -0.0062 -0.0944  0.0124 -0.1669 -0.2617 -0.3461 -0.2635

BANDWIDTH   0.4000
AMPLITUDE
 0.0401  0.0519  0.0621  0.0591  0.0369  0.0463  0.0433  0.0413  0.0309  0.0229
NORMALIZED AMPLITUDE
 0.8638  0.6791  0.9096  0.7971  0.7965  1.0000  0.9347  0.8914  0.6671  0.4922
PHASE
 0.0061  0.0946 -0.0910 -0.0265  0.1180  0.0628 -0.1642 -0.2535 -0.3561 -0.2453

BANDWIDTH   0.2000
AMPLITUDE
 0.0160  0.0189  0.0260  0.0219  0.0207  0.0276  0.0261  0.0248  0.0185  0.0136
NORMALIZED AMPLITUDE
 0.5791  0.6810  0.9392  0.7879  0.7455  1.0000  0.9455  0.8918  0.6662  0.4886
PHASE
 0.0196  0.0511 -0.0892 -0.0614  0.1521  0.0676 -0.1673 -0.2687 -0.3510 -0.2620

BANDWIDTH   0.1000
AMPLITUDE
 0.0047  0.0128  0.0179  0.0152  0.0127  0.0186  0.0179  0.0166  0.0123  0.0089
NORMALIZED AMPLITUDE
 0.2554  0.6906  0.9640  0.8195  0.6832  1.0000  0.9621  0.8925  0.6629  0.4806
PHASE
 0.0194  0.0675 -0.1159 -0.1118  0.2186  0.0799 -0.1692 -0.2867 -0.3457 -0.2337


S   0.7500
BANDWIDTH   1.2000
AMPLITUDE
 0.0950  0.1035  0.1111  0.1141  0.1066  0.0981  0.0855  0.0710  0.0537  0.0499
NORMALIZED AMPLITUDE
 0.8333  0.9071  0.9736  1.0000  0.9347  0.8625  0.7430  0.6223  0.5231  0.4369
PHASE
-0.0243 -0.0459 -0.0714 -0.1474 -0.2650 -0.3327 -0.3722 -0.3938 -0.3396 -0.2360

BANDWIDTH   0.8000
AMPLITUDE
 0.0815  0.0867  0.0888  0.0901  0.0815  0.0728  0.0630  0.0529  0.0449  0.0366
NORMALIZED AMPLITUDE
 0.9043  0.9604  0.9859  1.0000  0.9031  0.8079  0.6991  0.5877  0.4989  0.4063
PHASE
 0.1676  0.0792 -0.0282 -0.1135 -0.2444 -0.3294 -0.3812 -0.3710 -0.3346 -0.2195

BANDWIDTH   0.4000
AMPLITUDE
 0.0563  0.0529  0.0493  0.0491  0.0456  0.0405  0.0345  0.0303  0.0252  0.0199
NORMALIZED AMPLITUDE
 1.0000  0.9369  0.8754  0.8724  0.8090  0.7194  0.6124  0.5379  0.4475  0.3524
PHASE
 0.3947  0.2831  0.0737 -0.1404 -0.2748 -0.3542 -0.3825 -0.3757 -0.3272 -0.2031

BANDWIDTH   0.2000
AMPLITUDE
 0.0354  0.0326  0.0293  0.0284  0.0272  0.0252  0.0211  0.0172  0.0147  0.0125
NORMALIZED AMPLITUDE
 1.0000  0.9211  0.8246  0.8322  0.7698  0.7111  0.5970  0.4867  0.4166  0.3533
PHASE
 0.4339  0.3267  0.1053 -0.1902 -0.3045 -0.3421 -0.3471 -0.3463 -0.3361 -0.2422

BANDWIDTH   0.1000
AMPLITUDE
 0.0255  0.0228  0.0192  0.0179  0.0182  0.0175  0.0145  0.0110  0.0095  0.0088
NORMALIZED AMPLITUDE
 1.0000  0.8953  0.7558  0.7035  0.7157  0.6867  0.5699  0.4301  0.3722  0.3463
PHASE
 0.4921  0.3955  0.1597 -0.1682 -0.3515 -0.3536 -0.2999 -0.3104 -0.3562 -0.2761


S   1.5000
BANDWIDTH   1.2000
AMPLITUDE
 0.1329  0.1256  0.1151  0.1006  0.0888  0.0780  0.0696  0.0632  0.0557  0.0494
NORMALIZED AMPLITUDE
 1.0000  0.9454  0.8663  0.7569  0.6684  0.5870  0.5241  0.4756  0.4192  0.3719
PHASE
-0.3720 -0.3931 -0.3995 -0.4336 -0.4693 -0.4947 -0.4973 -0.4432 -0.3746 -0.2704

BANDWIDTH   0.8000
AMPLITUDE
 0.1075  0.1017  0.0936  0.0815  0.0707  0.0605  0.0524  0.0475  0.0426  0.0381
NORMALIZED AMPLITUDE
 1.0000  0.9461  0.8721  0.7598  0.6595  0.5623  0.4882  0.4431  0.3967  0.3555
PHASE
-0.4283 -0.4424 -0.4288 -0.4316 -0.4404 -0.4497 -0.4468 -0.4156 -0.3478 -0.2287

BANDWIDTH   0.4000
AMPLITUDE
 0.0619  0.0614  0.0564  0.0496  0.0421  0.0345  0.0291  0.0235  0.0206  0.0188
NORMALIZED AMPLITUDE
 1.0000  0.9612  0.8824  0.7767  0.6591  0.5400  0.4399  0.3681  0.3221  0.2941
PHASE
-0.4897 -0.4926 -0.4525 -0.4158 -0.3811 -0.3497 -0.3426 -0.3485 -0.3364 -0.2713

BANDWIDTH   0.2000
AMPLITUDE
 0.0388  0.0373  0.0344  0.0302  0.0256  0.0208  0.0167  0.0137  0.0119  0.0110
NORMALIZED AMPLITUDE
 1.0000  0.9620  0.8877  0.7803  0.6610  0.5370  0.4294  0.3526  0.3061  0.2833
PHASE
-0.4961 -0.5080 -0.4548 -0.4115 -0.3700 -0.3243 -0.3153 -0.3323 -0.3497 -0.3126

BANDWIDTH   0.1000
AMPLITUDE
 0.0263  0.0255  0.0236  0.0208  0.0175  0.0141  0.0109  0.0085  0.0072  0.0068
NORMALIZED AMPLITUDE
 1.0000  0.9662  0.8941  0.7881  0.6646  0.5338  0.4150  0.3241  0.2744  0.2596
PHASE
-0.5117 -0.5278 -0.4584 -0.4039 -0.3498 -0.2824 -0.2667 -0.2987 -0.3731 -0.3911


S   0.9000
BANDWIDTH   1.2000
AMPLITUDE
 0.1080  0.0989  0.0995  0.1040  0.1092  0.1063  0.0918  0.0810  0.0621  0.0538
NORMALIZED AMPLITUDE
 0.9890  0.9053  0.9106  0.9523  1.0000  0.9728  0.8401  0.7412  0.5689  0.4926
PHASE
 0.0112 -0.0618 -0.0358 -0.0316 -0.1056 -0.2146 -0.3131 -0.3529 -0.3198 -0.2768

BANDWIDTH   0.8000
AMPLITUDE
 0.0767  0.0722  0.0756  0.0812  0.0855  0.0806  0.0696  0.0607  0.0461  0.0402
NORMALIZED AMPLITUDE
 0.8966  0.8441  0.8819  0.9495  1.0000  0.9424  0.8138  0.7098  0.5387  0.4701
PHASE
 0.0073  0.0161  0.0710  0.0156 -0.0914 -0.2151 -0.3169 -0.3508 -0.3164 -0.2377

BANDWIDTH   0.4000
AMPLITUDE
 0.0246  0.0314  0.0414  0.0492  0.0496  0.0444  0.0388  0.0336  0.0258  0.0221
NORMALIZED AMPLITUDE
 0.4956  0.6332  0.8362  0.9915  1.0000  0.8957  0.7831  0.6786  0.5212  0.4458
PHASE
 0.0726  0.1190  0.1699  0.0597 -0.1017 -0.2097 -0.3209 -0.3595 -0.3125 -0.2029

BANDWIDTH   0.2000
AMPLITUDE
 0.0110  0.0169  0.0257  0.0302  0.0288  0.0266  0.0240  0.0196  0.0154  0.0135
NORMALIZED AMPLITUDE
 0.3635  0.5590  0.8520  1.0000  0.9551  0.8804  0.7964  0.6497  0.5095  0.4476
PHASE
 0.0231  0.0900  0.1531  0.0919 -0.0710 -0.2474 -0.3059 -0.3394 -0.3469 -0.1843

BANDWIDTH   0.1000
AMPLITUDE
 0.0030  0.0091  0.0178  0.0211  0.0186  0.0176  0.0166  0.0126  0.0103  0.0092
NORMALIZED AMPLITUDE
 0.1427  0.4313  0.8431  1.0000  0.8819  0.8373  0.7876  0.6003  0.4865  0.4374
PHASE
 0.0325  0.0350  0.1349  0.1328 -0.0305 -0.2877 -0.2912 -0.3185 -0.3092 -0.1561


S   1.0000
BANDWIDTH   1.2000
AMPLITUDE
 0.1193  0.1181  0.1133  0.1103  0.1019  0.0906  0.0777  0.0668  0.0576  0.0479
NORMALIZED AMPLITUDE
 1.0000  0.9916  0.9512  0.9325  0.8615  0.7659  0.6565  0.5646  0.4865  0.4052
PHASE
-0.0013 -0.0746 -0.1961 -0.2982 -0.3593 -0.4088 -0.4267 -0.4392 -0.3535 -0.2561

BANDWIDTH   0.8000
AMPLITUDE
 0.1045  0.1000  0.0925  0.0856  0.0782  0.0686  0.0587  0.0501  0.0427  0.0360
NORMALIZED AMPLITUDE
 1.0000  0.9575  0.8855  0.8193  0.7482  0.6571  0.5619  0.4795  0.4090  0.3444
PHASE
-0.0051 -0.0572 -0.1565 -0.2676 -0.3469 -0.3914 -0.3983 -0.3865 -0.3454 -0.2338

BANDWIDTH   0.4000
AMPLITUDE
 0.0691  0.0648  0.0565  0.0476  0.0407  0.0359  0.0320  0.0276  0.0235  0.0200
NORMALIZED AMPLITUDE
 1.0000  0.9368  0.8169  0.6888  0.5881  0.5187  0.4624  0.3997  0.3400  0.2890
PHASE
-0.0072 -0.0295 -0.0827 -0.1835 -0.3105 -0.4078 -0.4336 -0.4050 -0.3584 -0.2389

BANDWIDTH   0.2000
AMPLITUDE
 0.0428  0.0400  0.0345  0.0285  0.0237  0.0210  0.0192  0.0172  0.0146  0.0119
NORMALIZED AMPLITUDE
 1.0000  0.9359  0.8065  0.6651  0.5545  0.4900  0.4492  0.4021  0.3420  0.2786
PHASE
-0.0357 -0.0216 -0.0652 -0.1604 -0.3009 -0.4271 -0.4679 -0.4191 -0.3210 -0.1779

BANDWIDTH   0.1000
AMPLITUDE
 0.0300  0.0279  0.0237  0.0189  0.0151  0.0134  0.0129  0.0120  0.0102  0.0080
NORMALIZED AMPLITUDE
 1.0000  0.9299  0.7912  0.6294  0.5023  0.4460  0.4288  0.4014  0.3414  0.2658
PHASE
-0.0041 -0.0102 -0.0373 -0.1200 -0.2825 -0.4613 -0.5225 -0.4429 -0.2838 -0.1089


S   2.5000
BANDWIDTH   1.2000
AMPLITUDE
 0.1040  0.1019  0.0973  0.0905  0.0821  0.0729  0.0638  0.0556  0.0485  0.0431
NORMALIZED AMPLITUDE
 1.0000  0.9802  0.9359  0.8704  0.7890  0.7014  0.6138  0.5342  0.4665  0.4145
PHASE
-0.8161 -0.8019 -0.7768 -0.7321 -0.6733 -0.6099 -0.5530 -0.4902 -0.4303 -0.3713

BANDWIDTH   0.8000
AMPLITUDE
 0.0798  0.0785  0.0755  0.0710  0.0651  0.0586  0.0518  0.0453  0.0392  0.0342
NORMALIZED AMPLITUDE
 1.0000  0.9838  0.9463  0.8890  0.8156  0.7345  0.6490  0.5670  0.4912  0.4281
PHASE
-0.8621 -0.8473 -0.8194 -0.7697 -0.7026 -0.6261 -0.5486 -0.4616 -0.3771 -0.3001

BANDWIDTH   0.4000
AMPLITUDE
 0.0449  0.0443  0.0429  0.0408  0.0380  0.0347  0.0311  0.0274  0.0237  0.0202
NORMALIZED AMPLITUDE
 1.0000  0.9870  0.9556  0.9088  0.8460  0.7727  0.6927  0.6103  0.5278  0.4501
PHASE
-0.9098 -0.8929 -0.8612 -0.8067 -0.7307 -0.6383 -0.5356 -0.4188 -0.2957 -0.1770

BANDWIDTH   0.2000
AMPLITUDE
 0.0270  0.0266  0.0258  0.0246  0.0230  0.0210  0.0189  0.0167  0.0145  0.0125
NORMALIZED AMPLITUDE
 1.0000  0.9867  0.9566  0.9115  0.8512  0.7794  0.7008  0.6186  0.5362  0.4630
PHASE
-0.9189 -0.9010 -0.8698 -0.8135 -0.7365 -0.6421 -0.5342 -0.4109 -0.2796 -0.1400

BANDWIDTH   0.1000
AMPLITUDE
 0.0181  0.0178  0.0173  0.0166  0.0155  0.0143  0.0129  0.0114  0.0099  0.0084
NORMALIZED AMPLITUDE
 1.0000  0.9867  0.9584  0.9162  0.8596  0.7903  0.7141  0.6323  0.5502  0.4663
PHASE
-0.9325 -0.9134 -0.8828 -0.8243 -0.7452 -0.6470 -0.5312 -0.3969 -0.2533 -0.1037
```

PANAMETRICS
A Subsidiary of Esterline Corporation • 221 Crescent Street • Waltham, Massachusetts 02154 • (617) 899-2719
ESTERLINE

Technical Memorandum No. 5

Acoustic Emission Transducers and an Experimental Method of Verifying Their Performance

by

KENNETH A. FOWLER, P.E.
BRANCH CHIEF
MATERIALS EVALUATION

Invited Presentation

to

The Joint Meeting of the Boston Chapters of
ASNT, IEEE, AWS, ASM,
ASTM, ASME

September 23, 1970

ABSTRACT

The generic types of transducers useful in acoustic emission monitoring are reviewed. The basic modes of ultrasonic wave propagation and the interrelationships between structure geometry, propagation mode, material and transducer on the apparent form of acoustic emission signals are considered. An experimental method of comparing transducers, and determining the parameters that must be considered in the design of practical acoustic emission monitoring systems are proposed.

I. INTRODUCTION

Burst-type acoustic emissions, which are produced in a material undergoing micro-failure due to crack propagation, certain forms of deformation processes such as twining or some types of solid state phase transformations, vary widely in energy. Some acoustic emissions, notably those associated with micro-failure processes in mild steels, are of considerable practical interest but are also of very low energy. To monitor these emissions, high sensitivity transducers combined with high-gain, low-noise preamplifiers, must be used. With good quality transducers operating at a frequency of 100 kHz voltage gains of 100,000 or 100 dB to bring acoustic emission signals to an amplitude of one volt are not uncommon. The noise level of the best preamplifiers commonly available is about 5 μV peak-to-peak referenced to input. This means that at a gain of 100,000 the signal-to-noise level is typically 2 to 1. Clearly, this margin demands care in the selection and employment of transducers.

Today a variety of piezoelectric, ferroelectric, and magnetostrictive materials are available which, when properly fabricated, make excellent high-sensitivity acoustic emission transducers. These materials include lead-zirconate-titanates, commonly known as PZT, lead-metaniobate, lithium niobate, nickel-based magnetostrictive alloys and several other materials less widely known.

The lead-zirconate-titanates are probably the most widely used transducer material in acoustic emission work. They combine high sensitivity with low cost but, with a curie temperature of 320-365C, are limited with respect to high-temperature capabilities. For this reason lead metaniobate with a curie point of 550C and lithium niobate with the highest curie temperature presently available of 1210C have been receiving increasing attention as potential acoustic emission transducers for high temperature service. Bonding of these transducers for high-temperature operation is a difficult problem and although some progress is being made in th : area it appears that it will be some time before a reliable acoustic emission transducer is commercially available that utilizes the high-temperature capabilities of these materials. In the meantime, other solutions to the high-temperature problem are being sought. For example, wire waveguides can be used to carry the acoustic emission energy from a component at high temperature or under other adverse environment to a magnetostrictive or piezoelectric transducer up to 30 ft away. Because the mechanical impedance mismatch between the wire waveguide and more massive structures is quite large, this type of transducer is presently about a factor of five less sensitive than the best piezoelectric transducers. Other alternatives to the high-temperature problem include buffer rods either welded or pressure coupled to the component under test.

II. FACTORS INFLUENCING TRANSDUCER SELECTION

Perhaps more important than the selection of the transducer material, at least in many applications, is selecting the proper cut and/or mounting of the transducer element. The apparent sensitivity of a given transducer material to acoustic emissions is quite dependent on:

1. The cut, packaging (housing), and mounting.
2. The dominant modes of propagation at the point of measurement.
3. The frequency content of the emission and of any background noise at the point of measurement.

A. Modes of Propagation

A variety of propagation modes may be present in a structural component transmitting acoustic emissions. The most common basic propagation modes are shown in Fig. 1. Figure 1a illustrates a longitudinal wave in which the particle displacement is back and forth in the direction of propagation. The longitudinal wave can be transmitted through solids, liquids and gases; in solids it travels with the highest velocity. In the common structural metals longitudinal waves travel at speeds of about 0.25 in./μs. The shear wave shown in Fig. 1b is characterized by particle motion up and down at right angles to the direction of travel. Because liquids and gases do not, in general, support shear forces, the shear wave is transmitted only in solids and with a velocity approximately 0.6 times the longitudinal wave velocity in the same material. Surface or Rayleigh waves, as their names imply, travel along the surface of the solid material with a velocity equal to about half the longitudinal wave velocity. The particle motion, as indicated in Fig. 1c, is elliptical and a maximum of the surface. The effective depth of penetration of a surface wave is normally considered to be about one wavelength. This wave is readily damped or attenuated by surface films, liquids or other materials in contact with the surface. In thin sheet or plate materials Lamb or plate waves may be encountered. Both symmetric and asymmetric forms are allowed and particle motion may be quite complex as shown in Fig. 1d. The velocity of these waves is dispersive; that is to say, dependent on frequency and thickness, and may vary over a wide range. Like the surface wave they are readily damped by boundary materials. Another wave type that should be mentioned is the extensional wave. This is the wave utilized in the wire-type waveguide transducer and is quite similar to a longitudinal wave.

The acoustic emission source is usually small enough to be thought of as a point source and the emission itself is generally considered to be a step function containing frequency components as high as a few MHz at least.

In general, the emission after leaving the source may reflect from the surface of the structure a number of times before being detected by the transducer. This causes conversions or transformations from one type of wave to another which result in distortion of the original pulse and a spreading out of the energy in the time domain due to the various travel paths and changes in velocity assumed by the emission in arriving at the receiving transducer. Therefore, the dominant modes of propagation and the apparent frequency content of the burst as well as its apparent amplitude may depend on such factors as:

1. Distance traveled by the pulse from the emission source.
2. Dimensions and shape of the transmitting members.
3. Attenuation characteristics of the transmitting material.

In many cases several modes are propagating simultaneously and the pulse travels with an apparent velocity approaching the shear wave velocity in the material.

B. Characteristics of Transducers

Figure 2 illustrates, schematically, several types of transducer elements that have been used successfully as acoustic emission receivers. The compressional or longitudinal mode transducer in Fig. 2a is essentially omnidirectional. A special form of the compressional mode transducer is the differential type reported by Dunegan et al.[1] as being useful under conditions of high electrical noise. By splitting the basic transducer element and reassembling with one side upside down such that the poling directions are opposite the same emission will cause voltage outputs of opposite polarity from the two segments. When the leads attached to the tops of the segment are connected to a differential amplifier the two signals are added algebraically and the electrical noise is canceled by the common mode rejection.

A directional transducer can be achieved by using a thickness shear cut of the type shown in Fig. 2c. The sensitivity to emission sources in line with the direction of poling can be more than three times greater than at right angles to it. A variety of cross-coupled mode transducer elements are possible some of which can be quite small in comparison to the wavelength

of their resonant frequency. The extensional waveguide transducer, as mentioned previously, is attractive for high-temperature applications. The end of the wire is simply welded or brazed to the component to insure maximum coupling. Present experience with this type of transducer indicates that sensitivity under some conditions can be increased by adjusting the angle at which the wire intercepts the surface. This, in effect, maximizes the resolved component of the displacement in the axis of the wire. The transducer at the other end may be either magnetostrictive or piezoelectric. Magnetostrictive transducers using anodized aluminum wire will operate reliably at temperatures in excess of 1000F.

Figure 3 shows examples of actual transducers of several types together with a preamplifier. In practice, the preamplifier should be located as close to the transducer as possible. This reduces signal attenuation and noise pickup.

C. Transducer Bandwidth

The acoustic emission pulse, which, as we have already noted, may itself undergo considerable distortion, is rarely, if ever, faithfully reproduced by the transducer. In order to achieve maximum sensitivity and signal-to-noise ratio, acoustic emission transducers are often designed to operate at their resonant frequency. Therefore, the frequency spectrum of the pulse is modified by the bandpass characteristics of the transducer and/or preamplifiers. The bandwidth of the transducer, around its resonant frequency, may be controlled somewhat, as indicated in Fig. 4. If a free transducer element is struck by a mechanical impulse, it will ring at its resonant frequency. The duration of the ringing depends primarily on the mechanical Q of the transducer material. Under this condition the transducer will display quite a narrow bandwidth. In order to utilize a transducer element as an acoustic emission receiver, it must be mounted directly on the test part or in a housing and then on the part. In either case the transducer element is partially damped by virtue of the fact that part of the pulse energy is retransmitted into the part and/or backing member. The effect of this is an increased bandwidth. By matching the transducer with a backing critical damping is possible along with a further increase in bandwidth.

A second way to achieve flat response over a range of frequencies is to make the transducer resonant frequency much higher than the frequencies to be monitored. In general, however, increased bandwidth is achieved only at a sacrifice in sensitivity. Although some attempt at frequency analysis of acoustic emissions has been made in order to infer the nature of the emitting source, it now appears that frequency analysis

has little merit in most practical applications in view of the factors that have already been discussed which modify the frequency information. The exception to this is in the specialized area of acoustic emission that is better referred to as "signature analysis." Here one may be interested in the sound energy spectra of a motor or gear train where sound levels are much higher than in the acoustic emission associated with micro-failure, and true broadband techniques are readily adopted.

III. EXPERIMENTAL METHOD OF VERIFICATION - "THE ACOUSTIC EMISSION SIMULATION TEST SET"

Assume now that one is confronted with a structure that is to be monitored by acoustic emission techniques. How does the user determine the best transducer for the job taking into account:

1. The structure geometry?
2. The attenuation of the structure material?
3. The background or machine noise?
4. Distance and direction from transducer to the anticipated emission source?

Further, how does the user insure that all transducers are working properly and well bonded to the structure? How does he determine that material attenuation is within acceptable limits at the frequency to be monitored? How does he verify that triangulation equipment, if used, is working properly? Finally, during long tests, how does he insure that degradation of the system has not occurred?

One answer to these questions is to employ a controlled simulated emission source. The desirable characteristics of such a source are:

1. Repetitive sound source (constant repetition rate).
2. Point sound source.
3. Controlled short broadband pulse with center frequency approximately equal to the resonant frequency of the transducer.
4. Suitable for all transducer types.
5. Sound source can be either permanently or temporarily coupled to structure.
6. Means of evaluating pulse distortion by the structure.
7. Not limited by temperature or radiation.

A proposed sound source is shown in Fig. 5. A current pulse generator is connected to a wire-type waveguide transducer which now functions as a transmitter of ultrasonic pulses. The repetition rate of the pulse generator is normally 60 Hz. Pulse amplitude and waveform can be measured directly by observing the echo of the ultrasonic pulse reflected from the end of the wire prior to coupling. The ultrasonic pulse has a duration of one to two cycles and, therefore, is quite broadband and of known waveform and amplitude when transmitted into the structure. The amplitude is controlled by adjusting the amplitude of the excitation pulse and the center frequency of the pulse may be adjusted within the range of about 30 kHz to 1 MHz by the selection of transducer and pulse width.

The use of an "acoustic emission simulation test set" is demonstrated in Fig. 6. The set shown is designed for operation at a center frequency of 100 kHz, a frequency commonly used in acoustic emission monitoring systems. The ultrasonic pulse may be coupled into the structure simply by pressing the wire against the structure or for more permanent installations the wire may be brazed or tack welded to the surface.

Suppose the locations of an anticipated sound source and receiver transducer have been determined for a real or simulated structure. The preferred type of receiver transducer can be selected by monitoring the sound pulses transmitted by a thin wire probe placed at the probable source of emissions. The influence of path length between receiver and sound source can be rapidly and accurately determined by moving the acoustic emission "source" probe with respect to the receiver and the apparent material attenuation can be readily evaluated at the frequency being used for the tests.

If background machine noise is present the signal-to-noise ratio may be measured for different receiver frequencies and/or transducer types. Multiple transducer arrays may be checked for uniformity of response by monitoring the pulses transmitted by the emission probe. The accuracy of source location computation by triangulation techniques can be verified with the probe. Finally, the performance of the acoustic emission system during extended tests can be checked periodically with the acoustic emission simulation test set.

Reference

1. H. L. Dunegan, A. E. Brown and P. L. Krauss, Piezoelectric Transducers for Acoustic Emission Measurements, UCRL-50553, Lawrence Radiation Laboratory, University of California, Livermore (Dec. 13, 1968).

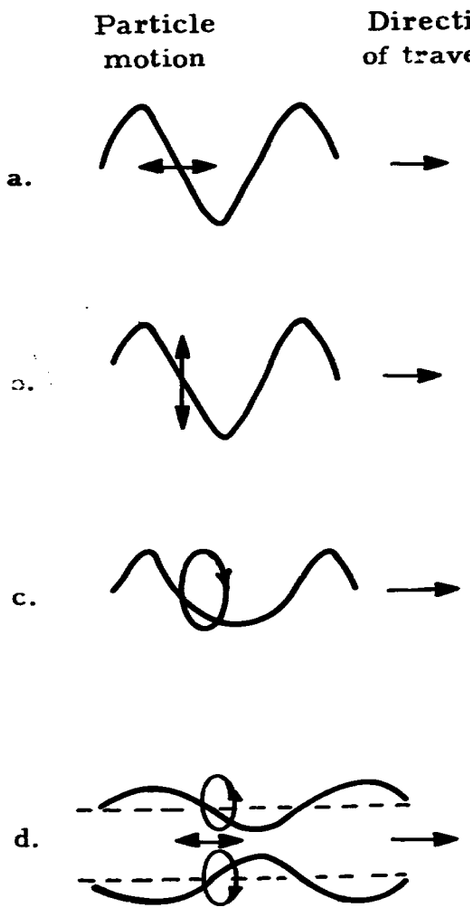

	Type of Wave	Relative Velocity
a.	Longitudinal or Compressional	Fastest $V_L = 1$
b.	Shear	Slower $V_S \cong 0.6\ V_L$
c.	Surface or Rayleigh	Slowest $V_R \cong 0.5\ V_L$
d.	Guided waves Lamb or plate symmetric or asymmetric	Both phase and group velocities vary

Fig. 1. Types of Traveling Waves Found in Acoustic Emission Monitoring

a.

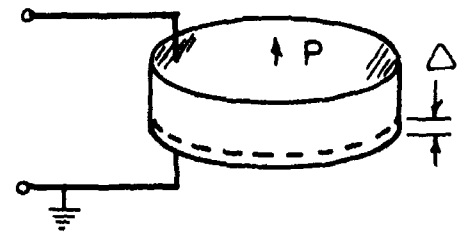

Compressional
Primarily sensitive to displacements normal to the surface

b.

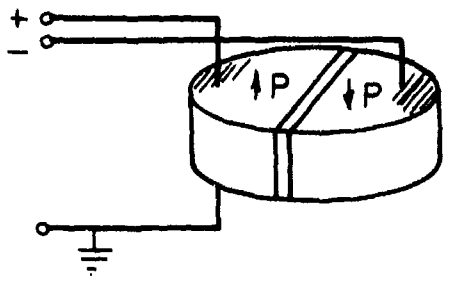

Differential compressional
Useful in high electrical noise environments

c.

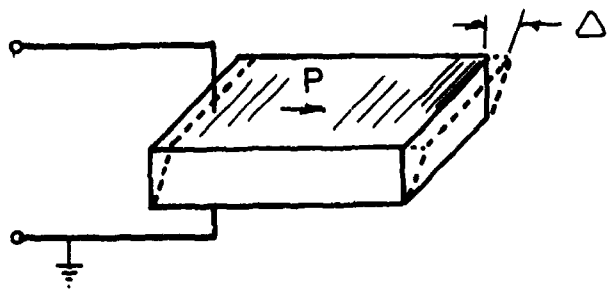

Thickness shear
(Directional)
Primarily sensitive to displacements parallel to the surface

d.

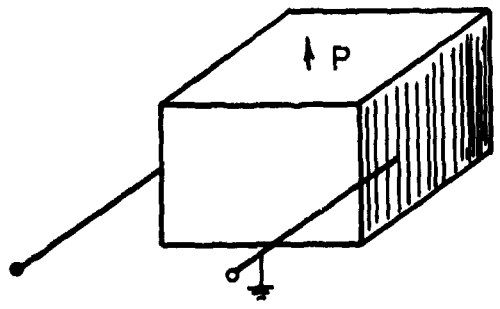

Cross-coupled
(Directional)

e.

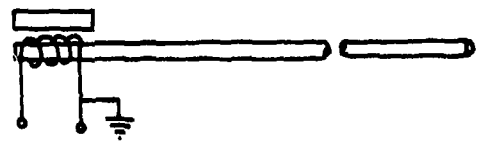

Waveguide
Extensional wave
magnetostrictive
or
piezoelectric
Useful for high temperature or nuclear radiation

Fig. 2. Types of Transducers Useful for Acoustic Emission

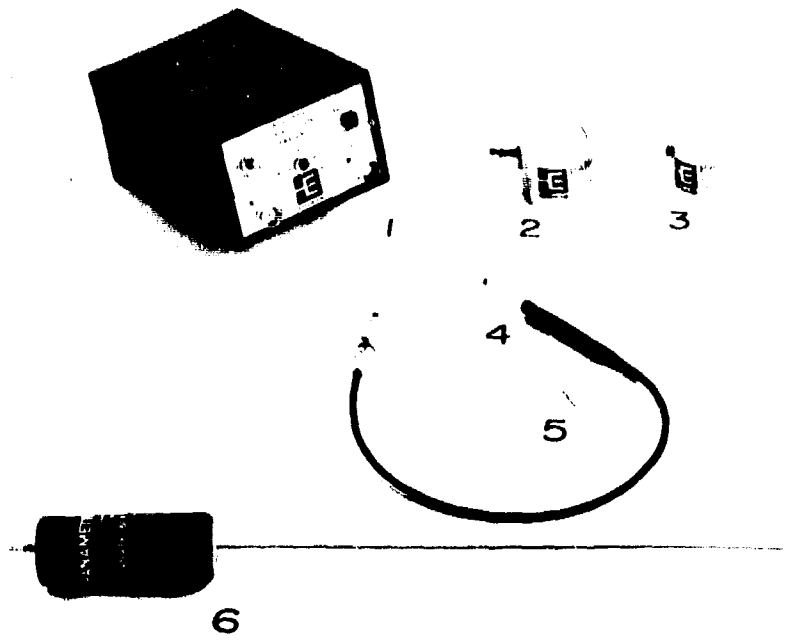

1. Acoustic Emission Preamplifier.

2. Acoustic Emission Transducer, compressional, housed and shielded, mode transducer resonant at ~100 kHz.

3. Acoustic Emission Transducer, housed and shielded, directional shear wave, resonant at ~100 kHz.

4. Acoustic Emission Transducer, high sensitivity transducer element with leads, cable, and BNC connector, resonant at ~100 kHz.

5. Acoustic Emission Transducer, High-Frequency, directional, shear mode transducer element with leads attached, resonant at ~1 MHz.

6. Acoustic Emission Transducer, High sensitivity magnetostrictive transducer including wire waveguide that carries emissions from high temperature or radiation environments or other remote locations. Wire line useful to 1000C. Broadband response centered at 100 kHz. Patent pending.

Fig. 3. Examples of Acoustic Emission Transducers and Preamplifiers

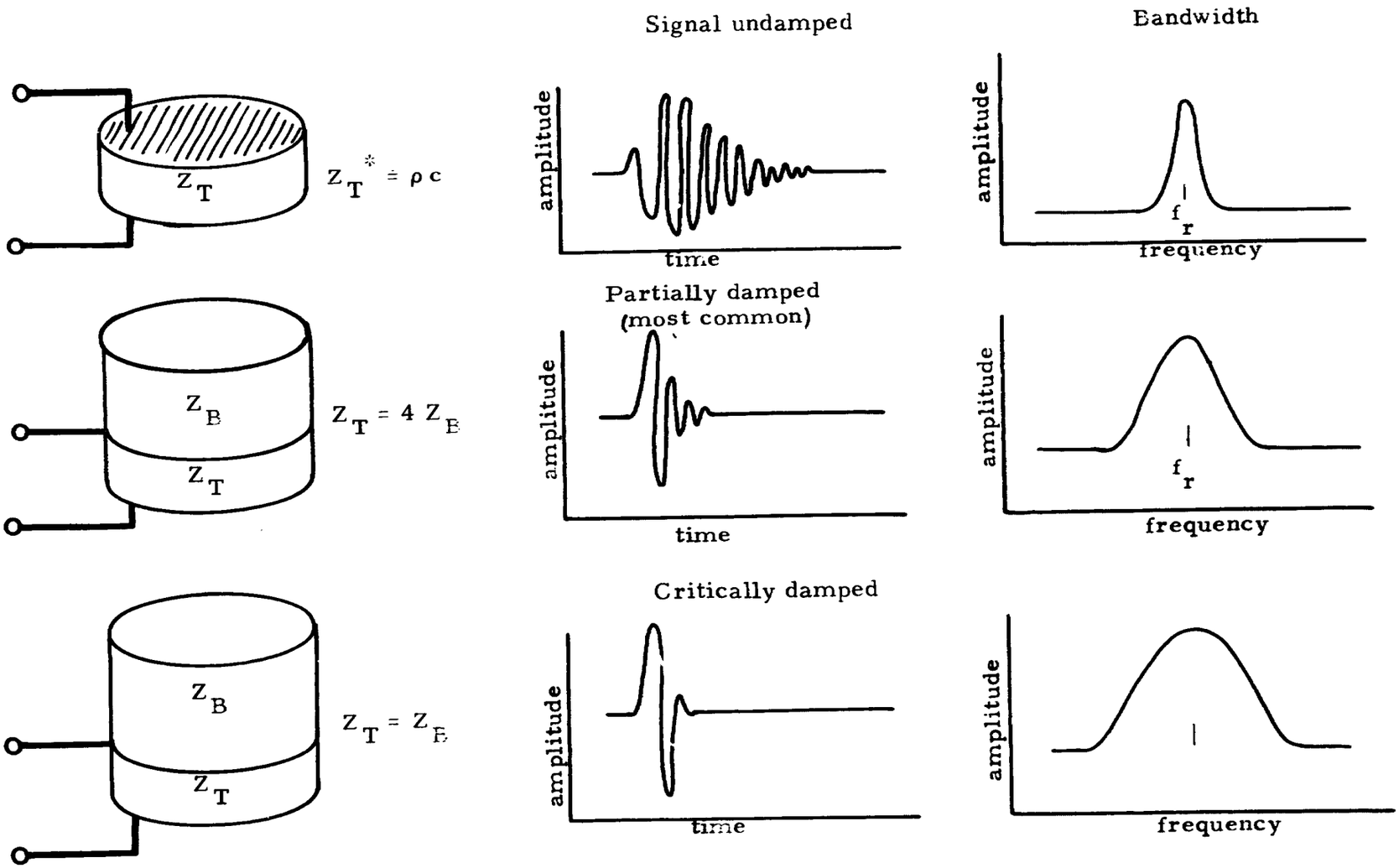

*Acoustic impedance, Z is equal to the product of the material density and its sound velocity

Fig. 4. Damping and Bandwidth of Piezoelectric Transducers

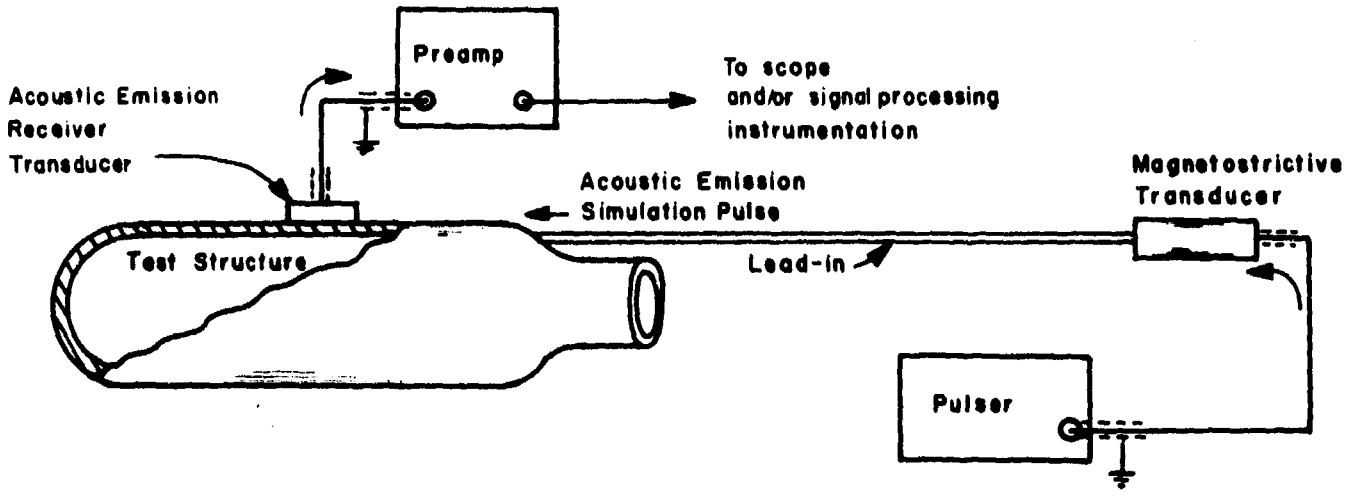

Fig. 5. Block Diagram of "Acoustic Emission Simulation Test Set"

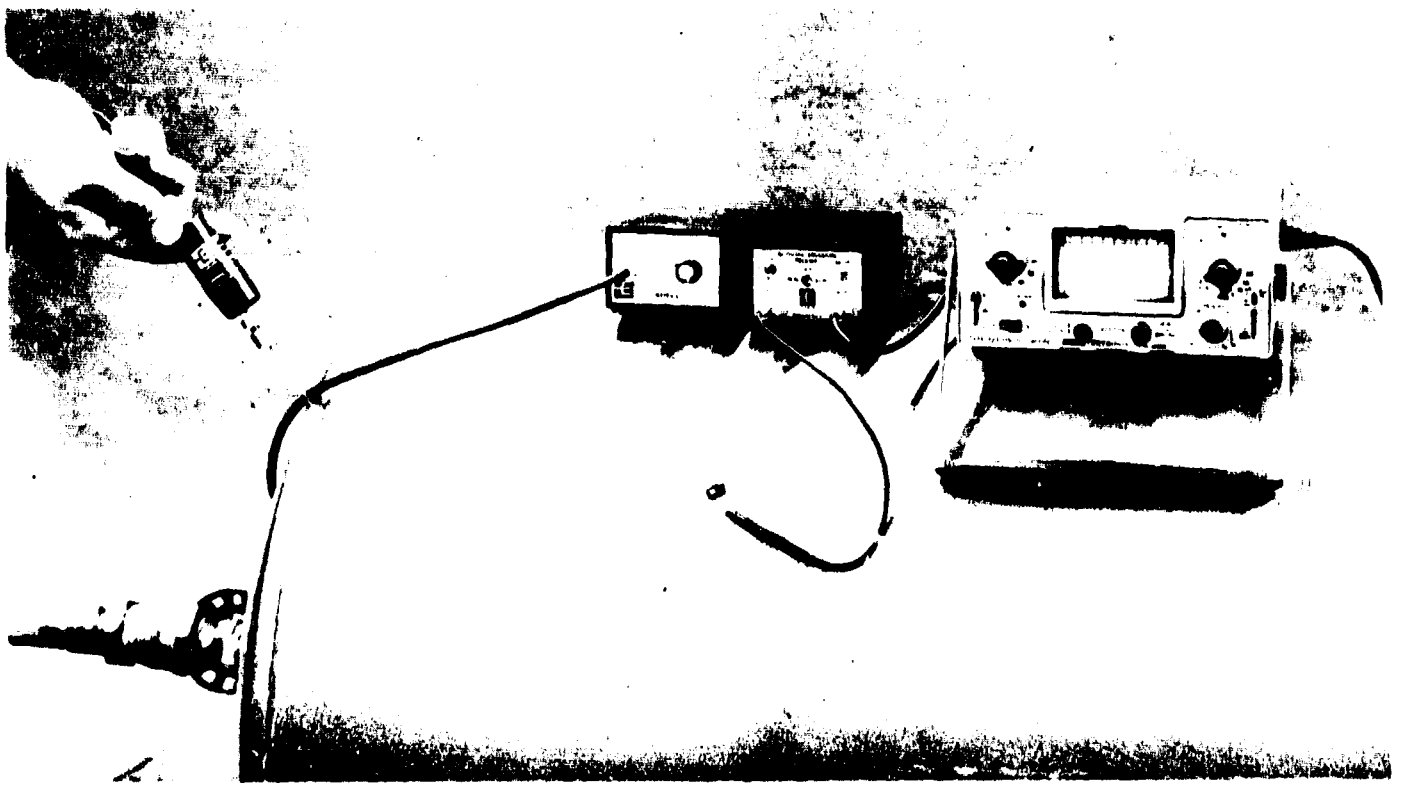

Fig. 6. Demonstration of the Use of the Acoustic Emission Simulation Test Set